

All Theses and Dissertations

2015-03-01

Deployable and Foldable Arrays of Spatial Mechanisms

Thomas Evans

Brigham Young University - Provo

Follow this and additional works at: <https://scholarsarchive.byu.edu/etd>

Part of the [Mechanical Engineering Commons](#)

BYU ScholarsArchive Citation

Evans, Thomas, "Deployable and Foldable Arrays of Spatial Mechanisms" (2015). *All Theses and Dissertations*. 5321.
<https://scholarsarchive.byu.edu/etd/5321>

This Thesis is brought to you for free and open access by BYU ScholarsArchive. It has been accepted for inclusion in All Theses and Dissertations by an authorized administrator of BYU ScholarsArchive. For more information, please contact scholarsarchive@byu.edu, ellen_amatangelo@byu.edu.

Deployable and Foldable Arrays of Spatial Mechanisms

Thomas Andrew Evans

A thesis submitted to the faculty of
Brigham Young University
in partial fulfillment of the requirements for the degree of
Master of Science

Larry L. Howell, Chair
Spencer P. Magleby
Jonathan D. Blotter

Department of Mechanical Engineering
Brigham Young University
March 2015

Copyright © 2015 Thomas Andrew Evans
All Rights Reserved

ABSTRACT

Deployable and Foldable Arrays of Spatial Mechanisms

Thomas Andrew Evans
Department of Mechanical Engineering, BYU
Master of Science

This work evaluates a specific origami device known as the kaleidocycle and the broad class of rigidly foldable origami. Both of these have potential for application in the design of deployable and foldable arrays of spatial mechanisms.

Origami is considered a compliant mechanisms because it achieves its motion through the deflection of paper creases. Compliant mechanisms generally do not allow for continuous rotation; however, the compliant kaleidocycle represents an exception to this generality. Along with their ability to rotate continuously, kaleidocycles may also be designed to exhibit multistable behavior during this rotation. These two characteristics make the kaleidocycle an interesting device with potential for applications in engineering. This work presents the multistable characteristics of kaleidocycles, showing that devices can be made which exhibit one, two, three, or four distinct stable equilibrium positions. Kaleidocycles may also be designed to exhibit a range over which the device is neutrally stable.

The second type of origami presented in this work is rigidly foldable origami, a special class of origami in which all deflection occurs at the creases, allowing the panels to remain rigid. This type of origami is of particular interest because of its ability to be constructed from materials much stiffer than paper while retaining its mobility. This property allows rigidly foldable origami to be applied to fields such as architecture and deployable mechanisms. This work presents a method for evaluating rigid foldability in origami tessellations. This method is used to define seven theorems for the rigid foldability of origami twists and to develop new rigidly foldable origami “gadgets” and tessellations.

Keywords: rigid foldability, tessellation, crease pattern, kaleidocycle, origami, multistable

ACKNOWLEDGMENTS

I would like to thank my advisor, Dr. Howell, for his instruction and advice. I would also like to thank Drs. Magleby and Blotter for being members of my graduate committee. Thanks also to Dr. Robert Lang for instructing me in origami matters and teaching me much about the field. And thanks to those who helped me construct prototypes, including Matthew Gong and Bryce Edmondson, and to all other members of the lab who helped me with ideas and concepts, without which this research would have been much more difficult. Finally, I would like to thank my family for their support throughout all of my educational endeavors.

This work is supported in part by the National Science Foundation and the Air Force Office of Scientific Research through NSF Grant No. EFRI-ODISSEI-1240417.

TABLE OF CONTENTS

LIST OF TABLES	vi
LIST OF FIGURES	vii
Chapter 1 Introduction	1
1.1 Problem Statement	1
1.2 Background	1
1.3 Research Objectives	3
1.4 Research Approach	4
Chapter 2 Multistable Behavior of Compliant Kaleidocycles	5
2.1 Introduction	5
2.2 Method	9
2.3 Behavior	11
2.4 Hardware	14
2.5 Conclusions	15
Chapter 3 Rigidly Foldable Origami Twists	19
3.1 Introduction	19
3.2 Rigidly Foldable Origami	19
3.2.1 Flat Foldability in Degree-4 Vertices	20
3.2.2 Fold-Angle Multipliers	21
3.2.3 Rigidly Foldable Polygons	22
3.3 Rigid Foldability of Origami Twists	22
3.4 Triangle Twists	24
3.5 Quadrilateral Twists	26
3.5.1 Rectangle and Square Twists	26
3.5.2 Parallelogram, Rhombus, and Isosceles Trapezoid Twists	27
3.5.3 Scalene Trapezoid Twists	28
3.5.4 Kite Twists	30
3.6 Regular Polygon Twists	31
3.7 Conclusions	33
Chapter 4 Rigidly Foldable Origami Gadgets and Tessellations	36
4.1 Introduction	36
4.2 Rigidly Foldable Origami	37
4.2.1 Flat-Foldability in Degree-4 Vertices	38
4.2.2 Fold-Angle Multipliers	39
4.2.3 Rigidly Foldable Polygons	40
4.2.4 Rigidly Foldable Origami Tessellations	40
4.3 Known Rigidly Foldable Tessellations	40
4.3.1 Huffman Grid	40

4.3.2	Chicken Wire Tessellation	43
4.3.3	Barreto’s “Mars”	44
4.3.4	Miura-ori	44
4.3.5	Yoshimura Pattern	45
4.3.6	Generalised Quadrilateral Mesh Origami	47
4.3.7	Generalised Miura-ori	48
4.4	Gadgets	49
4.4.1	Corner Gadget	51
4.4.2	Triple Parallel Gadget	51
4.4.3	Level Shifters	55
4.5	Directly Modified Rigidly Foldable Patterns	56
4.5.1	Miura-ori with Corner Gadget	56
4.5.2	Barreto’s “Mars” with Corner Gadget	57
4.6	New Rigidly Foldable Patterns	57
4.6.1	Dual Square Twist Tessellation	57
4.6.2	Alternating Level Shifter Tessellation	58
4.6.3	Level Shifter Tessellation	60
4.6.4	Miura-ori and Level Shifter Combination	61
4.6.5	Triple Parallel Tessellation	63
4.7	Conclusion	64
Chapter 5 Conclusions and Recommendations		66
5.1	Summary	66
5.2	Conclusions	66
5.3	Recommendations	67
REFERENCES		68
Appendix A Derivation of the Relationship between Dihedral Angles in a Degree-4 Flat-Foldable Origami Vertex		71
Appendix B Proof of Average Polygon Size		74
Appendix C Crease Patterns for Rigidly Foldable Origami Tessellations		77

LIST OF TABLES

2.1	Special Cases for Kaleidocycle Stability	12
3.1	Rigidly Foldable Scalene Trapezoid Twist Vertex Types	30
3.2	Twist Angles for Rigidly Foldable Regular Polygon Twists	35

LIST OF FIGURES

1.1	Kaleidocycle	2
2.1	Kinematic equivalence of the $n = 6$ kaleidocycle and the Bricard 6R. θ and ϕ joints are labeled and links are numbered	6
2.2	Compliant kaleidocycle laser cut from acrylic	7
2.3	θ and ϕ during one complete revolution	10
2.4	Strain energy diagram. $\theta_0 = \phi_0 = 0$, $K_\phi/K_\theta = 1.15$	11
2.5	Stability contour plot for special case where $K_\theta = K_\phi$	13
2.6	3D stability contour plot. Regions of quadstability are enclosed by red. Regions of tristability are enclosed by yellow. The boundary between regions of bistability and monostability as marked in blue with the monostable region between the blue surfaces.	14
2.7	Strain energy diagram for sharply stable kaleidocycle. $\theta_0 = -50^\circ$, $\phi_0 = 0^\circ$, $K_\theta/K_\phi = 1/5$	15
2.8	Strain energy diagram for sharply unstable kaleidocycle. $\theta_0 = 0$, $\phi_0 = 0$, $K_\theta/K_\phi = 5/1$	16
2.9	Strain energy diagram for neutrally stable kaleidocycle. $\theta_0 = 0$, $\phi_0 = 60^\circ$, $K_\theta/K_\phi = 1/3$	17
2.10	Kaleidocycle prototype. (a) shows adjustment mechanism for θ_0 or ϕ_0 . Each half of the joint may be adjusted by 0° or $\pm 25^\circ$, resulting in 0° , $\pm 25^\circ$, or $\pm 50^\circ$ adjustment for the entire joint. (b) shows the complete kaleidocycle	18
3.1	A Degree-4 origami vertex is its (a) unfolded and (b) partially folded states.	20
3.2	Rigidly foldable triangle. (a) Sector angles shown. (b) Fold angle multipliers for each consecutive pair of creases.	23
3.3	(a) A rigidly foldable square twist with twist angle θ . Arrows point from the minor to the major crease lines. (b) A Type-A vertex. (c) A Type-B vertex.	23
3.4	Two flat-foldable triangle twist configurations. The α and β vertices in (a) are both Type-A while the third is Type-B. The α vertex in (b) is Type-A while the other two are Type-B.	25
3.5	Flat foldable rectangular twists. (a) and (b) are rigidly foldable while (c) and (d) are not. The vertex label for each twist starts at the lower left vertex and runs counterclockwise.	27
3.6	Rigidly foldable parallelogram twist configurations for $\theta < \alpha_{min}$	28
3.7	Rigidly foldable parallelogram twist configurations for $\alpha_{min} < \theta < 90^\circ$	28
3.8	Rigidly foldable isosceles trapezoidal twist configurations for $\theta < \alpha_{min}$	29
3.9	Rigidly foldable isosceles trapezoidal twist configurations for $\alpha_{min} < \theta < 90^\circ$	29
3.10	Rigidly Foldable Kite Twists with Integer Angles. The α vertex is shown on the bottom in these figures ($\alpha = 15^\circ$ in (a)) and the β vertex is shown on top ($\beta = 105^\circ$ in (a)). The alphabetical labeling lists the α vertex first and then moves clockwise around the central polygon. Note that cases (e) and (f) may be rotated and/or mirrored to obtain any of the four configurations listed.	32

4.1	A Degree-4 origami vertex in its (a) unfolded and (b) partially folded states.	38
4.2	Rigidly foldable tessellations. New tessellations are shown with a bold outline. . .	41
4.3	Huffman grid	42
4.4	Single vertex of the Huffman grid. (a) labels the sector angles and (b) gives the fold-angle multipliers associated with the sectors	43
4.5	Single polygon of the Huffman grid. (a) labels the sector angles and (b) gives the fold-angle multipliers associated with the sectors. This polygon is rigidly foldable because $3.73 * -0.27 * -3.73 * 0.27 = 1$	44
4.6	Chicken wire tessellation	45
4.7	Barreto's "Mars"	46
4.8	Miura-ori	47
4.9	Yoshimura pattern	48
4.10	Quadrilateral meshed pattern	49
4.11	Generalised Miura-ori pattern	50
4.12	Corner gadget. This gadget is rigidly foldable for $\frac{\pi}{2} < \alpha_1 < \beta < \pi$. The value of β does not have any effect on the fold-angle multipliers between exterior creases. .	52
4.13	Recursive corner gadget. Note that each successive interior vertex is a rotation of the previous interior vertex by 180°	53
4.14	Symmetric corner gadget. This gadget is rigidly foldable for $\frac{\pi}{2} < \alpha < \beta < \pi$. The value of β does not have any effect on the fold-angle multipliers between exterior creases.	54
4.15	Triple parallel gadget. This gadget is rigidly foldable for $0 < \alpha, \beta < \pi/2$ and $\alpha \neq \beta$. The original vertex is superimposed with light weight on the gadget in (b). .	54
4.16	A set of triple parallel gadgets	55
4.17	Asymmetric level shifter. This gadget is rigidly foldable for $0 < \alpha_1, \alpha_2 < \frac{\pi}{2}$ and $\alpha_1 + \alpha_2 \neq \frac{\pi}{2}$. (a) and (b) show the two possible crease assignments. The gadget may also be mirrored across itself and remain rigidly foldable. All vertices in this gadget are flat foldable (opposite sector angles sum to π).	56
4.18	Symmetric level shifter. This gadget is rigidly foldable for $0 < \alpha < \frac{\pi}{2}$ and $\alpha \neq \frac{\pi}{4}$. This gadget may be repeated by mirroring itself and repeating as seen in (b).	57
4.19	Miura-ori pattern with corner gadgets	58
4.20	Barreto's "Mars" with corner gadgets	59
4.21	Dual square twist tessellation	60
4.22	Alternating level shifter tessellation	61
4.23	Non-parallel alternating level shifter tessellation	62
4.24	Level shifter tessellation	62
4.25	Non-parallel level shifter tessellation	63
4.26	Combination of Miura-ori and level shifter patterns	63
4.27	Triple parallel tessellation	64
A.1	Degree-4 flat-foldable origami vertex with sector angles (α_i), dihedral angles (γ_i) and unit vectors along each crease (a_i)	72
B.1	Arbitrary polygon mesh with subdividing triangles	74

C.1	Triple parallel tessellation. This tessellation is constructed using sets of triple parallel gadgets. Self-intersection generally occurs before the secondary flat position is reached.	77
C.2	Barreto’s “Mars” with corner gadgets. This tessellation modifies Barreto’s “Mars” by replacing vertices with corner gadgets. This replacement does not change the overall motion of the tessellation and the secondary flat position is obtainable without self-intersection.	78
C.3	Miura-ori pattern with corner gadgets. This tessellation modifies the Miura-ori by replacing vertices with corner gadgets. This replacement does not change the overall motion of the tessellation and the secondary flat position is obtainable without self-intersection.	79
C.4	Collapsed Miura-ori pattern with corner gadgets. This tessellation is created by eliminating creases between corner gadgets in the previous tessellation. As such, pairs of degree-4 vertices are combined to form degree-6 vertices. Even with the presence of degree-6 vertices, this tessellation has only one degree of freedom and the secondary flat position is obtainable without self-intersection.	80
C.5	Kite twist tessellation. This tessellation is constructed using two types of kite twists. Self-intersection generally occurs before the secondary flat position is reached.	81
C.6	Alternating level shifter tessellation. This tessellation contains parallel chains of level shifters which alternate in direction. The secondary flat position is obtainable without self-intersection.	82
C.7	Level shifter tessellation. This tessellation contains parallel chains of level shifters separated by vertical creases. Crease assignments of adjacent chains mirror each other. The secondary flat position is obtainable without self-intersection.	83
C.8	Trapezoidal tessellation. This tessellation is constructed entirely of trapezoids and the secondary flat position is obtainable without self-intersection.	84
C.9	Modified Yoshimura pattern. This tessellation is constructed by replacing creases on the Yoshimura pattern with pairs of creases with opposite parity and by replacing vertices with a rectangle and two isosceles trapezoids. The motion is similar to the Yoshimura pattern and self-intersection generally occurs before the secondary flat position is reached.	85
C.10	Dual square twist tessellation. This tessellation contains square twists of two twist angles. The secondary flat position is obtainable without self-intersection.	86

CHAPTER 1. INTRODUCTION

1.1 Problem Statement

Origami has recently been considered for applications in deployable structures and devices [1–3]. Rigidly foldable origami, in which panels remain rigid during deployment, is especially applicable to deployable mechanisms. This research addresses two factors which limit the application of origami designs to deployable mechanisms. The first factor is the difficulty of analyzing rigidly foldable tessellations. Several methods for evaluating rigid foldability in origami tessellations exist [4–7]. However, the difficulty of using these methods decreases their effectiveness. The second factor is the inability of compliant mechanisms (including origami) to undergo continuous rotation [8]. This research presents an analysis of the kaleidocycle, an origami device which is capable of continuous revolution, and also presents a new method which simplifies the analysis and design of rigidly foldable origami tessellations. This new method provides a useful tool in the design of deployable and foldable arrays of spatial mechanisms based on origami patterns.

1.2 Background

Origami can easily be seen for its value in art and entertainment, but it has also seen increased application in the engineering community in recent years [9, 10]. Designs influenced by origami patterns have been considered for application in deployable structures such as solar panels [1] and recent developments have included self-deployable origami stent grafts [11], self-folding membranes [12], and sandwich panel cores [13]. In these applications, the motion of origami was used to deploy mechanisms from a compact state to a final expanded state.

Compliant mechanisms are mechanisms which use the flexibility of materials to achieve at least some of their mobility. These mechanisms have advantages over traditional mechanisms

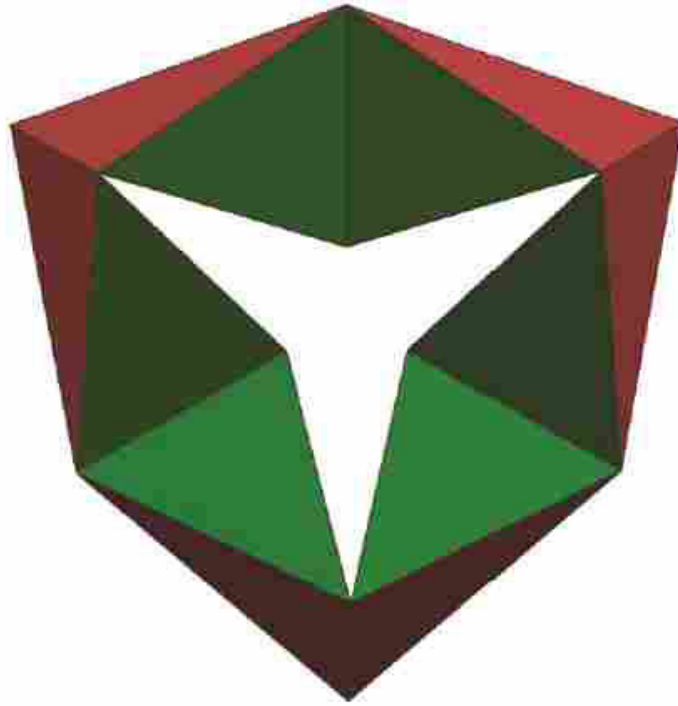


Figure 1.1: Kaleidocycle

such as reduced part count, simplified manufacturing, and increased precision and reliability [8]. Because the motion is achieved through the deflection of the paper, origami is an example of a compliant mechanism and methods derived for compliant mechanisms can be applied to origami. Like other compliant mechanisms, origami devices are generally unable to undergo continuous rotation; however, the kaleidocycle (see Figure 1.1) provides an exception and is able to continuously rotate. Because of this property, kaleidocycles have potential to be used in applications which previously have not been possible with compliant mechanisms. Kaleidocycles have been considered for use in deployable structures [14] and a retractable structure based on the kaleidocycle has been proposed for use in space [15]. In Chapter 2, another characteristic of kaleidocycles is evaluated: multistability. It is shown that kaleidocycles may be designed to have up to four positions of stable equilibrium and that these positions may be tuned to be sharply stable (requiring a large amount of force to perturb) or neutrally stable (requiring minimal force to perturb). This chapter was produced in conjunction with Dr. Larry L. Howell, Dr. Spencer P. Magleby, and Brett G. Rowberry.

Also considered in this work is the specific class of rigidly foldable origami. With a rigidly foldable origami pattern, creases may be represented as compliant members and the panels as rigid links. This type of origami generally has one degree of freedom and is useful in the design of deployable structures which incorporate materials much stiffer than paper. Rigidly foldable origami has received much interest in recent years [5, 6]. Produced in conjunction with Dr. Larry L. Howell, Dr. Spencer P. Magleby, and Dr. Robert J. Lang, Chapter 3 presents a new method, fold-angle multipliers, to evaluate rigid foldability. This method uses equations derived from loop closure equations to compare the dihedral angles in origami patterns. The result is a method for determining if an origami pattern is rigid foldable without the requirement of solving systems of nonlinear equations. This method simplifies the analysis of rigidly foldable origami and allows for the construction of more complex arrays of spatial mechanisms.

Origami twists are mechanisms that appear often in origami patterns and can facilitate the design of rigidly foldable tessellations. Chapter 3 evaluates origami twists using the fold-angle multiplier method and shows under what conditions they are rigidly foldable. The fold-angle multiplier method is also used in Chapter 4 to characterize and compare existing rigidly foldable tessellations and to create new origami “gadgets” which, like origami twists, can facilitate the design of rigidly foldable tessellations. New tessellations are designed by modifying existing tessellations and using gadgets as design tools. Both Chapters 3 and 4 were developed in conjunction with Drs. Howell, Magleby, and Lang.

1.3 Research Objectives

The research objectives are to:

- Evaluate the multistability characteristics of compliant kaleidocycles and design kaleidocycles which are sharply stable, sharply unstable, and neutrally stable;
- Characterize and compare existing rigidly foldable tessellations
- Characterize rigidly foldable origami twists which may be used as building blocks for deployable arrays;

- Use the fold-angle multiplier method to evaluate the rigid foldability of existing origami tessellations with potential to be used in deployable arrays;
- Design rigidly foldable origami “gadgets” which may be used to facilitate the construction of rigidly foldable tessellations;
- Design new rigidly foldable origami tessellations.

1.4 Research Approach

The multistable characteristics of $n=6$ compliant kaleidocycles are evaluated using the strain energy in the compliant joints. It is assumed that these compliant joints act as idealized torsional springs. Optimization techniques are used to design kaleidocycles which are sharply stable, sharply unstable, and neutrally stable. Prototypes are constructed to verify the stability characteristics of these kaleidocycles.

Origami twists are evaluated using the fold-angle multiplier method to determine under what conditions they are rigid foldable. Existing origami tessellations are studied to find patterns which would be useful for deployable structures. These arrays are evaluated using fold-angle multipliers to determine if they are rigid foldable. Rigid foldable tessellations are verified using graphical models.

New rigidly foldable origami patterns are constructed using origami twists and gadgets as design tools. The rigid foldability of these patterns is verified using fold-angle multipliers and graphical models. Optimization methods are used to aid the process of designing rigid foldable patterns. Origami patterns are constructed using paper and other paper-like materials to ensure that the motion is as expected and that no global self-intersection occurs.

CHAPTER 2. MULTISTABLE BEHAVIOR OF COMPLIANT KALEIDOCYCLES

2.1 Introduction

Compliant mechanisms are devices that achieve their motion from the bending of flexible components rather than using hinges and bearings [8]. They are common in natural systems that have motion (consider a pumping heart or the motion of a Venus fly trap), and are appreciated in human-designed systems because of their high precision, low mass, low part count, and ability to be made at many size scales. An obvious disadvantage of compliant mechanisms has been their inability to undergo continuous rotation. However, a violation of this constraint is found in a surprising place: folded paper art in the form of a kaleidocycle [15, 16].

Kaleidocycles are closed rings composed of at least 6 tetrahedra that have the ability to rotate continuously. Every tetrahedron shares one edge with each of its two adjacent tetrahedra. These joining edges correspond to revolute kinematic joints. The number of tetrahedra is designated as n . Figure 2.1 shows a paper kaleidocycle and its kinematic equivalent. The creases act as revolute joints and the kaleidocycle can be modeled as a spatial mechanism. The kinematic equivalence shown in Figure 2.1 can be exploited by combining with compliant mechanism theory to create non-paper compliant mechanisms with continuous rotation. Figure 2.2 shows a compliant mechanism laser cut from acrylic with motion obtained from surrogate folds [17].

The conversion of the kaleidocycle from paper to other materials reveals intriguing properties: 1) depending on the configuration of the compliance, it can have one, two, three, or four stable equilibrium positions, 2) it is possible to construct them with distinctly sharp unstable equilibrium positions (which can be critical in safety applications), 3) distinctly sharp stable equilibrium positions (important for high precision instruments), and 4) large range of neutral stable positions, making in effect a frictionless bearing.

Kaleidocycles are single-loop spatial mechanisms and are overconstrained as defined by the Grubler-Kutzbach criterion [18]

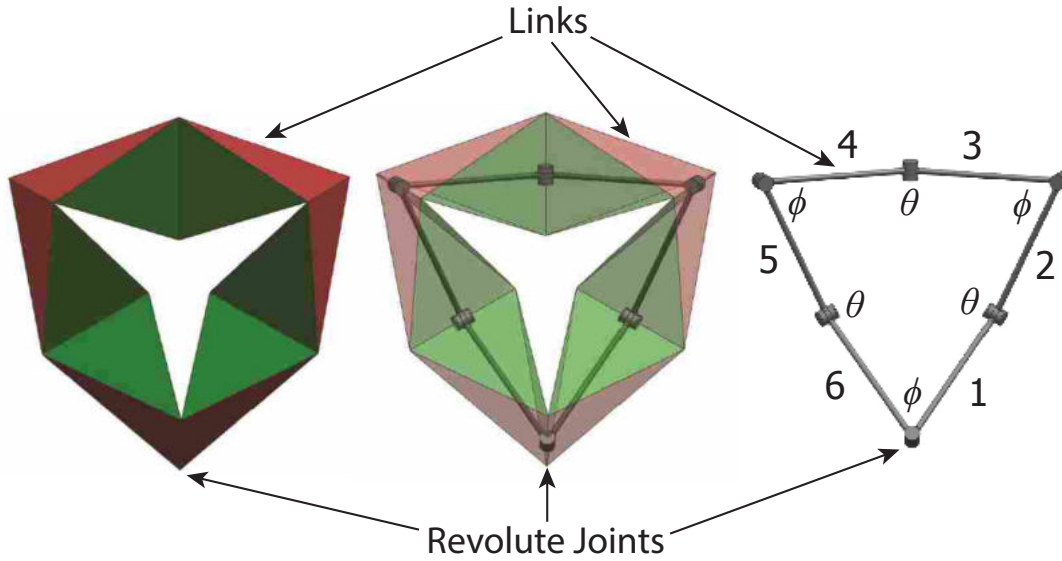
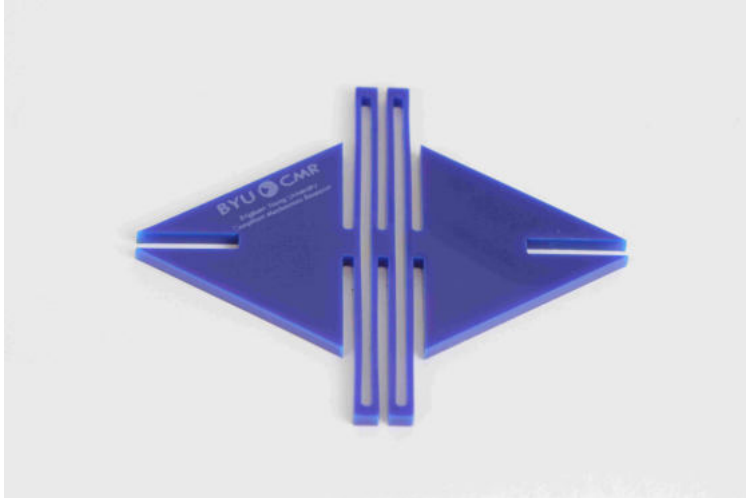


Figure 2.1: Kinematic equivalence of the $n = 6$ kaleidocycle and the Bricard 6R. θ and ϕ joints are labeled and links are numbered

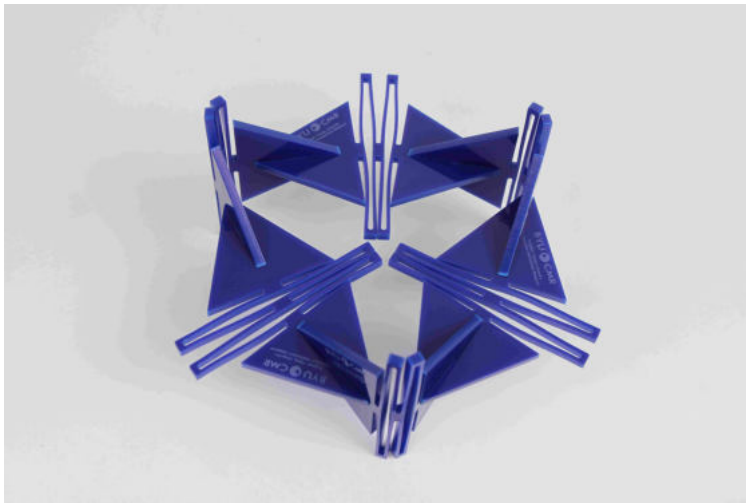
$$m = 6(L - 1) - 5J_1 - 4J_2 - 3J_3 - 2J_4 - J_5 \quad (2.1)$$

where m is the mobility of the mechanism, L is the number of links, and $J_1, J_2, J_3, J_4,$ and J_5 are the number of joints that remove 5, 4, 3, 2, and 1 degrees of freedom, respectively. When $m \leq 0$, a mechanism is a structure. However, some mechanisms are overconstrained and have more degrees of freedom than predicted by Equation 2.1. For all kaleidocycles, $L = J_1 = n$ and $J_2 = J_3 = J_4 = J_5 = 0$, thus $m = L - 6 = n - 6$. This indicates that $n = 6$ kaleidocycles are structures and should be immobile. However, these kaleidocycles are overconstrained and able to achieve mobility through symmetry and have a single degree of freedom.

It is also possible to construct kaleidocycles from polyhedra other than tetrahedra; though the range of motion may be limited [15] and continuous rotation may not be possible. Isosceles



(a) Surrogate fold



(b) Complete kaleidocycle

Figure 2.2: Compliant kaleidocycle laser cut from acrylic

tetrahedra, like those present in closed isosceles kaleidocycles, represent the maximum volume possible for links without interference.

As defined by Engel [19], kaleidocycles can be regular, normal, or special. This chapter focuses on the stability of $n = 6$ normal and special, right-angled kaleidocycles where the two opposite edges which connect adjacent tetrahedra are pairwise orthogonal. To simplify analysis and maintain generality, the tetrahedra may be reduced to straight-line links between joints, resulting in a Bricard 6R with $\alpha = 90^\circ$, which is kinematically equivalent to the $n = 6$ kaleidocycle [20]. Figure 2.1 shows this equivalence. Like its related kaleidocycles, the Bricard 6R rotates contin-

uously while any particular joint experiences $\pm 120^\circ$ of rotation [14]. Because of this kinematic equivalence, analysis conducted on the Bricard 6R, such as in [21], can be applied to $n = 6$ kaleidocycles. Methods have been developed for kinematic analysis of closed loop structures [22] and a reconfigurable robot has been recently developed using a closed loop mechanism [23].

The ball-on-the-hill analogy illustrates the different types of equilibrium positions. A ball at the top of a hill can be in equilibrium if balanced at the peak, but a small disturbance will cause a large output, thus it is an unstable equilibrium position. A ball resting at the bottom of a valley is in a stable equilibrium position because it will return to that position after a small disturbance. A ball on a flat surface is in a neutrally stable position. A hill with a particularly sharp peak makes it difficult to balance the ball in an unstable equilibrium position, and a valley with sharp sides will maintain the ball in a specific position.

Sharply stable mechanisms require a relatively large force to perturb the mechanism from a stable equilibrium position. Sharp stability has potential applications in precision machinery and safety devices. On the other hand, sharply unstable mechanisms ensure that it is difficult for the mechanism to balance at an unstable equilibrium. This is important in applications such as electrical switches where binary operation is required and sparking can occur when the mechanism balances at an intermediate position. Neutrally stable mechanisms exhibit a region over which any perturbation of the mechanism will result in the mechanism remaining in the new position [24]. Neutral stability can be advantageous because it allows for smooth motion over a certain range.

Of particular interest in this chapter are the stability characteristics of multistable kaleidocycles, including their sharply stable (ball in a sharp valley), sharply unstable (ball on a pointed hill), and neutrally stable (ball on flat ground) positions. Previous analysis has been performed on the compliant Sarrus mechanism, another overconstrained mechanism. The analysis showed the possibility of constructing a multistable compliant Sarrus mechanism with up to four stable positions [25].

Multistable mechanisms have more than one stable equilibrium position over their range of motion. Multistability is of particular interest to the engineering community because it reduces system complexity, decreases actuation power required, and can improve the performance of devices [26, 27]. Some traditional mechanisms use detents or latching mechanisms to achieve

multistability, but compliant mechanisms achieve it through the strain energy in the compliant members.

2.2 Method

Unlike planar mechanisms, which can be entirely described in two dimensions, the Bricard 6R and kaleidocycle are spatial mechanisms and must be described in three-dimensional space. However, their motion can be completely described by the angles of rotation experienced at their joints. The special geometry of the Bricard 6R results in two unique angles; θ is defined as the input angle and ϕ as the output angle, as shown in Figure 2.1. Joints represented by θ and joints represented by ϕ will be referred to as θ -type and ϕ -type joints, respectively. The angles θ and ϕ are defined by their deviation from the collinearity of adjacent links; therefore, a 0° angle corresponds to collinear links.

The relationship between θ and ϕ for the Bricard 6R is

$$\sec \theta + \sec \phi + 1 = 0 \quad (2.2)$$

or

$$\phi = \pm \arccos \left(-\frac{\cos \theta}{\cos \theta + 1} \right) \quad (2.3)$$

Figure 2.3 shows a plot of θ and ϕ vs. the rotation of the kaleidocycle. This rotation will be used in all subsequent plots. The kaleidocycle has a period of rotation of 480° ; therefore, 0° and 480° are equivalent.

The energy storage elements placed at the hinges of kaleidocycles can be modeled as idealized torsional springs. The strain energy stored in a torsional spring at a θ -type joint (E_θ) is

$$E_\theta = \frac{k_\theta}{2} (\theta - \theta_0)^2 \quad (2.4)$$

where k_θ represents the torsional spring constant, and θ_0 represents the angle at which the torsional spring is unstrained (the potential energy stored is zero). This angle is an important parameter in the stability characteristics of the mechanism and is not necessarily equal to zero.

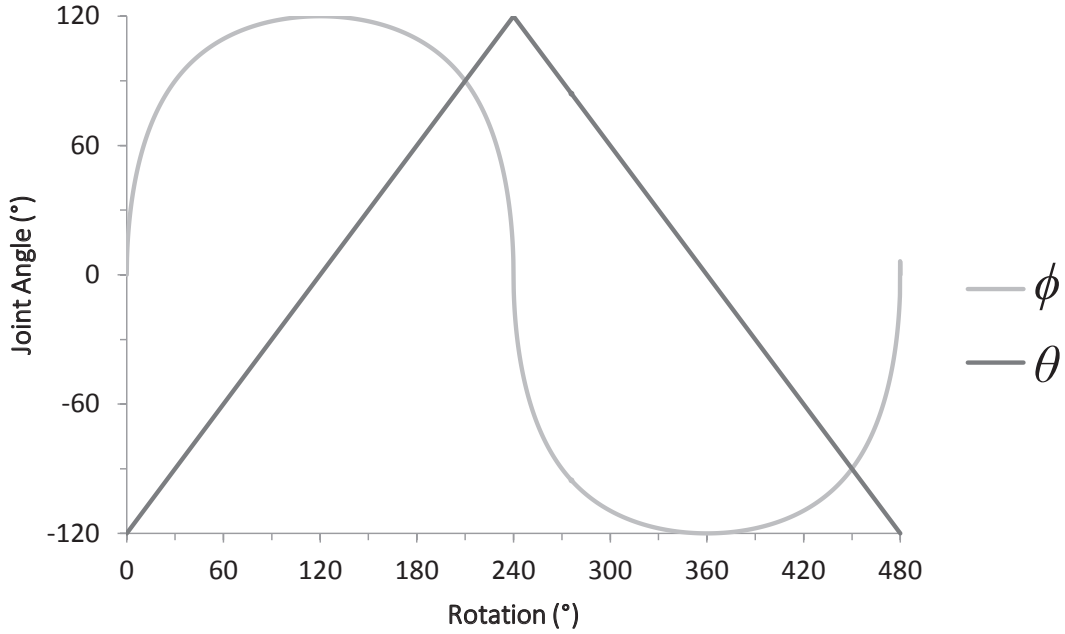


Figure 2.3: θ and ϕ during one complete revolution

Because all θ -type joints see the same deflection, they can be modeled as springs in parallel. Therefore, the combined spring constant for all θ -type joints (K_θ) is equal to the individual spring constants in each θ -type joint:

$$K_\theta = \sum_{i=1}^{n/2} k_{\theta_i} \quad (2.5)$$

where k_{θ_i} is the torsional spring constant on joint i . A similar equation for springs at ϕ -type joints is

$$K_\phi = \sum_{i=1}^{n/2} k_{\phi_i} \quad (2.6)$$

Thus the total strain energy stored in the mechanism is given by

$$E = \frac{K_\theta}{2} (\theta - \theta_0)^2 + \frac{K_\phi}{2} (\phi - \phi_0)^2 \quad (2.7)$$

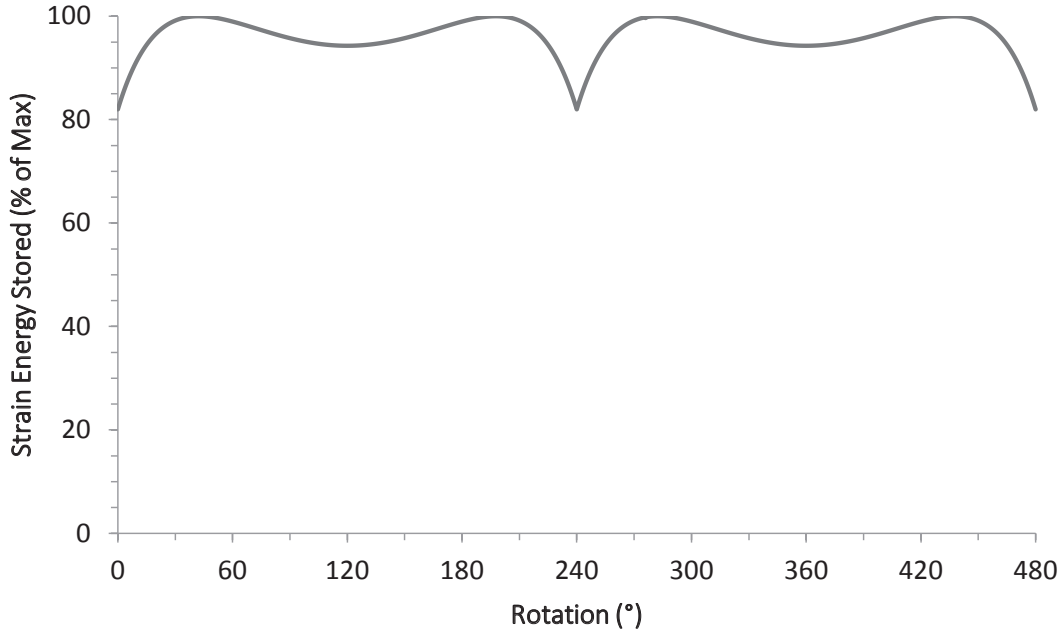


Figure 2.4: Strain energy diagram. $\theta_0 = \phi_0 = 0$, $K_\phi/K_\theta = 1.15$

This energy model includes the assumption of linear springs. It also includes the assumption that all springs on θ -type joints are undeflected at the same θ_0 and all springs on ϕ -type joints are undeflected at the same ϕ_0 .

A critical point on the energy curve is defined where $\frac{dE}{d\theta} = 0$. The stability characteristics of the point depend on the second derivative test. If $\frac{d^2E}{d\theta^2} > 0$, the position is at a stable equilibrium, if $\frac{d^2E}{d\theta^2} < 0$, the position is at an unstable equilibrium, and if $\frac{d^2E}{d\theta^2} = 0$, the position is neutrally stable. Recall that from Equation 2.3, ϕ is a function of θ and, therefore, these derivatives are non-trivial.

Figure 2.4 shows the strain energy diagram for one complete revolution of a kaleidocycle with $\theta_0 = \phi_0 = 0$ and $K_\phi/K_\theta = 1.15$. This mechanism has stable equilibrium positions at $0^\circ(480^\circ)$, 120° , 240° , and 360° . Unstable equilibrium positions exist at 42° , 198° , 282° , and 438° . This particular mechanism does not contain any neutrally stable positions.

2.3 Behavior

Numerical methods were used to evaluate the stability characteristics for kaleidocycles. It was found that kaleidocycles may exhibit one, two, three, or four stable positions, depending on

the values of θ_0 and ϕ_0 and the ratio between K_θ and K_ϕ . Although the nominal values of the spring constants affect the overall strain energy in the system, the shape of the energy curve is only dependent on the ratio between K_θ and K_ϕ .

Several special cases of kaleidocycle parameters provide consistent stability characteristics. These cases are presented in Table 2.1. Note that in Cases 5 and 6, switching all θ and ϕ conditions results in the same stability characteristics.

Cases 1-4 may be visualized by viewing a contour plot representing the number of stable positions for the special case where the spring constants are equal to each other (see Figure 2.5). As can be seen from the plot, quadstability may be achieved when both θ_0 and ϕ_0 are near zero, tristability and bistability may be achieved with a small range of values for θ_0 and ϕ_0 , and monostability is present with large values for either angle. For a set of parameters that are not included in the special cases mentioned, a 3D contour plot (Figure 2.6) may be referenced to determine the number of stable positions in the motion of the kaleidocycle.

For use in describing the sharpness of a stable or unstable position, we define a non-dimensional stability index ξ is as

$$\xi = \frac{\left| \frac{dE}{d\theta} \right| \operatorname{sgn} \left(\frac{d^2E}{d\theta^2} \right)}{E_{max} - E_{min}} \quad (2.8)$$

where E_{max} and E_{min} are the maximum and minimum strain energy found over the entire cycle, respectively. The signum function causes a positive stability index for stable equilibrium positions, a negative index for unstable equilibrium positions, and a zero index for neutrally stable positions. The greater the magnitude of the stability index, the sharper the instability or stability.

Table 2.1: Special Cases for Kaleidocycle Stability

Case Number	Condition 1	Condition 2	Condition 3	Result
1	$K_\theta = K_\phi$	$K_\theta, K_\phi = 0$		Neutrally Stable
2	$K_\theta = K_\phi$	$ \theta_0 = \phi_0 \leq 11.56^\circ$		Quadstable
3	$K_\theta = K_\phi$	$11.57^\circ \leq \theta_0 = \phi_0 \leq 32.70^\circ$		Bistable
4	$K_\theta = K_\phi$	$ \theta_0 = \phi_0 \geq 32.71^\circ$		Monostable
5	$K_\phi = 0$	$K_\theta > 0$	$ \theta_0 \geq 120^\circ$	Monostable
6	$K_\phi = 0$	$K_\theta > 0$	$ \theta_0 < 120^\circ$	Bistable

Figure 2.5: Stability contour plot for special case where $K_\theta = K_\phi$

Along with the multistability characteristics of the kaleidocycle, another important discovery was the distinct stable and unstable positions possible. For example, with $\theta_0 = -50^\circ$, $\phi_0 = 0^\circ$, and $K_\theta/K_\phi = 1/5$, sharply stable positions are obtained at $0^\circ(480^\circ)$ and 240° (see Figure 2.7). The stability index of this position $\xi = 1.26$. With $\theta_0 = 0$, $\phi_0 = 0$, and $K_\theta/K_\phi = 5/1$, sharply unstable equilibrium positions are obtained at $0^\circ(480^\circ)$ and 240° with a $\xi = -0.80$ (see Figure 2.8).

It is also possible to design a mechanism which experiences a large range of neutral stability, requiring small actuation force for motion over that range. For example, with $\theta_0 = 0$, $\phi_0 = 60^\circ$, and $K_\theta/K_\phi = 1/3$, the energy diagram (Figure 2.9) shows a statically balanced mechanism where over a range of 202° of θ (42% of the cycle) the potential energy has a variation of less than 1% from the average potential energy over that range. The maximum stability index over this range is 0.03.

Stability Contour Plot

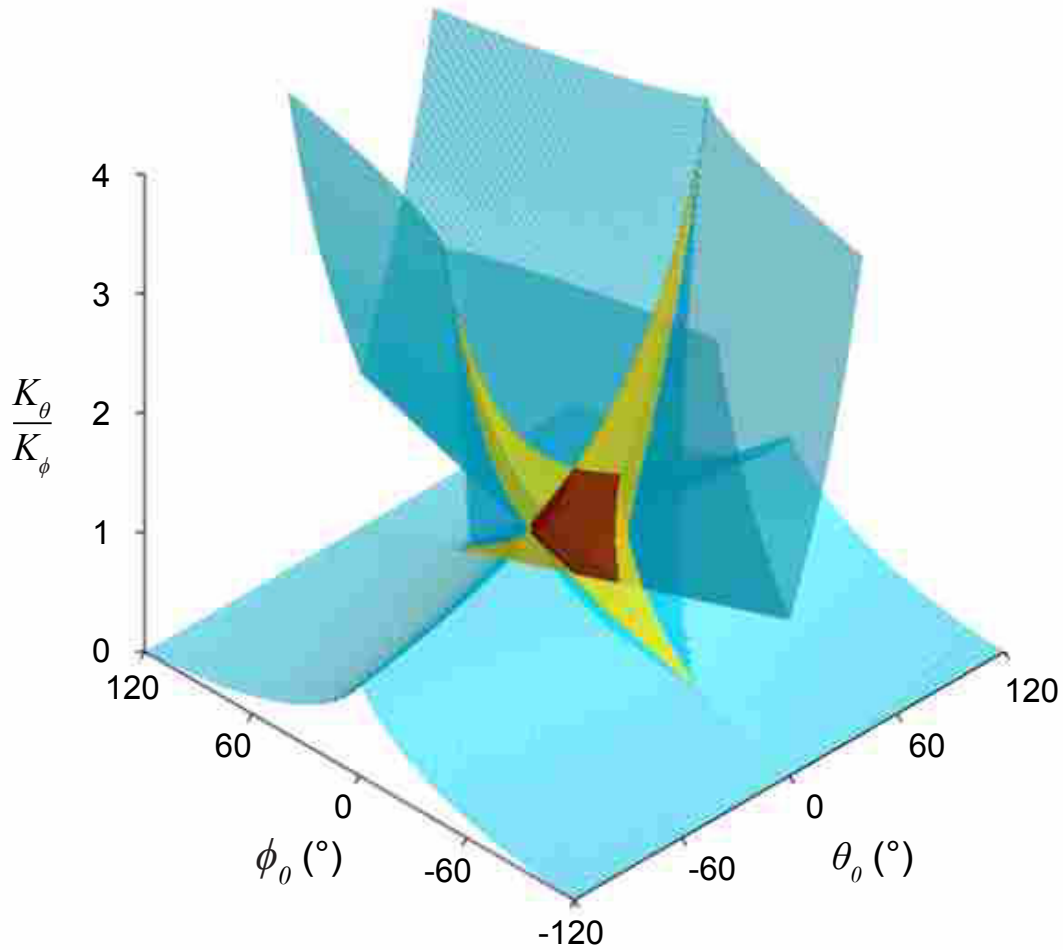


Figure 2.6: 3D stability contour plot. Regions of quadstability are enclosed by red. Regions of tristability are enclosed by yellow. The boundary between regions of bistability and monostability as marked in blue with the monostable region between the blue surfaces.

2.4 Hardware

A prototype multistable kaleidocycle was constructed to validate the results. The prototype was constructed with flexural joints made of 0.38 mm acetal resin (Delrin®), housing for the joints 3D printed using polylactic acid, and links constructed from 25.4 mm aluminum tubing (see Figure 2.10). The joint housing allowed for values for θ_0 and ϕ_0 of 0° , $\pm 25^\circ$, and $\pm 50^\circ$. Two sizes of joints were made, allowing a ratio between K_θ and K_ϕ of 2:5, 1:1, or 5:2. The prototype was assembled using each possible combination of the three parameters and it behaved as predicted by

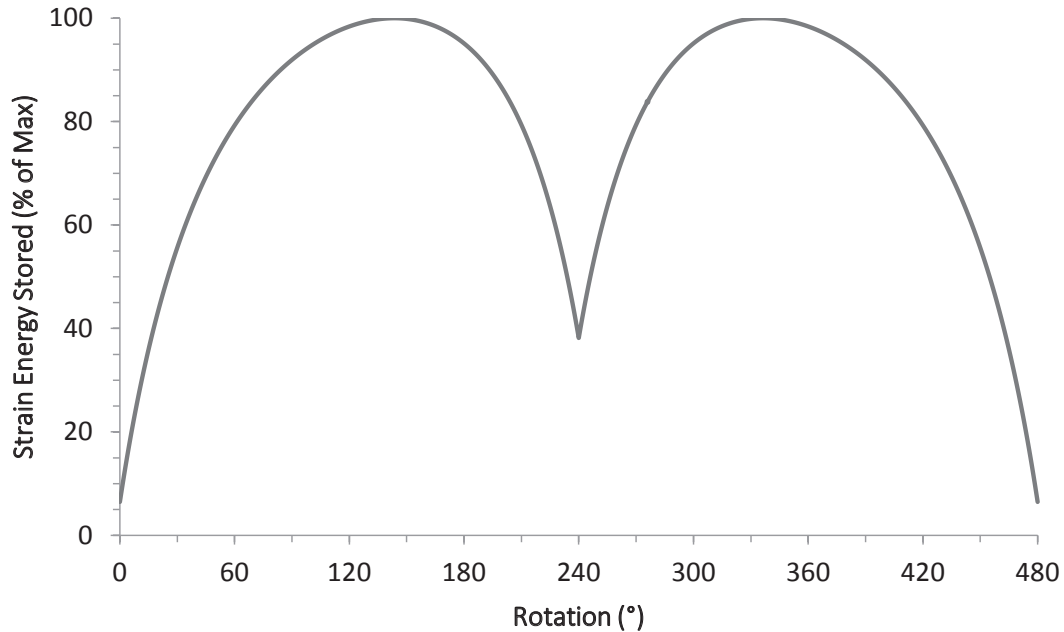


Figure 2.7: Strain energy diagram for sharply stable kaleidocycle. $\theta_0 = -50^\circ$, $\phi_0 = 0^\circ$, $K_\theta/K_\phi = 1/5$

the contour plots and the special cases. Kaleidocycles were assembled exhibiting one, two, three, and four stable positions, as predicted.

2.5 Conclusions

It has been shown that compliant kaleidocycles may be designed with one, two, three, or four positions of stable equilibrium, depending on the stiffness and neutral position of the revolute joints. The degree of stability of stable positions may be designed to vary from sharp to neutrally stable.

Because kaleidocycles represent an exception to the general rule that compliant mechanisms do not allow for continuous rotation, they provide the potential opportunity for compliant mechanisms to be used in applications which previously were not considered. With the possibility of continuous revolution and the varied stability characteristics, the kaleidocycle has the potential to increase the scope for compliant mechanisms in engineering applications. Possible applications

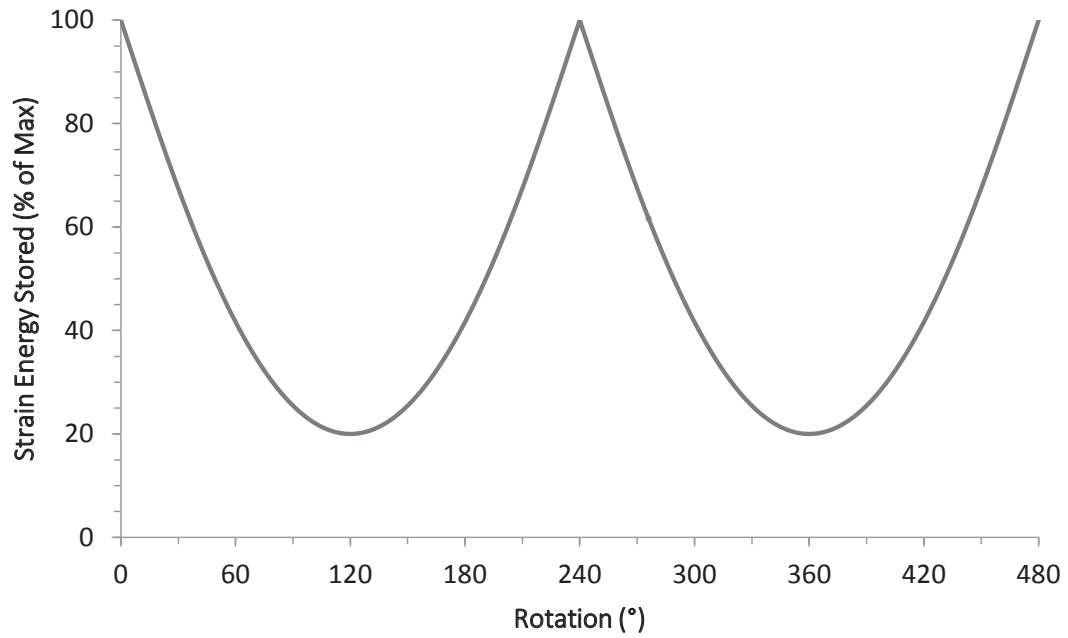


Figure 2.8: Strain energy diagram for sharply unstable kaleidocycle. $\theta_0 = 0$, $\phi_0 = 0$, $K_\theta/K_\phi = 5/1$

include mechanical detents, mechanical one-way valves, ratchets, and safety features involving discrete stable positions.

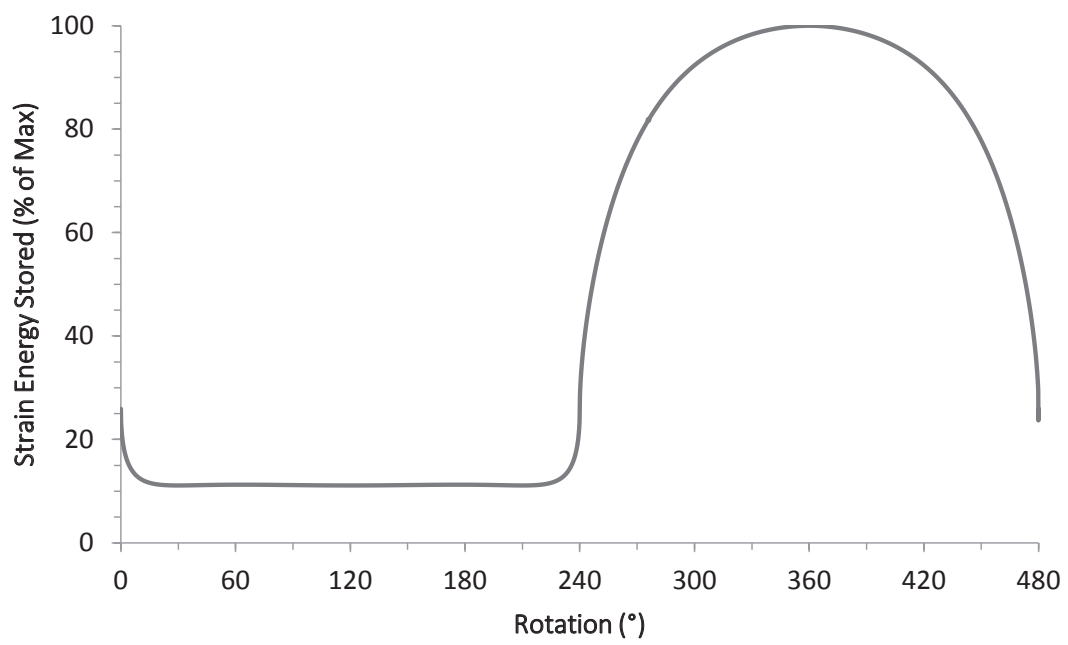
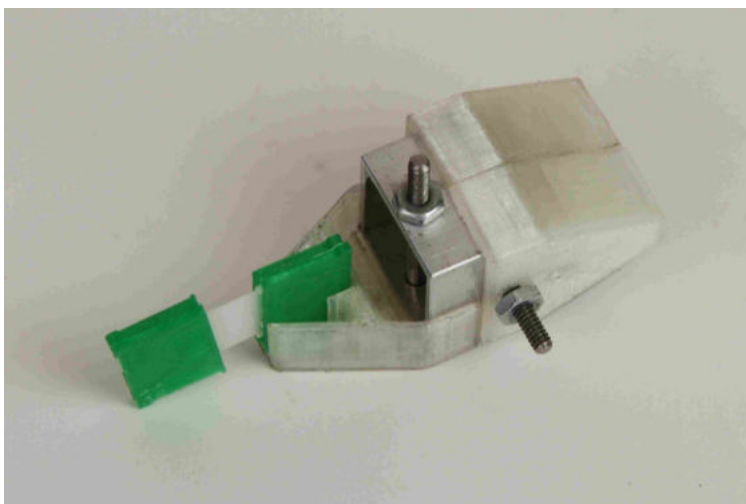
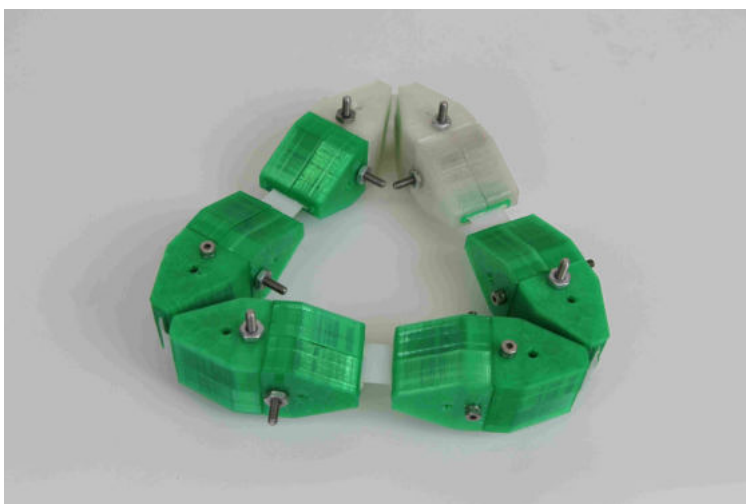


Figure 2.9: Strain energy diagram for neutrally stable kaleidocycle. $\theta_0 = 0$, $\phi_0 = 60^\circ$, $K_\theta/K_\phi = 1/3$



(a) Joint housing



(b) Complete kaleidocycle

Figure 2.10: Kaleidocycle prototype. (a) shows adjustment mechanism for θ_0 or ϕ_0 . Each half of the joint may be adjusted by 0° or $\pm 25^\circ$, resulting in 0° , $\pm 25^\circ$, or $\pm 50^\circ$ adjustment for the entire joint. (b) shows the complete kaleidocycle

CHAPTER 3. RIGIDLY FOLDABLE ORIGAMI TWISTS

3.1 Introduction

Rigid foldability is an important characteristic of origami structures that becomes significant with non-paper materials. A rigidly foldable origami tessellation is one where the sectors remain rigid and all deflection occurs at the crease lines. Many rigidly foldable patterns have only one degree of freedom, making them potentially useful for deployable structures. Methods have been developed to construct rigidly foldable origami tessellations using materials with finite thickness based on zero-thickness rigidly foldable patterns. [28].

Origami methods have been considered for application in deployable structures such as solar panels [1] [2] and sterile shrouds [3]. Other recent developments have included self-deployable origami stent grafts [11], self-folding membranes [12], and sandwich panel cores [13]. A better understanding of how to create rigidly foldable tessellations can lead to previously unexplored applications.

This chapter develops a method for evaluating the rigid foldability of origami tessellations by examining relationships between the dihedral angles in the pattern. The method is then used to determine what configurations allow origami twists, in particular, to be rigidly foldable. Rigidly foldable twists may be arrayed in a tessellation, providing a foundation for deployable origami-based structures to be constructed out of rigid materials.

3.2 Rigidly Foldable Origami

We will focus on patterns composed of degree-4 vertices, where a typical vertex is illustrated in Figure 3.1. Four creases meet at each vertex; the paper between adjacent creases is a *sector* and the angle between adjacent creases is a *sector angle*, designated α . The angle of the fold itself is the *dihedral angle*, denoted by γ , which is the angle between the surface normals

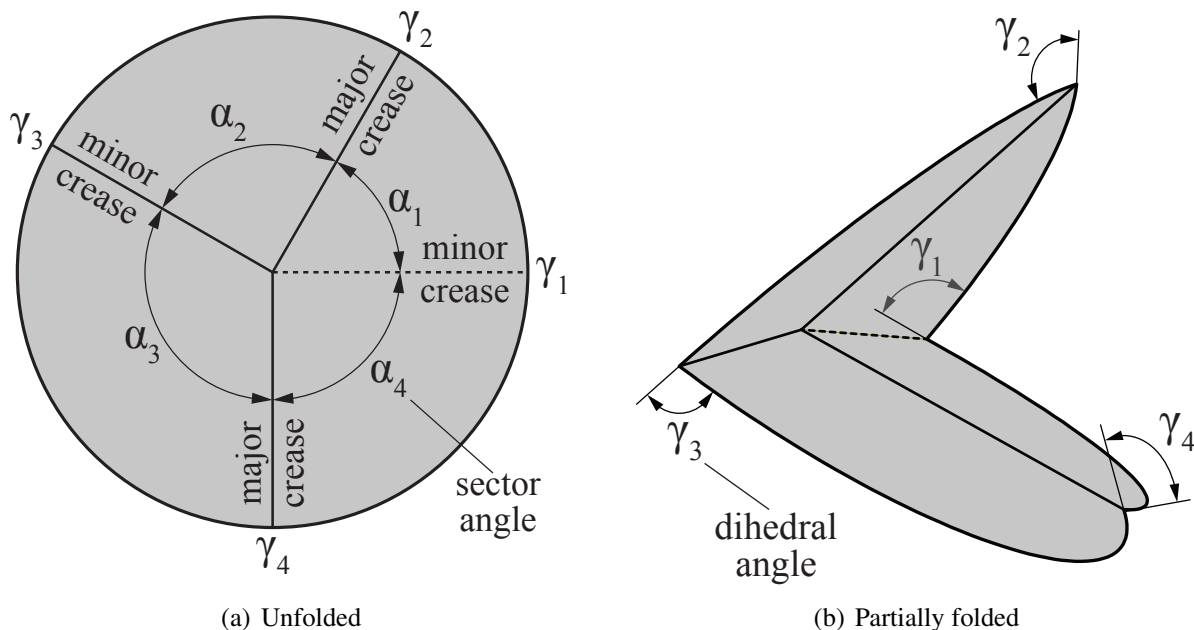


Figure 3.1: A Degree-4 origami vertex is its (a) unfolded and (b) partially folded states.

of the two incident sectors. A crease may be a *mountain fold* ($\gamma < 0$), a *valley fold* ($\gamma > 0$), or *unfolded* ($\gamma = 0$). We will indicate valley folds by dashed lines and mountain folds by solid lines. We index the sector angles α_i and dihedral angles γ_i so that sector α_i lies between folds γ_i and γ_{i+1} , as illustrated in the figure.

3.2.1 Flat Foldability in Degree-4 Vertices

A flat-foldable vertex can be folded so that all dihedral angles are equal to $\pm\pi$. Likewise, an origami pattern is considered flat foldable if there exists a configuration where all dihedral angles in the pattern are equal to $\pm\pi$. The conditions for flat-foldability are well known (see, e.g., [29]); for degree-4 vertices, they can be summarized as:

- Opposite sector angles sum to π ;
- There exist three folds of one parity and one fold of the other;
- The smallest-angled sector, if unique, is incident to folds of opposite parity (“anto”);
- The largest-angled sector, if unique, is incident to folds of the same parity (“iso”).

If there exist two equal smallest angled sectors, at least one of these sectors must be anto and its opposite sector must be iso. We call the two opposite creases with equal parity the *major* creases and the other two the *minor* creases.

These conditions imply a relationship between the sector angles:

$$\alpha_1 + \alpha_3 = \alpha_2 + \alpha_4 = \pi. \quad (3.1)$$

These are necessary conditions, not sufficient; an origami pattern composed entirely from flat foldable vertices may still not be flat-foldable due to self-intersection. However, any origami tessellation containing one or more non-flat-foldable vertices cannot be flat-foldable.

3.2.2 Fold-Angle Multipliers

We now introduce relationships between dihedral angles in a flat-foldable degree-4 vertex. Huffman [4], Lang [29], and Tachi [7] derived several relationships (which were equivalent under trigonometric transformation). We present equivalent, but new, and somewhat simpler expressions here. A derivation for this relationship is presented in Appendix A.

For the degree-4 vertex of Figure 3.1 where γ_2 and γ_4 are the major creases and γ_1 and γ_3 are the minor creases, in all configurations between the unfolded and fully folded states, the following relationships apply:

$$\gamma_3 = -\gamma_1, \gamma_2 = \gamma_4 = 2 \arctan \left(\frac{\sin \left(\frac{1}{2}(\alpha_1 + \alpha_2) \right)}{\sin \left(\frac{1}{2}(\alpha_1 - \alpha_2) \right)} \tan \left(\frac{1}{2}\gamma_1 \right) \right) \quad (3.2)$$

or equivalently,

$$\frac{\tan \left(\frac{1}{2}\gamma_2 \right)}{\tan \left(\frac{1}{2}\gamma_1 \right)} = \frac{\tan \left(\frac{1}{2}\gamma_4 \right)}{\tan \left(\frac{1}{2}\gamma_1 \right)} = \frac{\sin \left(\frac{1}{2}(\alpha_1 + \alpha_2) \right)}{\sin \left(\frac{1}{2}(\alpha_1 - \alpha_2) \right)} \quad (3.3)$$

The ratio between the half-angle tangents of any two dihedral angles in a flat-foldable degree-4 vertex is a constant that depends solely on the (fixed) values of the sector angles. We call this ratio the “fold-angle multiplier”, μ :

$$\mu \equiv \frac{\sin \left(\frac{1}{2}(\alpha_1 + \alpha_2) \right)}{\sin \left(\frac{1}{2}(\alpha_1 - \alpha_2) \right)} = \frac{\tan \left(\frac{1}{2}\gamma_2 \right)}{\tan \left(\frac{1}{2}\gamma_1 \right)} = \frac{\tan \left(\frac{1}{2}\gamma_4 \right)}{\tan \left(\frac{1}{2}\gamma_1 \right)} \quad (3.4)$$

We further define μ_i to be the ratio between the half-angle tangents of the dihedral angles adjacent to the i^{th} sector, i.e., $\mu_i \equiv \tan(\frac{1}{2}\gamma_{i+1})/\tan(\frac{1}{2}\gamma_i)$. Then

$$\mu_1 = -\mu_3 = \mu, \mu_2 = -\mu_4 = -\frac{1}{\mu} \quad (3.5)$$

There is a special case to note: when the major crease fold lines are collinear ($\alpha_2 + \alpha_3 = \pi$), zero and infinite fold-angle multipliers are obtained. This occurs because the major crease lines must be completely folded before the minor crease lines begin folding.

3.2.3 Rigidly Foldable Polygons

The fold angle multipliers $\{\mu_i\}$ capture the relationship between consecutive folds around a vertex. They can therefore be used to evaluate the rigid foldability of arrays of vertices. For an origami tessellation to be rigidly foldable, each vertex and each closed polygon in the tessellation must be rigidly foldable. (Again, there are longer-range self-intersection issues that must be considered for global rigid foldability, which we are intentionally not addressing.) For an n -degree polygon with interior angles 1 through n the fold angle multipliers (μ_i) associated with the crease pairs at each vertex define a loop condition that enforces consistency around the polygon, namely

$$\prod_{i=1}^n \mu_i = 1 \quad (3.6)$$

Figure 3.2 shows the sector angles and fold-angle multipliers for a rigidly foldable triangle. Each vertex is rigidly foldable in isolation; since the product of the fold angle multipliers around the interior polygon is 1 ($-0.246 \times 5.671 \times -0.718 = 1$), the entire pattern is similarly rigidly foldable.

3.3 Rigid Foldability of Origami Twists

The origami twist is a building block of many origami patterns that have application to deployable structures. It consists of a central polygon plus parallel pairs of creases extended from each side of the central polygon, as shown in Figure 3.3(a). The angle between each parallel pair

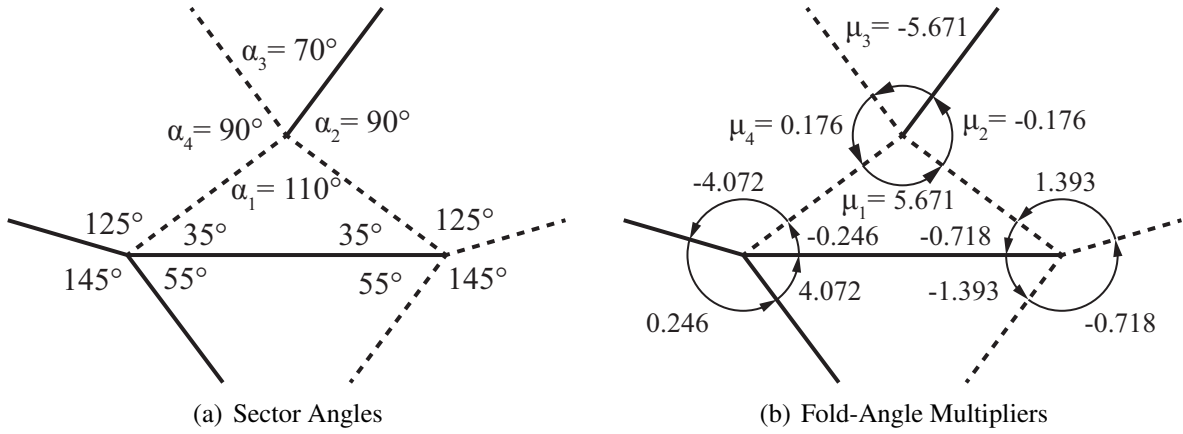


Figure 3.2: Rigidly foldable triangle. (a) Sector angles shown. (b) Fold angle multipliers for each consecutive pair of creases.

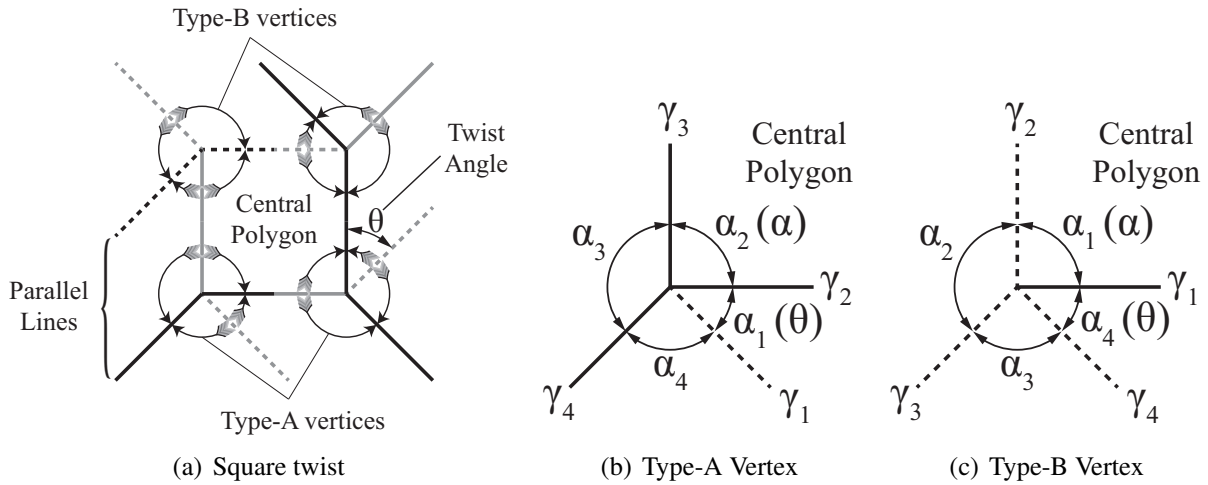


Figure 3.3: (a) A rigidly foldable square twist with twist angle θ . Arrows point from the minor to the major crease lines. (b) A Type-A vertex. (c) A Type-B vertex.

and its adjacent side is the *twist angle*; in a flat-foldable origami twist, all vertices have the same twist angle.

We will classify twist vertices as one of two types. If conventional numbering is used and the first sector lies counterclockwise from a minor crease, a vertex is of Type-A if the sector which includes the central polygon is evenly numbered (see Figure 3.3(b)). Conversely, if this sector is oddly numbered, the vertex is of Type-B (see Figure 3.3(c)). Another method of differentiating vertex types is shown in Figure 3.3(a). If an arrow is drawn from minor crease lines to major crease lines at each vertex, a Type-A vertex will have a clockwise arrow in the central polygon while a

Type-B vertex will have a counterclockwise arrow. A twist polygon can be characterized by the sequence of its vertices; the square twist of Figure 3.3(a) is AABB.

Note that zero and infinite multipliers can occur if the twist angle is equal to the interior angle of a Type-B vertex or if the twist angle is equal to the complement of the interior angle of a Type-A vertex.

For a Type-A vertex of a twist with interior angle $\alpha = \alpha_2$ and twist angle $\theta = \alpha_1$, we can evaluate the fold-angle multiplier (μ_A) for that vertex:

$$\mu_A = -\frac{\sin\left(\frac{1}{2}(\theta - \alpha)\right)}{\sin\left(\frac{1}{2}(\theta + \alpha)\right)} = \frac{\sin\left(\frac{1}{2}(\alpha - \theta)\right)}{\sin\left(\frac{1}{2}(\alpha + \theta)\right)}. \quad (3.7)$$

For a Type-B vertex with interior angle $\alpha = \alpha_1$ and twist angle $\theta = \alpha_4$, we have

$$\mu_B = \frac{\sin\left(\frac{1}{2}(\alpha + \pi - \theta)\right)}{\sin\left(\frac{1}{2}(\alpha - \pi + \theta)\right)} = -\frac{\cos\left(\frac{1}{2}(\alpha - \theta)\right)}{\cos\left(\frac{1}{2}(\alpha + \theta)\right)}. \quad (3.8)$$

With the constraints $0 < \alpha < 180^\circ$ and $0 < \theta < 180^\circ$, it follows that

$$|\mu_A| < 1 < |\mu_B|. \quad (3.9)$$

This gives us the following result.

Theorem 3.3.1 (No Rigidly Foldable Vertex-Uniform Twists) *No origami twist with degree-4 vertices having all Type-A or all Type-B vertices is rigidly foldable.*

The proof follows directly from Equations 3.9 and 3.6.

3.4 Triangle Twists

We now consider triangular twists. In this section we will prove the following:

Theorem 3.4.1 (No Rigidly Foldable Triangle Twist) *No origami triangle twist is rigidly foldable.*

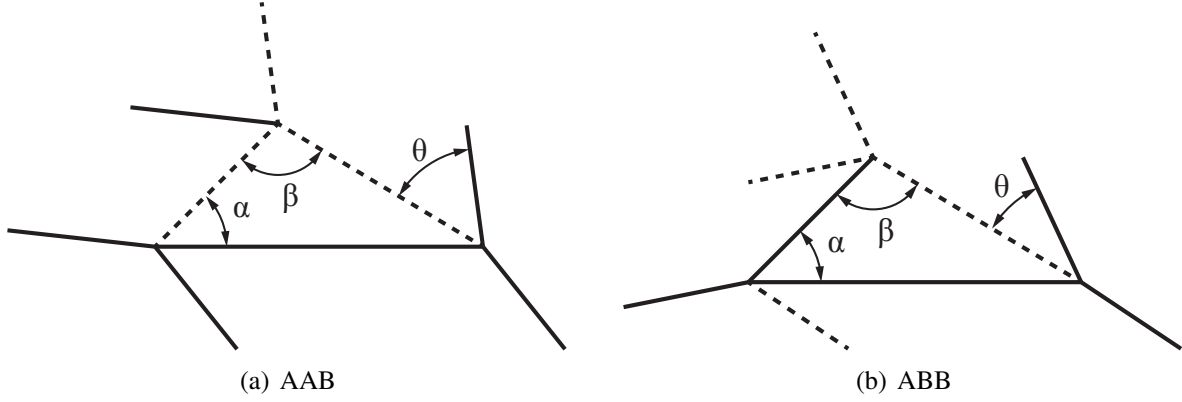


Figure 3.4: Two flat-foldable triangle twist configurations. The α and β vertices in (a) are both Type-A while the third is Type-B. The α vertex in (b) is Type-A while the other two are Type-B.

To prove this theorem we will consider the two basic configurations with potential to be rigidly foldable for a triangle twist. These two configurations are ABA and ABB (cyclic permutations are equivalent).

For the ABA configuration (see Figure 3.4(a)), substituting Equations (3.7) and (3.8) into Equation (3.6) results in the condition

$$\frac{\sin\left(\frac{\alpha-\theta}{2}\right) \sin\left(\frac{\beta-\theta}{2}\right) \cos\left(\frac{\alpha+\beta+\theta}{2}\right)}{\sin\left(\frac{\alpha+\theta}{2}\right) \sin\left(\frac{\beta+\theta}{2}\right) \cos\left(\frac{\alpha+\beta-\theta}{2}\right)} = 1. \quad (3.10)$$

This equation is satisfied only if $\theta = \pi$ or $\alpha + \beta = 2\pi$. In the first case the angle opposite of the twist angle becomes zero and in the second case the triangle violates geometric compatibility. Therefore, there is no rigidly foldable ABA triangle twist.

For the ABB configuration (see Figure 3.4(b)), Equation (3.6) results in

$$\frac{\sin\left(\frac{\alpha-\theta}{2}\right) \cos\left(\frac{\theta-\beta}{2}\right) \cos\left(\frac{\alpha+\beta+\theta}{2}\right)}{\sin\left(\frac{\alpha+\theta}{2}\right) \cos\left(\frac{\beta+\theta}{2}\right) \cos\left(\frac{\alpha+\beta-\theta}{2}\right)} = 1 \quad (3.11)$$

This equation is satisfied only if $\theta = 0$ or $\alpha + \beta = \pi$. In the first case the twist angle becomes zero and in the second case the third interior angle becomes zero. Therefore, there is no rigidly foldable ABB triangle twist. Because all other triangle twists with two Type-A and one Type-B or two Type-B and one Type-A vertices may be obtained by rotating the AAB or ABB

twists, we conclude that no triangle twist is rigidly foldable. Because our definition of an origami twist requires parallel pleats, Theorem 3.4.1 does not eliminate the possibility of rigidly foldable triangles with non-parallel pleats.

3.5 Quadrilateral Twists

For simplification, quadrilateral twists have been divided into several standard types of quadrilaterals. These are discussed below.

3.5.1 Rectangle and Square Twists

Since side length does not factor into the fold-angle multipliers, square and rectangular twists have the same conditions for rigid foldability.

Theorem 3.5.1 (Rectangle and Square Twists) *A square or rectangular twist is rigidly foldable if and only if it contains two Type-A and two Type-B vertices, with a twist angle not equal to 90° .*

The proof is as follows. For a rectangular twist, $\alpha = 90^\circ$. Therefore, Equations (3.7) and (3.8) simplify to give the following result:

$$\mu_A = \cot\left(\frac{\pi}{4} + \frac{\theta}{2}\right) \quad (3.12)$$

$$\mu_B = -\tan\left(\frac{\pi}{4} + \frac{\theta}{2}\right) \quad (3.13)$$

As can be seen from Equations (3.12) and (3.13), the fold angle multipliers for Type-A and Type-B vertices in such a twist are negative reciprocals of one another. Therefore, any rectangular twist with two Type-A and two Type-B vertices will satisfy Equation (3.6) and is rigidly foldable. The only exception is when $\theta = 90^\circ$, where multipliers become infinite. Conversely, those with unequal numbers of Type-A and Type-B vertices cannot satisfy Equation (3.6) and are not rigidly foldable. Figure 3.5 shows all of the possibilities (to within cyclic permutation and/or global parity reversal).

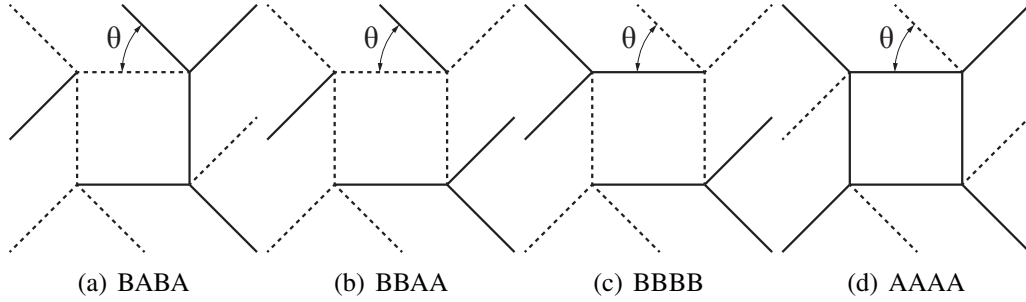


Figure 3.5: Flat foldable rectangular twists. (a) and (b) are rigidly foldable while (c) and (d) are not. The vertex label for each twist starts at the lower left vertex and runs counterclockwise.

3.5.2 Parallelogram, Rhombus, and Isosceles Trapezoid Twists

All three of these types of polygons contain two sets of supplementary interior angles, although the order in which these angles are arranged differs. Since this order does not affect rigid foldability, rhombus, parallelogram, and isosceles trapezoid twists have the same conditions for rigid foldability.

Theorem 3.5.2 (Parallelogram, Rhombus, and Isosceles Trapezoid Twists) *A parallelogram, rhombus, or isosceles trapezoid twist is rigidly foldable if and only if it contains two Type-A and two Type-B vertices, with a twist angle not equal to the interior angle of a Type-A vertex.*

To prove this we will define α as the value of one of the interior angles of the polygon. Of necessity, there are two interior angles with a value of α and two with a value of $\pi - \alpha$. The multipliers for the α -vertices may be calculated using Equations (3.7) and/or (3.8). The multipliers for the other two vertices are found by substituting into Equations (3.7) and (3.8), resulting in

$$\mu_A = \frac{\cos\left(\frac{1}{2}(\alpha + \theta)\right)}{\cos\left(\frac{1}{2}(\alpha - \theta)\right)} \quad (3.14)$$

$$\mu_B = -\frac{\sin\left(\frac{1}{2}(\alpha + \theta)\right)}{\sin\left(\frac{1}{2}(\alpha - \theta)\right)} \quad (3.15)$$

The product of any two of these Type-A multipliers and two of these Type-B vertices is equal to one, satisfying Equation (3.6). Therefore, a parallelogram, rhombus, or isosceles trapezoid twist is rigidly foldable if it contains two Type-A and two Type-B vertices. The exception is where the twist angle is equal to the interior angle of a Type-A vertex, where infinite multipliers are

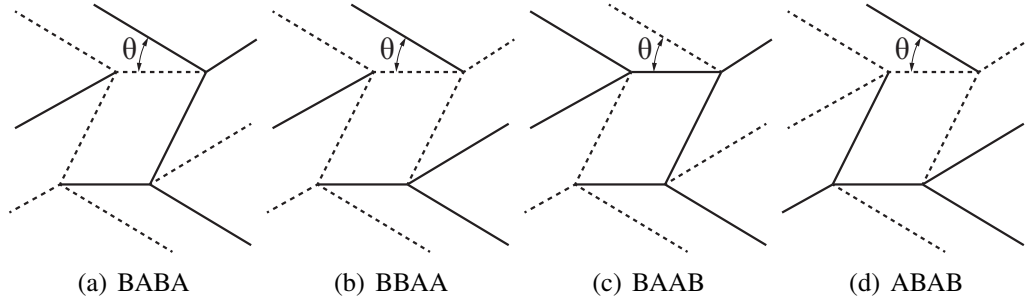


Figure 3.6: Rigidly foldable parallelogram twist configurations for $\theta < \alpha_{min}$.

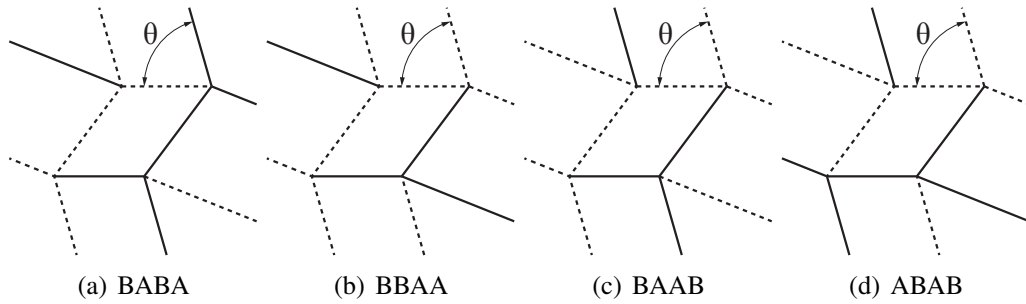


Figure 3.7: Rigidly foldable parallelogram twist configurations for $\alpha_{min} < \theta < 90^\circ$.

obtained. Conversely, twists with unequal numbers of Type-A and Type-B vertices cannot satisfy Equation (3.6) and are not rigidly foldable.

Figure 3.6 shows the four rigidly foldable configurations for a parallelogram twist where the twist angle (θ) is smaller than any of the interior angles (again allowing for cyclic permutation and/or global parity reversal). Figure 3.7 shows the four rigidly foldable configurations for the case where one of the sets of interior angles is less than θ . Figure 3.8 shows the six rigidly foldable configurations for an isosceles trapezoid for the case where the twist angle is less than any of the interior angles. Figure 3.9 shows the six rigidly foldable configurations for the case where the twist angle is greater than one pair of interior angles.

3.5.3 Scalene Trapezoid Twists

Theorem 3.5.3 (Scalene Trapezoid Twists) *A scalene trapezoid twist is rigidly foldable if and only if the pairs of supplementary interior angles each include a Type-A and a Type-B vertex and the twist angle is not equal to the interior angle of a Type-A vertex.*

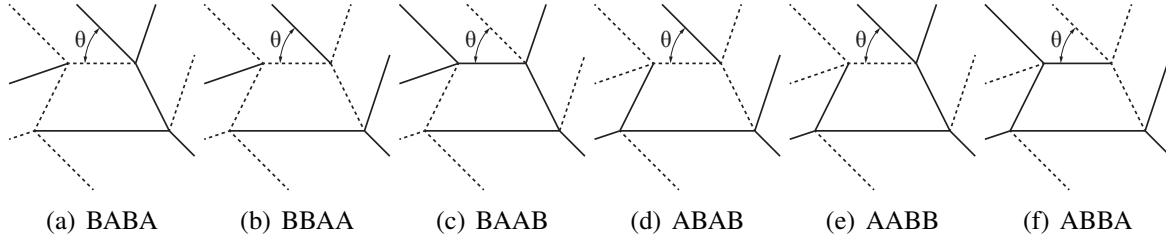


Figure 3.8: Rigidly foldable isosceles trapezoidal twist configurations for $\theta < \alpha_{min}$.

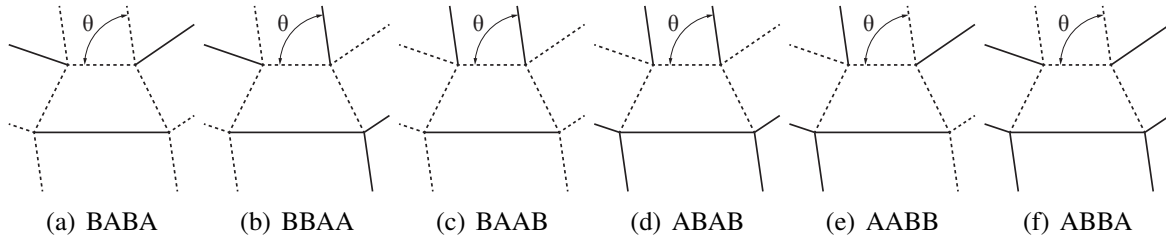


Figure 3.9: Rigidly foldable isosceles trapezoidal twist configurations for $\alpha_{min} < \theta < 90^\circ$.

The proof is as follows. If α_1 and α_2 are two non-supplementary interior angles, then of necessity the other two interior angles must be the supplements to α_1 and α_2 . As can be seen from Equations (3.7), (3.8), (3.14), and (3.15), the product of the multipliers for two supplementary-angled vertices of opposite type is -1. Therefore, the product of two such sets is equal to 1, satisfying Equation (3.6). Therefore, a scalene trapezoidal twist is rigidly foldable if the two sets of supplementary interior angles each have a Type-A and a Type-B vertex. Table 3.1 shows the possible vertex configurations for a rigidly foldable scalene trapezoid twist where Vertex 1 and Vertex 2 contain supplementary interior angles, as do Vertex 3 and Vertex 4. The exception is if the twist angle is equal to the interior angle of a Type-A vertex, in which case infinite multipliers are obtained.

Theorem 3.3.1 rules out the possibility of a twist with all vertices of the same type. Any scalene trapezoid twist with 3 vertices of one type must include a set of supplementary vertices of opposite type. Since the product of the multipliers for such vertices is equal to -1, the product of the multipliers of the other two vertices must also be -1 for it to be rigidly foldable. This dismisses the possibility of a scalene trapezoid twist with three vertices of the same type. The only remaining possibility is that one set of supplementary vertices of one type, and the other set

is of the opposite type. However, this configuration is only rigidly foldable if $\alpha_1 = \alpha_2$, resulting in an isosceles trapezoid or a parallelogram. Therefore, no conditions other than those stated in the previous paragraph result in a rigidly foldable scalene trapezoid twist.

3.5.4 Kite Twists

The previous discussions apply for kites that are squares, rectangles, parallelograms, rhombuses, or trapezoids and the rigidly foldable configurations having two Type-A and two Type-B vertices. However, unlike the parallelogram, rectangle, or trapezoid twists, a kite twist can be rigidly foldable with three vertices of one type and one vertex of the other type.

We will call α and β the two unique interior angles of a kite and θ the twist angle. For any combination of α and β where $\alpha \neq \beta$ and $\alpha + \beta \neq \pi$ there exists a unique θ which results in a rigidly foldable kite twist for each of the six configurations with 3 vertices of one type and 1 of the other. The type labeling in this section labels the α vertex first and the β vertex third, with the other two vertices second and fourth.

For the configuration with Type-A α and β vertices and one other vertex of each type (AAAB/ABAA), a kite twist is rigidly foldable if

$$\cos(\theta) = \frac{\sin(\alpha + \beta)}{\sin(\alpha) + \sin(\beta)} \quad (3.16)$$

For the configuration with Type-B α and β vertices and one other vertex of each type (BABB/BBBA), a kite twist is rigidly foldable if

$$\cos(\theta) = -\frac{\sin(\alpha + \beta)}{\sin(\alpha) + \sin(\beta)} \quad (3.17)$$

Table 3.1: Rigidly Foldable Scalene Trapezoid Twist Vertex Types

Case	Vertex 1	Vertex 2	Vertex 3	Vertex 4
1	B	A	B	A
2	B	A	A	B
3	A	B	B	A
4	A	B	A	B

For the configuration with Type-A α vertex, Type-B β vertex, and two other Type-A vertices (AABA), a kite twist is rigidly foldable if

$$\cos^2\left(\frac{\theta}{2}\right) = \frac{4 \cos\left(\frac{\alpha}{2}\right) \sin\left(\frac{\beta}{2}\right) \sin^2\left(\frac{\alpha+\beta}{4}\right)}{\sin(\alpha) - \sin(\beta) + 2 \sin\left(\frac{\alpha+\beta}{2}\right)} \quad (3.18)$$

For the configuration with Type-A α vertex, Type-B β vertex, and two other Type-B vertices (ABBB), a kite twist is rigidly foldable if

$$\cos^2\left(\frac{\theta}{2}\right) = \frac{4 \cos\left(\frac{\alpha}{2}\right) \sin\left(\frac{\beta}{2}\right) \cos^2\left(\frac{\alpha+\beta}{4}\right)}{\sin(\beta) - \sin(\alpha) + 2 \sin\left(\frac{\alpha+\beta}{2}\right)} \quad (3.19)$$

For the configuration with Type-B α vertex, Type-A β vertex, and two other Type-A vertices (BAAA), a kite twist is rigidly foldable if

$$\cos^2\left(\frac{\theta}{2}\right) = \frac{4 \sin\left(\frac{\alpha}{2}\right) \cos\left(\frac{\beta}{2}\right) \sin^2\left(\frac{\alpha+\beta}{4}\right)}{\sin(\beta) - \sin(\alpha) + 2 \sin\left(\frac{\alpha+\beta}{2}\right)} \quad (3.20)$$

For the configuration with Type-B α vertex, Type-A β vertex, and two other Type-B vertices (BBAB), a kite twist is rigidly foldable if

$$\cos^2\left(\frac{\theta}{2}\right) = \frac{4 \sin\left(\frac{\alpha}{2}\right) \cos\left(\frac{\beta}{2}\right) \cos^2\left(\frac{\alpha+\beta}{4}\right)}{\sin(\alpha) - \sin(\beta) + 2 \sin\left(\frac{\alpha+\beta}{2}\right)} \quad (3.21)$$

Figure 3.10 shows the twists which result from the integer angle solutions to Equations (3.16) to (3.21).

3.6 Regular Polygon Twists

For an n -sided regular polygon, we define the interior angle at each vertex as α , where

$$\alpha = \pi - \frac{2\pi}{n} \quad (3.22)$$

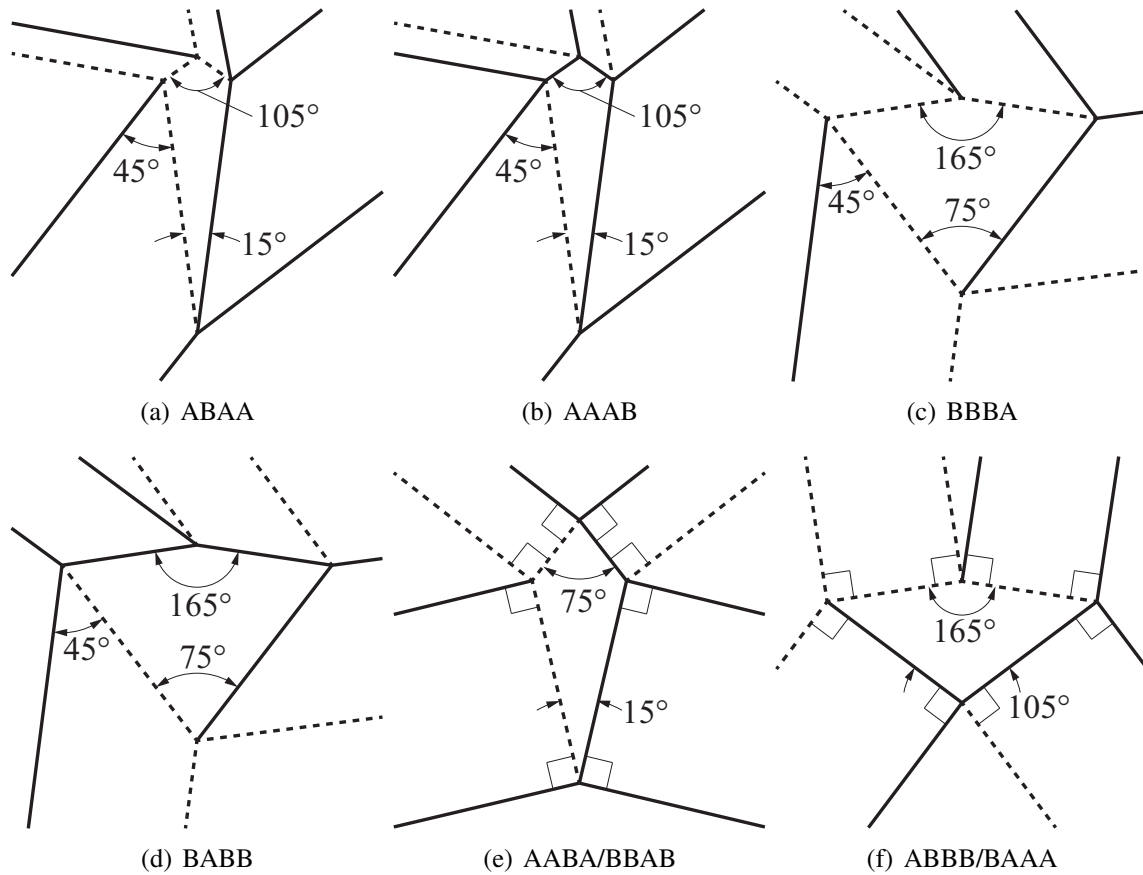


Figure 3.10: Rigidly Foldable Kite Twists with Integer Angles. The α vertex is shown on the bottom in these figures ($\alpha = 15^\circ$ in (a)) and the β vertex is shown on top ($\beta = 105^\circ$ in (a)). The alphabetical labeling lists the α vertex first and then moves clockwise around the central polygon. Note that cases (e) and (f) may be rotated and/or mirrored to obtain any of the four configurations listed.

If an n -degree regular polygon twist has a Type-A vertices and b Type-B vertices, then from Equation (3.6)

$$\mu_A^a \times \mu_B^b = 1 \tag{3.23}$$

where of necessity

$$a + b = n \tag{3.24}$$

Substituting Equations (3.7) and (3.8) into Equation (3.23) and simplifying gives

$$\left(\frac{\sin\left(\frac{1}{2}(\alpha - \theta)\right)}{\sin\left(\frac{1}{2}(\alpha + \theta)\right)} \right)^a \left(\frac{-\cos\left(\frac{1}{2}(\alpha - \theta)\right)}{\cos\left(\frac{1}{2}(\alpha + \theta)\right)} \right)^b = 1 \quad (3.25)$$

Substituting Equation (3.22) into Equation (3.25) yields

$$\left(\frac{\cos\left(\frac{\pi}{n} + \frac{\theta}{2}\right)}{\cos\left(\frac{\pi}{n} - \frac{\theta}{2}\right)} \right)^a \left(-\frac{\sin\left(\frac{\pi}{n} + \frac{\theta}{2}\right)}{\sin\left(\frac{\pi}{n} - \frac{\theta}{2}\right)} \right)^b = 1 \quad (3.26)$$

This results in the following theorem:

Theorem 3.6.1 (Rigidly Foldable Regular Polygon Twists) *A regular, n -degree polygon twist with a Type-A vertices, b Type-B vertices, and twist angle θ is rigidly foldable if and only if Equation (3.26) is satisfied.*

From Equations (3.9) and (3.23) it can be seen that there exist no rigidly foldable regular polygon twists where all vertices are of the same type. However, for each unique a , b and n , with $0 < a < n$ and $n > 4$, there exists one unique twist angle which satisfies Equation (3.26). This gives us the following result for regular polygon twists:

Theorem 3.6.2 (Rigidly Foldable Regular Polygon Twist Angles) *For an n -degree regular polygon twist with $n > 4$, there exist $n - 1$ unique twist angles which result in a rigidly foldable twist.*

Table 3.2 shows the twist angles which result in a rigidly foldable twist for regular pentagon, hexagon, heptagon, and octagon twists. For any even polygon twist, a 90° twist angle is rigidly foldable with $a = n/2$ and $b = n/2$. It can be seen that the twist angles larger than 90° are complementary to the twist angles for the opposite configuration. For $n > 4$ rigidly foldable regular polygon twists, all interior folds must have the same parity because the interior angle is the largest angle at each vertex. For a square twist with $a = b = 2$, Equation (3.26) is true for any value of θ other than 90° , where it becomes undefined.

3.7 Conclusions

We described a method for evaluating the rigid foldability of origami tessellations. We then applied this method to origami twists to discover what parameters allow an origami twist

to be rigidly foldable. It was shown that there is no possible configuration for a rigidly foldable triangle twist. It was also shown that many possible rigidly foldable quadrilateral twists exist. Finally, a method for determining twist angles for a rigidly foldable regular polygon twist was presented. This method was used to calculate all possible twist angles for rigidly foldable regular polygons of degree eight or less.

Table 3.2: Twist Angles for Rigidly Foldable Regular Polygon Twists

Degree n	Type-A a	Type-B b	Twist Angle θ ($^\circ$)	Inner Angle β ($^\circ$)
4	2	2	$\neq 90.0$	90.0
5	1	4	107.1	108.0
5	2	3	96.8	108.0
5	3	2	83.2	108.0
5	4	1	72.9	108.0
6	1	5	117.4	120.0
6	2	4	104.5	120.0
6	3	3	90.0	120.0
6	4	2	75.5	120.0
6	5	1	62.6	120.0
7	1	6	124.1	128.6
7	2	5	110.7	128.6
7	3	4	96.8	128.6
7	4	3	83.2	128.6
7	5	2	69.3	128.6
7	6	1	55.9	128.6
8	1	7	129.6	135.0
8	2	6	115.9	135.0
8	3	5	102.7	135.0
8	4	4	90.0	135.0
8	5	3	77.3	135.0
8	6	2	64.1	135.0
8	7	1	50.4	135.0

CHAPTER 4. RIGIDLY FOLDABLE ORIGAMI GADGETS AND TESSELLATIONS

4.1 Introduction

Rigid foldability is an important characteristic of origami structures. An origami tessellation is rigidly foldable if all sectors remain rigid and deflection only occurs at the crease lines. Because many materials used in engineering are much stiffer than paper, non-rigidly foldable tessellations (those that require deflection of the paper sectors) may have restricted movement when constructed out of these rigid materials. However, rigidly foldable tessellations may be constructed using stiff materials, leading to potential applications such as architecture and deployable arrays.

The study of origami has inspired engineering applications in recent years, including deployable structures such as solar panels [1] [2] and sterile shrouds [3], as well as sandwich panel cores [13], self-folding membranes [12], a self-deployable origami stent graft [11], and tunable metamaterials [30]. Origami techniques have also been used in packaging [31] and an origami-folding robot has been developed [32]. Origami is also of interest to the architectural community and has been used as inspiration in the design of a timber constructed chapel in Switzerland [33].

Origami research has focused on several related areas. Hull developed theorems which govern flat-foldable origami patterns [34] and evaluated the possible crease assignments which result in flat-foldable origami [29]. Schenk and Guest described the kinematics of two folded metamaterials based on the Miura-ori fold pattern [35]. Wei et al. characterised the elastic response of a simple periodically folded Miura-ori structure [36]. Demaine et al. showed that adding additional creases to an origami model can allow the model to be mathematically folded [37].

Research on rigidly foldable origami has addressed the issue in several different ways. Huffman derived basic relationships between the various dihedral angles in a rigidly foldable degree-4 polyhedral vertex using spherical trigonometry [4]. Wu used quaternions and dual quaternions to model rigid origami [5], resulting in a system of six nonlinear equations where constrained nonlinear optimisation was used to converge to a solution. Tachi developed conditions for partially

folded quadrilateral surfaces [6]. These methods resulted in systems of nonlinear equations, requiring optimisation techniques to converge to solutions. Tachi also developed equations which compare the dihedral angles of quadrilateral mesh origami [7].

A method for analysing the rigid foldability of origami patterns composed entirely from flat-foldable, degree-4 vertices has been developed previously by the authors [38]. While mathematically equivalent to Tachi’s matrix formalism [6, 7], it has a simple geometric interpretation that facilitates evaluation of rigid foldability, in many cases, by inspection alone. In this chapter, we use this method to evaluate previously existing tessellations for rigid foldability. These tessellations are characterised and a comparison of these tessellations is presented. We develop several new origami *gadgets*, which are tools in the modification and creation of rigidly foldable tessellations. These gadgets are used in two different ways. First, they are used to replace portions of existing rigidly foldable tessellations to create slightly modified tessellations. Second, the gadgets are tessellated to make new rigidly foldable patterns.

4.2 Rigidly Foldable Origami

An origami pattern is said to be rigidly foldable if all panels remain rigid while all deflection occurs at the crease lines during deployment. We previously presented a method for determining if an origami pattern composed of degree-4 vertices is rigidly foldable [38]. Because of its relevance to this work, the method is briefly reviewed here.

In this chapter, we focus on patterns composed of degree-4 vertices. As is illustrated in Figure 4.1, a degree-4 vertex is formed by the junction of four creases. The paper between adjacent creases is called a *sector* and the angle between adjacent creases is called a *sector angle*, designated α . The angle of the fold itself is the *dihedral angle* or *fold angle*, denoted by γ , which is the angle between the surface normals of the two incident sectors. A crease may be a *valley fold* ($\gamma > 0$), a *mountain fold* ($\gamma < 0$), or *unfolded* ($\gamma = 0$). We will indicate mountain folds by solid lines and valley folds by dashed lines. We index the sector angles α_i and dihedral angles γ_i so that sector α_i lies between folds γ_i and γ_{i+1} , as illustrated in Figure 4.1.

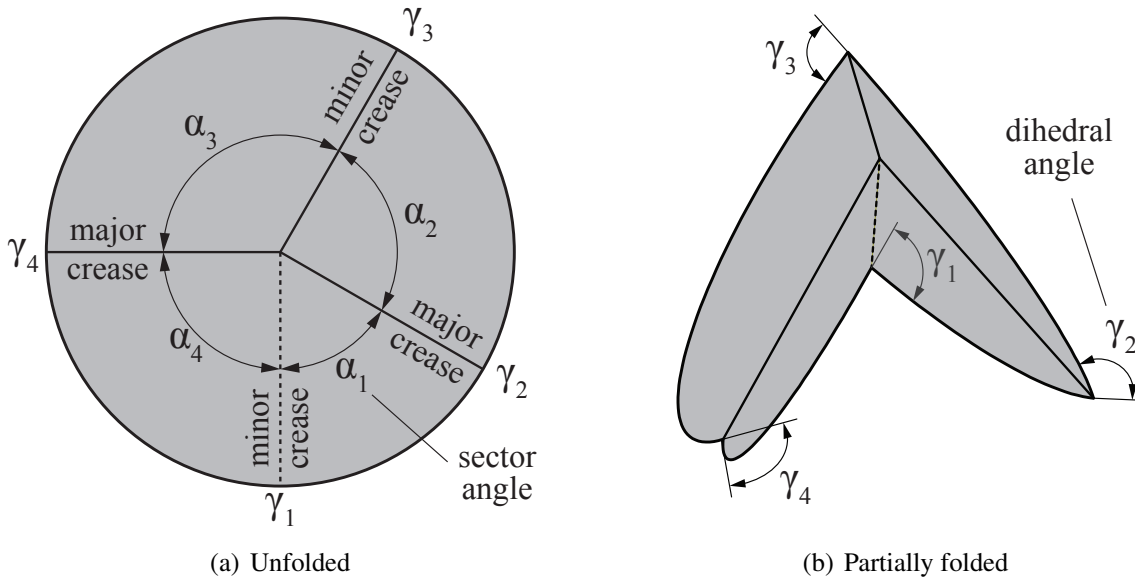


Figure 4.1: A Degree-4 origami vertex in its (a) unfolded and (b) partially folded states.

4.2.1 Flat-Foldability in Degree-4 Vertices

A flat-foldable vertex begins in an initial flat position and can be folded to achieve a secondary flat position. All dihedral angles are equal to $\pm\pi$ in the secondary flat position of a degree-4 vertex. Likewise, an origami pattern composed entirely of degree-4 vertices is considered flat foldable if there exists a configuration where all dihedral angles in the pattern are equal to $\pm\pi$. The conditions for flat-foldability are well known (see, e.g., [29]); for degree-4 vertices, they are as follows:

- There exist three folds of one parity and one fold of the other;
- The smallest-angled sector, if unique, is incident to folds of opposite parity (“anto”);
- The largest-angled sector, if unique, is incident to folds of the same parity (“iso”).
- Opposite sector angles sum to π ;

If there exist two equally valued smallest angled sectors, at least one of these sectors must be anto and its opposite sector must be iso. We call the two opposite creases with opposite parity the *minor* creases and the two opposite creases with equal parity the *major* creases.

These conditions give us the following relationship between sector angles in a degree-4 vertex [34]:

$$\alpha_1 + \alpha_3 = \alpha_2 + \alpha_4 = \pi. \quad (4.1)$$

These are necessary conditions, not sufficient; an origami pattern composed entirely from flat-foldable vertices may self-intersect before the final flat state. Such a pattern is considered non-flat-foldable. Also, any origami tessellation containing one or more non-flat-foldable vertices cannot be flat-foldable.

4.2.2 Fold-Angle Multipliers

We will use fold-angle multipliers to evaluate tessellations. Fold-angle multipliers, as defined in [38], define the ratio between the half-angle tangents of adjacent dihedral angles in an origami vertex. This ratio is constant in any flat-foldable degree-4 origami vertex throughout the entire motion of the vertex [6]. The fold-angle multiplier, μ_i , for the i^{th} sector is defined as follows:

$$\mu_i \equiv \frac{\tan\left(\frac{1}{2}\gamma_{i+1}\right)}{\tan\left(\frac{1}{2}\gamma_i\right)} \quad (4.2)$$

The multipliers for each sector in a vertex may be evaluated as follows:

$$\mu_1 \equiv \frac{\tan\left(\frac{1}{2}\gamma_2\right)}{\tan\left(\frac{1}{2}\gamma_1\right)} = \frac{\sin\left(\frac{1}{2}(\alpha_1 + \alpha_2)\right)}{\sin\left(\frac{1}{2}(\alpha_1 - \alpha_2)\right)} \quad (4.3)$$

$$\mu_2 \equiv \frac{\tan\left(\frac{1}{2}\gamma_3\right)}{\tan\left(\frac{1}{2}\gamma_2\right)} = -\frac{1}{\mu_1} = -\frac{\cos\left(\frac{1}{2}(\alpha_2 + \alpha_3)\right)}{\cos\left(\frac{1}{2}(\alpha_2 - \alpha_3)\right)} \quad (4.4)$$

$$\mu_3 \equiv \frac{\tan\left(\frac{1}{2}\gamma_4\right)}{\tan\left(\frac{1}{2}\gamma_3\right)} = -\mu_1 = \frac{\sin\left(\frac{1}{2}(\alpha_3 + \alpha_4)\right)}{\sin\left(\frac{1}{2}(\alpha_3 - \alpha_4)\right)} \quad (4.5)$$

$$\mu_4 \equiv \frac{\tan\left(\frac{1}{2}\gamma_1\right)}{\tan\left(\frac{1}{2}\gamma_4\right)} = \frac{1}{\mu_1} = -\frac{\cos\left(\frac{1}{2}(\alpha_4 + \alpha_1)\right)}{\cos\left(\frac{1}{2}(\alpha_4 - \alpha_1)\right)} \quad (4.6)$$

There is a special case to note: when the major crease fold lines are collinear ($\alpha_2 + \alpha_3 = \pi$), zero and infinite fold-angle multipliers are obtained. This occurs because the major crease lines must be completely folded before the minor crease lines begin folding. Because such vertices have more than one degree of freedom, they are not considered in this chapter.

4.2.3 Rigidly Foldable Polygons

A polygon in an origami tessellation is rigidly foldable only if the product of all fold-angle multipliers in the polygon is equal to one [38]. Therefore, an n -degree polygon with interior angles 1 through n is rigidly foldable if the following equation is satisfied:

$$\prod_{i=1}^n \mu_i = 1 \quad (4.7)$$

This provides a method for determining if a polygon is rigidly foldable. First, fold-angle multipliers must be evaluated for each vertex. Then all fold-angle multipliers associated with a polygon must be multiplied to determine if Equation (4.7) is satisfied.

4.2.4 Rigidly Foldable Origami Tessellations

An origami tessellation may contain many polygons. A tessellation can be rigidly foldable only if each of these polygons is rigidly foldable. However, an origami tessellation containing only rigidly foldable polygons may only be rigidly foldable over a restricted range because of global self-intersection (tessellations with inner portions cut out may not be rigidly foldable at all). In this chapter we first evaluate existing tessellation to identify those that are rigidly foldable. We then present gadgets that facilitate the creation of rigidly foldable tessellations and show some resulting tessellations.

4.3 Known Rigidly Foldable Tessellations

There are several origami tessellations which have been known to be rigidly foldable. Figure 4.2 shows an organisation of rigidly foldable periodic tessellations. This chart does not represent a chronology of the development of these tessellations but rather a way to see how they are related. These tessellations are described in the following sections.

4.3.1 Huffman Grid

The first tessellation we consider was presented by David Huffman [4], which we call the Huffman grid. This basic tessellation involves only a single degree-4 vertex that is rotated and

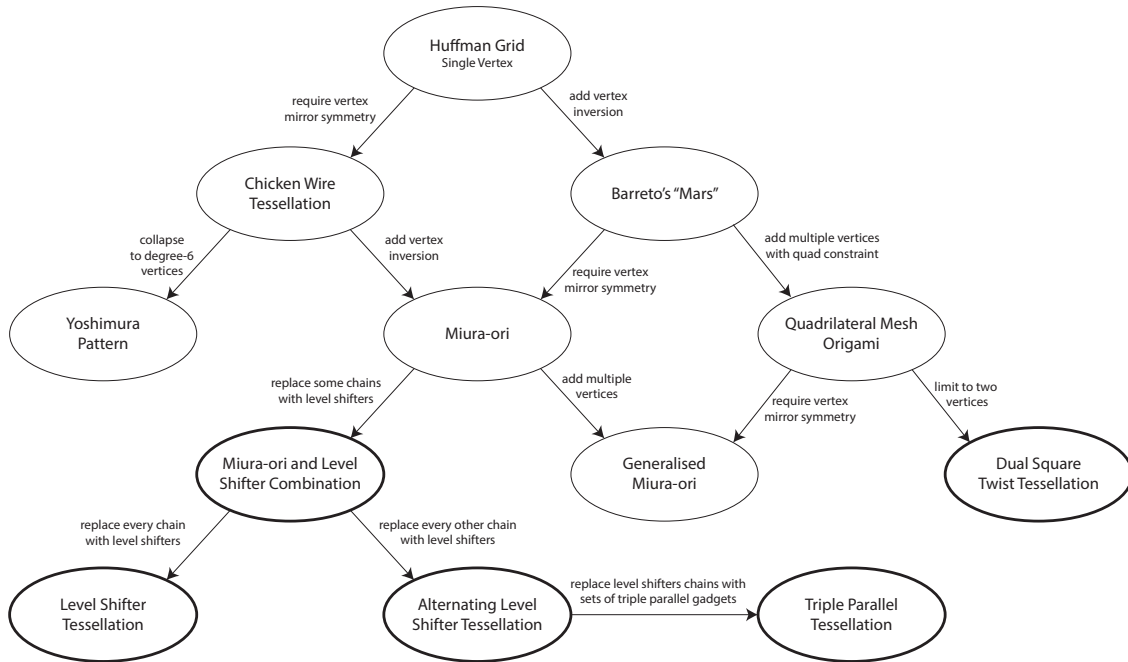
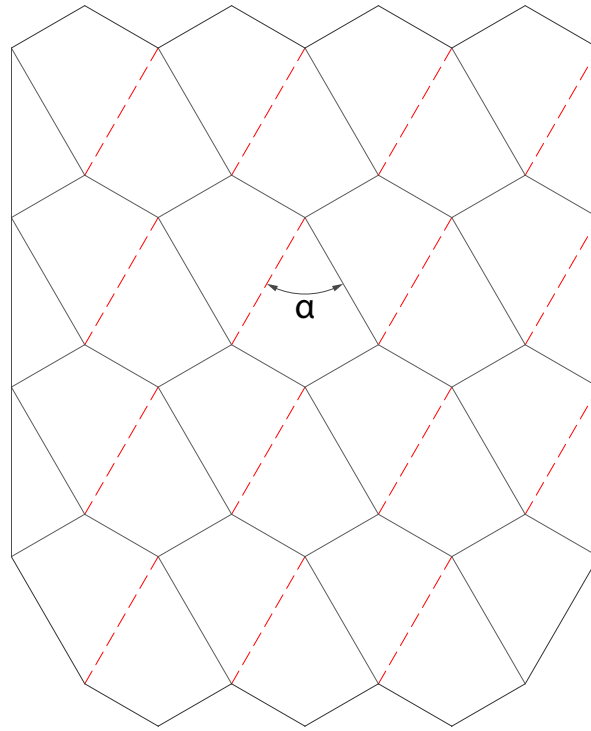


Figure 4.2: Rigidly foldable tessellations. New tessellations are shown with a bold outline.

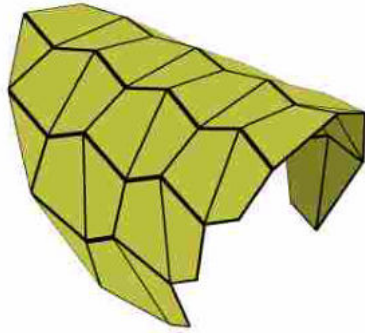
repeated continuously through the tessellation as shown in Figure 4.3(a). Two of the sector angles are equal to $\pi/2$ and the other two are equal α and $\pi - \alpha$. The tessellation is locally rigidly foldable for any $\alpha \neq \pi/2$. However, as seen in Figure 4.3(c), this tessellations folds into a cylindrical form and global self-intersection occurs before it reaches the final flat state.

Equations (4.3 - 4.6) show that opposite dihedral angles in a degree-4 vertex are equal in magnitude. This characteristic is useful in determining how many unique dihedral angles a tessellation contains. In this chapter we define all fold angles with equal magnitude to share one unique dihedral angle. At any position during deployment, this pattern contains fold angles of only two magnitudes; all fold lines with a positive slope in Figure 4.3(a) have equal fold angle magnitude, as do all crease lines with a negative slope. As a result, this tessellation contains two unique dihedral angles.

We will use this tessellation to provide an example for the calculation of fold-angle multipliers and the evaluation of rigidly foldable polygons. Figure 4.4 shows a single vertex in the Huffman grid. Figure 4.4(a) shows the sector angles of this vertex and labels the dihedral angles γ_1 through γ_4 . The fold-angle multipliers associated with this vertex may be calculated using



(a) Fold pattern



(b) Partially folded position



(c) Pre-interference position

Figure 4.3: Huffman grid

Equations (4.3 - 4.6). For example, using Equation (4.3)

$$\mu_1 = \frac{\sin\left(\frac{1}{2}\left(\frac{\pi}{3} + \frac{\pi}{2}\right)\right)}{\sin\left(\frac{1}{2}\left(\frac{\pi}{3} - \frac{\pi}{2}\right)\right)} = -3.73 \quad (4.8)$$

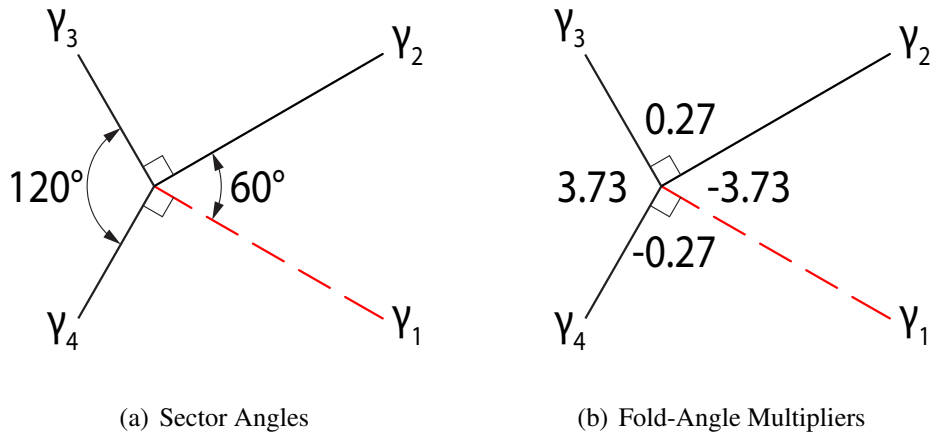


Figure 4.4: Single vertex of the Huffman grid. (a) labels the sector angles and (b) gives the fold-angle multipliers associated with the sectors

The other fold-angle multipliers are then calculated using Equations (4.4 - 4.6). The results are shown in Figure 4.4(b). For any polygon, this procedure is repeated for all vertices of the polygon. Because the Huffman grid includes only one unique vertex, further calculations are not necessary.

Figure 4.5 shows a single polygon of the tessellation with its associated fold-angle multipliers. This polygon is rigidly foldable because the product of all multipliers in the polygon is equal to 1. For any tessellation, this process is repeated for all unique enclosed polygons. Because the Huffman grid contains only one unique polygon, further calculations are not necessary and we conclude that it is locally rigidly foldable. Note that global rigid foldability is not ensured because of possible self-intersection.

4.3.2 Chicken Wire Tessellation

The chicken wire tessellation (also known as the hexagonal pattern [39]) is constructed using a single vertex with mirror symmetry, as shown in Figure 4.6. This tessellation is rigidly foldable for $\alpha < \pi/2$ although it folds into a cylindrical form and global self-intersection occurs before a second flat position is obtained, as is seen in Figure 4.6(c). This tessellation contains two unique dihedral angles; all valley creases have the same fold angle, as do all mountain creases.

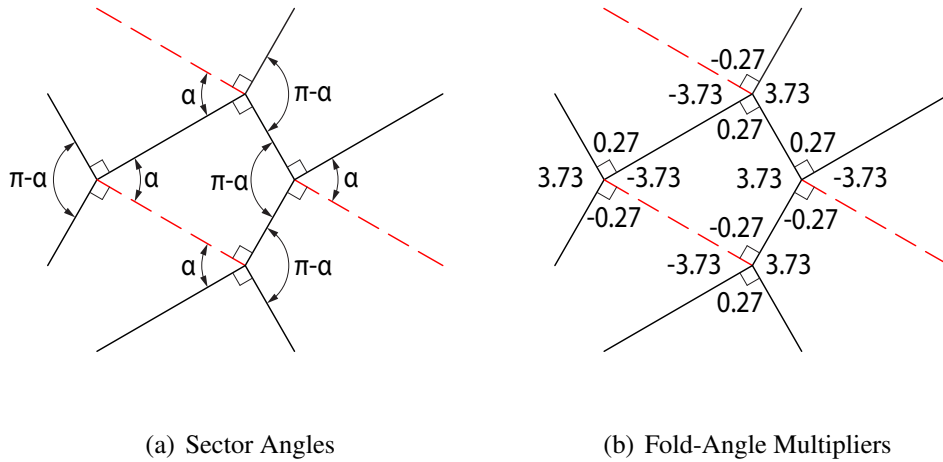


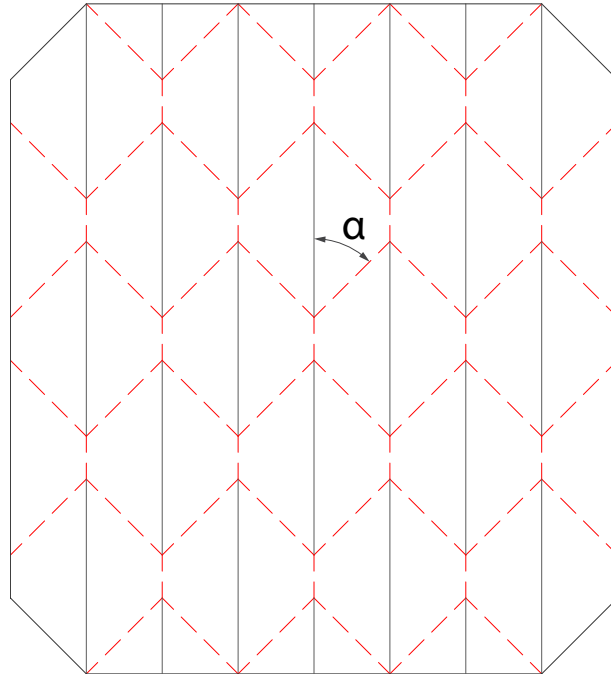
Figure 4.5: Single polygon of the Huffman grid. (a) labels the sector angles and (b) gives the fold-angle multipliers associated with the sectors. This polygon is rigidly foldable because $3.73 * -0.27 * -3.73 * 0.27 = 1$.

4.3.3 Barreto’s “Mars”

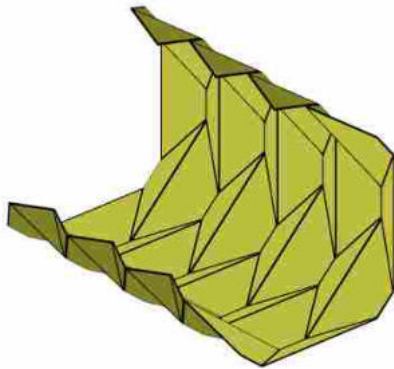
Paulo Barreto presented a tessellation, “Mars”, which included a single degree-4 vertex and its inversion [40] as shown in Figure 4.7. The vertex and its inversion are mirrored, rotated, and repeated continuously through the tessellation. This tessellation includes square twists and parallelogram twists with configurations proved in [38] to be rigidly foldable. It is rigidly foldable for $\alpha < \pi/2$. The pattern stays in a planar form, as shown in Figures 4.7(b) and 4.7(c), and is able to reach its final flat state without self-intersection. This tessellation contains two unique dihedral angles; all vertical moving chains are equal in fold angle magnitude, as are all horizontal chains.

4.3.4 Miura-ori

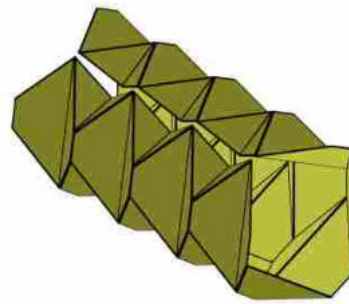
The Miura-ori is an origami tessellation developed by Koryo Miura [1] that is comprised entirely from parallelograms. The tessellation is created by patterning a single degree-4 vertex and its inversion with a constraint of mirror symmetry of the vertex. As such, it is the result of a combination of the constraints on the chicken wire tessellation and Barreto’s “Mars” tessellation. This tessellation is rigidly foldable for any $\alpha < \pi/2$. Figure 4.8(a) shows the fold pattern for the Miura-ori. The pattern stays in a planar form as shown in Figures 4.8(b) and 4.8(c) and thus is able



(a) Fold pattern



(b) Partially folded position



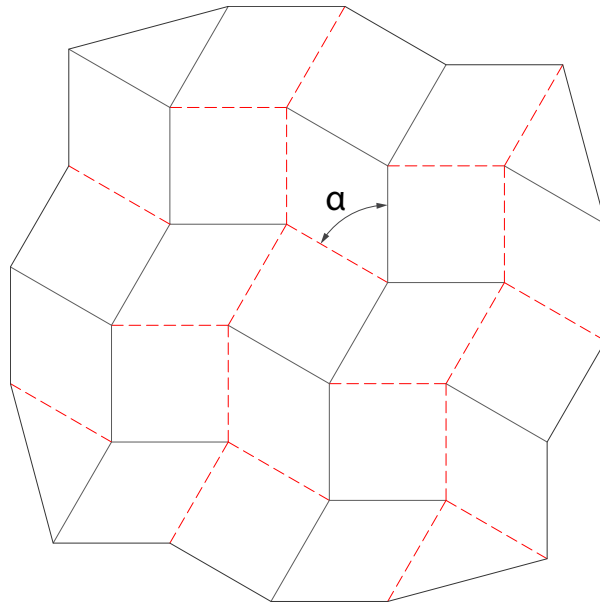
(c) Pre-interference position

Figure 4.6: Chicken wire tessellation

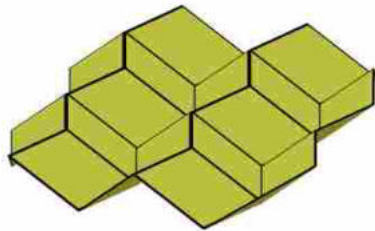
to reach its final flat state without self-intersection. The Miura-ori has two unique dihedral angles; all vertical creases are equal in angle, as are all other creases.

4.3.5 Yoshimura Pattern

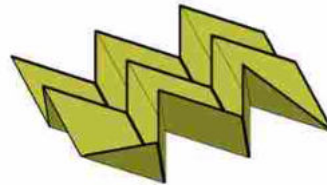
Yoshimura developed an origami pattern [41] based on the observed behaviour of thin cylinders under an axial buckling load. This pattern (also referred to as the diamond pattern [42])



(a) Fold pattern



(b) Partially folded position

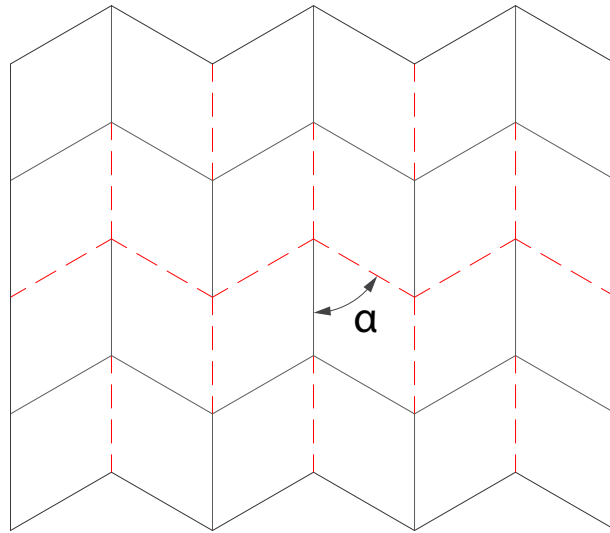


(c) Mostly folded position

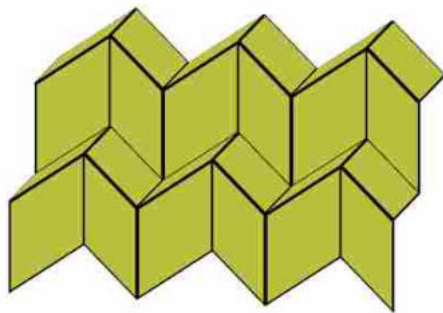
Figure 4.7: Barreto's "Mars"

is constructed by repeating a single degree-6 vertex with mirror symmetry. Unlike previously considered tessellations, this pattern has more than one degree of freedom due to the three degrees of freedom in the degree-6 vertices. Figure 4.9(a) shows the fold lines for the Yoshimura pattern. Figures 4.9(b) and 4.9(c) show one of the possible fold paths for this tessellation. Although the pattern is locally rigidly foldable for $\alpha < \pi/2$, except under specific circumstances, global self-intersection occurs before the second flat state can be reached with this fold path.

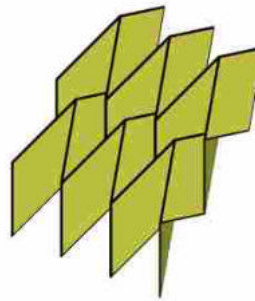
As is noted in Figure 4.2, the Yoshimura pattern may be obtained by collapsing the chicken wire tessellation into degree-6 vertices. Because this tessellation has more than one degree of



(a) Fold pattern



(b) Partially folded position



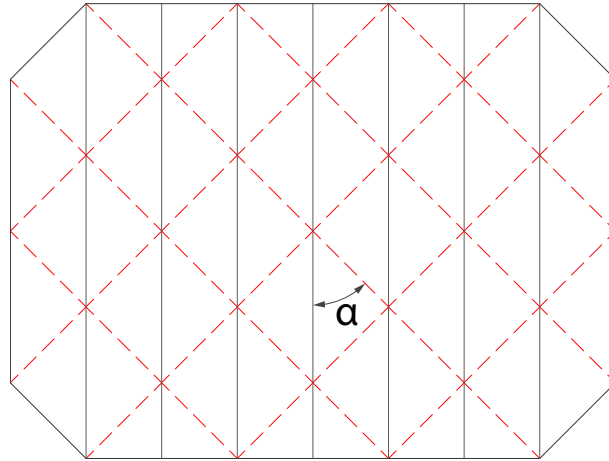
(c) Mostly folded position

Figure 4.8: Miura-ori

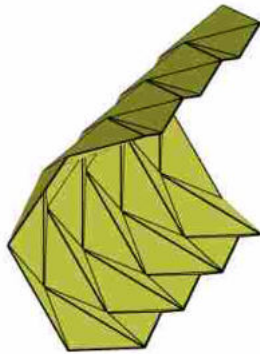
freedom, the number of unique dihedral angles is not constant. However, in the positions shown in Figure 4.9, there are two unique fold angles; all valley creases have the same fold angle, as do all mountain creases.

4.3.6 Generalised Quadrilateral Mesh Origami

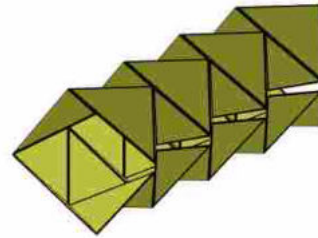
Tachi analysed quadrilateral mesh origami and presented conditions for rigid foldability [6]. As the name implies, this origami consists entirely of quadrilateral panels joined by creases meeting in degree-4 vertices. Quadrilateral mesh origami can also be evaluated using the method presented in [38], and may be rigidly foldable under the condition that Equations (4.1) and (4.7) are



(a) Fold pattern



(b) Partially folded position



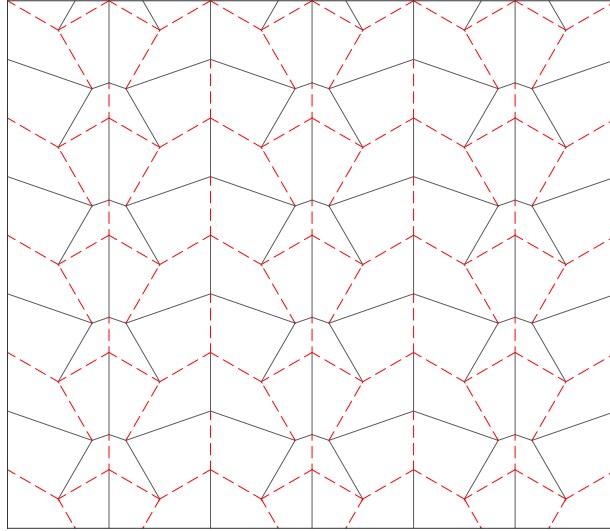
(c) Mostly folded position

Figure 4.9: Yoshimura pattern

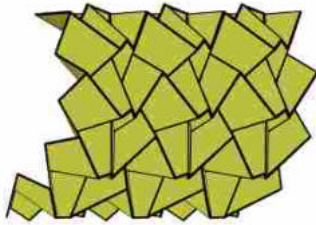
satisfied for all vertices and polygons, respectively. Unlike the previously mentioned tessellations, this mesh does not need to include the repetition of a single, flat-foldable vertex, but may contain multiple vertices. Figure 4.10 shows one of the many possible rigidly foldable quadrilateral mesh patterns. Generalised quadrilateral mesh patterns may have any number of unique dihedral angles.

4.3.7 Generalised Miura-ori

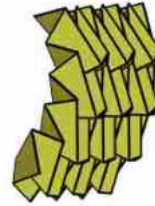
By requiring a quadrilateral mesh origami to contain vertices with mirror symmetry, the generalised Miura-ori is obtained (see Figure 4.11). The generalised Miura-ori differs from the Miura-ori in that it allows for multiple vertices. It can therefore be thought of as stemming from both the Miura-ori and the generalised quadrilateral mesh origami, as shown in Figure 4.2. The



(a) Fold pattern



(b) Partially folded position



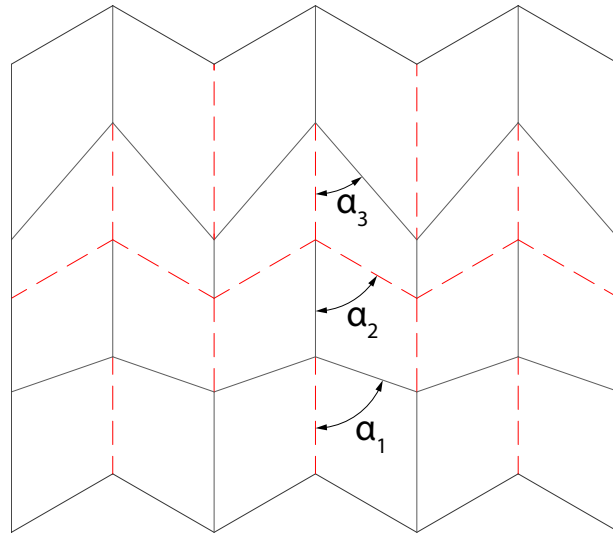
(c) Mostly folded position

Figure 4.10: Quadrilateral meshed pattern

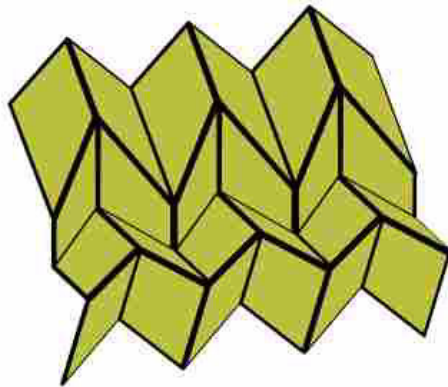
generalised Miura-ori is globally rigidly foldable for all $\alpha_i < \pi/2$. The generalised Miura-ori may have many unique dihedral angles. All vertical creases have the same fold angle while all chains of intersecting creases have another unique fold angle. (Chains with equal values of α have equal fold angles.)

4.4 Gadgets

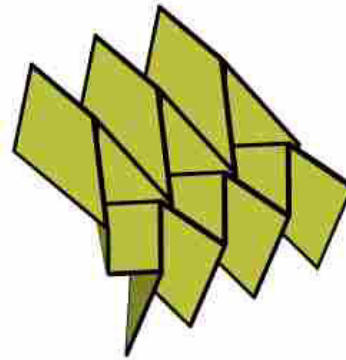
Author Lang defined an origami *gadget* as a localised section of crease pattern that can replace an existing patch to add functionality or otherwise modify the pattern [43]. As a gadget replaces a single vertex or multiple vertices it does not necessarily preserve the rest of the pattern, but may make manageable changes to surrounding creases. However, any rigidly foldable gadget



(a) Fold pattern



(b) Partially folded position



(c) Mostly folded position

Figure 4.11: Generalised Miura-ori pattern

which exactly replaces an existing rigidly foldable patch (all boundaries are equivalent) will not modify the motion of the pattern.

The average polygon degree in a repeatable tessellation containing only degree-4 vertices must be equal to 4 (see Appendix B). As a result, any tessellation constructed using only degree-4 vertices and featuring polygons of more than fourth degree must also contain triangles. Because of this, of particular interest are gadgets which include triangles and allow for the use of $n > 4$ polygons in rigidly foldable tessellations.

4.4.1 Corner Gadget

A flat-foldable degree-4 vertex may be modified to create a rigidly foldable network of four degree-4 vertices with four outwardly extending creases in the same location as the original creases as shown in Figure 4.12. The fold-angle multipliers between these four creases remain the same as in the original vertex, therefore, the overall motion remains the same. As such, this gadget follows the conventional definition of a gadget. This gadget is the result if a vertex is depressed into a second rigidly foldable form. The depression can be repeated as many times as is desired as shown in Figure 4.13. The value of β changes the size and shape of the depression, but does not change the fold-angle multipliers between any of the exterior creases. It is required that $\beta > \alpha_1$. Replacing a vertex with a corner gadget adds one unique dihedral angle to the tessellation. (The folds along the boundaries of the quadrilateral in the corner gadget are all of equal fold angle.)

Symmetric Corner Gadget

A special case of the corner gadget is one where the minor crease lines of the original vertex are collinear. As a result, the gadget created is symmetric about this crease line as seen in Figure 4.14. As with the general corner gadget, the fold-angle multipliers between the exterior creases remain the same as in the original vertex, regardless of the value of β . As with the original, it is also required that $\beta > \alpha$.

4.4.2 Triple Parallel Gadget

Any flat-foldable degree-4 origami vertex which does not contain two collinear crease lines and does not contain 90° sector angles may be modified to become a network of four vertices enclosing two isosceles triangles. This network contains six outwardly extending creases, three of which are parallel to one of the original minor creases and the other three are each coincident to each of the other three original creases (see Figure 4.15). The fold-angle multipliers between the three non-parallel creases remain the same as in the original vertex. The two non-adjacent parallel creases have dihedral angles equal in magnitude but opposite in sign. Replacing a vertex with a triple parallel gadget adds one unique dihedral angle. The middle parallel crease has a dihedral

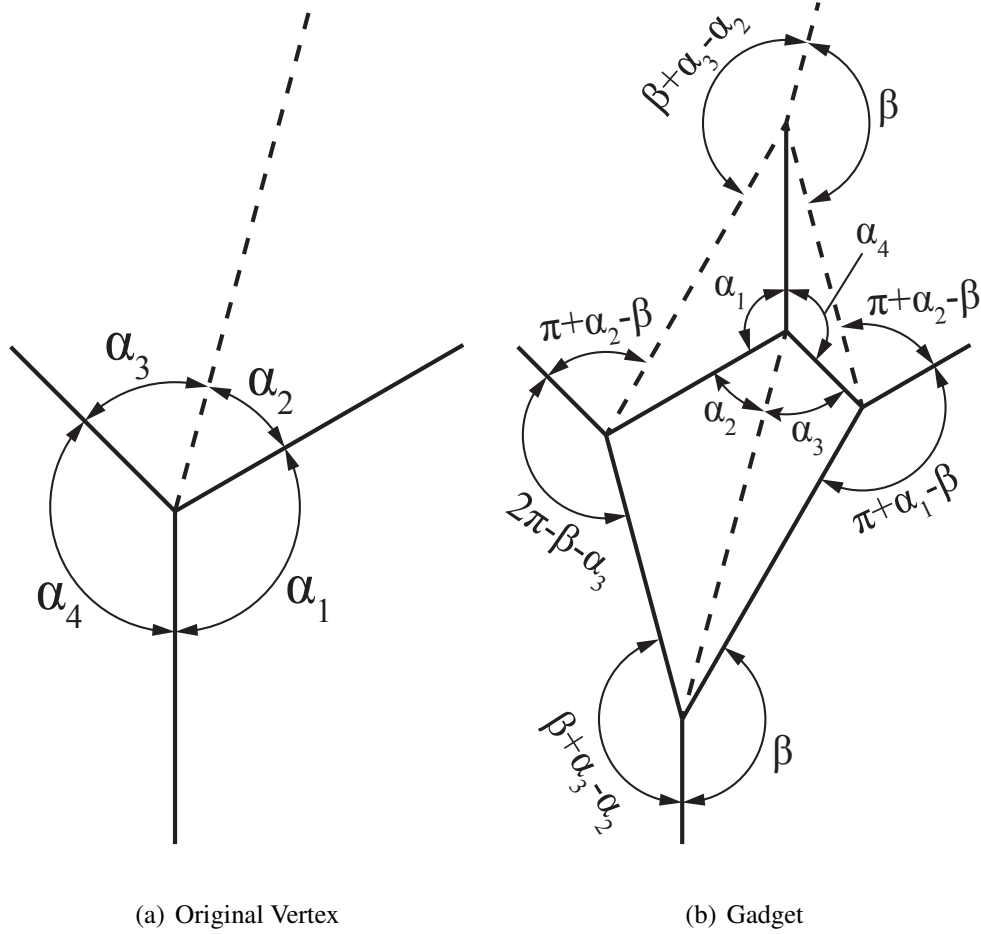


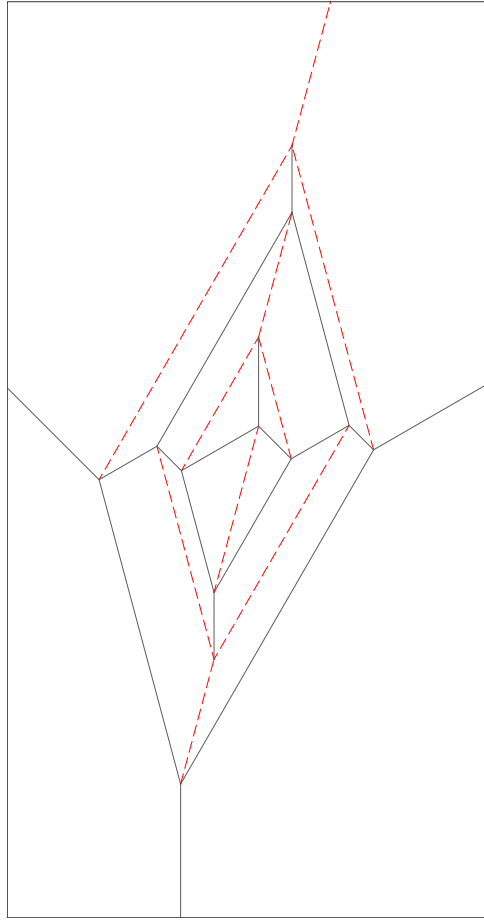
Figure 4.12: Corner gadget. This gadget is rigidly foldable for $\frac{\pi}{2} < \alpha_1 < \beta < \pi$. The value of β does not have any effect on the fold-angle multipliers between exterior creases.

angle equal to the original crease while the outer parallel creases are equal in magnitude to each other.

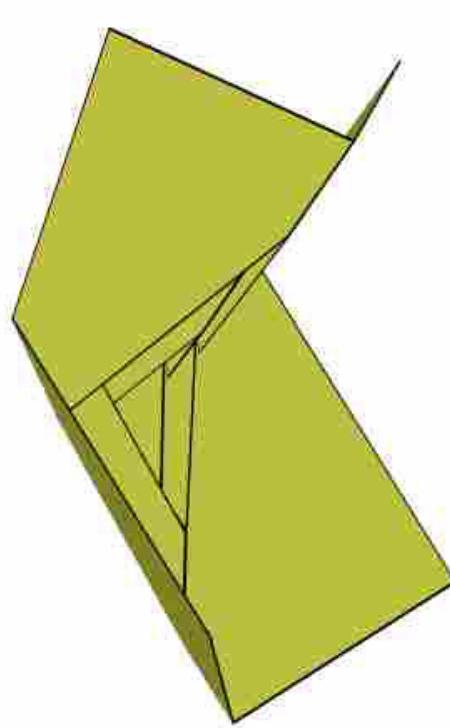
Labeling the opposite crease as crease number one and numbering counter-clockwise (see Figure 4.15), the multipliers are as follows:

$$\mu_1 \equiv \frac{\tan\left(\frac{1}{2}\gamma_2\right)}{\tan\left(\frac{1}{2}\gamma_1\right)} = -\frac{\cos\left(\frac{1}{2}(\alpha - \beta)\right)}{\cos\left(\frac{1}{2}(\alpha + \beta)\right)} \quad (4.9)$$

$$\mu_2 \equiv \frac{\tan\left(\frac{1}{2}\gamma_3\right)}{\tan\left(\frac{1}{2}\gamma_2\right)} = -\frac{\sin\left(\frac{1}{2}(\alpha - \beta)\right)}{\sin\left(\frac{1}{2}(\alpha + \beta)\right)} \quad (4.10)$$



(a) Fold Pattern



(b) Partially-folded state

Figure 4.13: Recursive corner gadget. Note that each successive interior vertex is a rotation of the previous interior vertex by 180°

$$\mu_3 \equiv \frac{\tan\left(\frac{1}{2}\gamma_4\right)}{\tan\left(\frac{1}{2}\gamma_3\right)} = -\frac{\sin(\alpha + \beta)}{\sin(\alpha - \beta)} \quad (4.11)$$

$$\mu_4 \equiv \frac{\tan\left(\frac{1}{2}\gamma_5\right)}{\tan\left(\frac{1}{2}\gamma_4\right)} = \frac{\sin(\alpha - \beta)}{\sin(\alpha + \beta)} \quad (4.12)$$

$$\mu_5 \equiv \frac{\tan\left(\frac{1}{2}\gamma_6\right)}{\tan\left(\frac{1}{2}\gamma_5\right)} = \frac{\sin\left(\frac{1}{2}(\alpha + \beta)\right)}{\sin\left(\frac{1}{2}(\alpha - \beta)\right)} \quad (4.13)$$

$$\mu_6 \equiv \frac{\tan\left(\frac{1}{2}\gamma_1\right)}{\tan\left(\frac{1}{2}\gamma_6\right)} = -\frac{\cos\left(\frac{1}{2}(\alpha + \beta)\right)}{\cos\left(\frac{1}{2}(\alpha - \beta)\right)} \quad (4.14)$$

Of particular interest is an arrangement where two of these gadgets are combined in such a way that the three parallel crease lines from one gadget meet the three parallel crease lines from

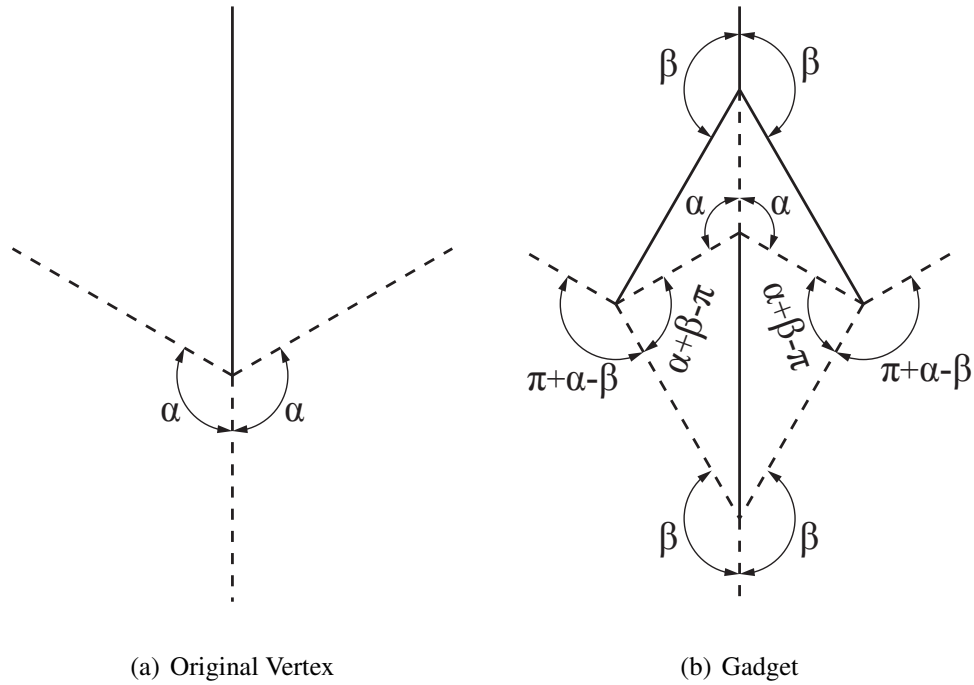


Figure 4.14: Symmetric corner gadget. This gadget is rigidly foldable for $\frac{\pi}{2} < \alpha < \beta < \pi$. The value of β does not have any effect on the fold-angle multipliers between exterior creases.

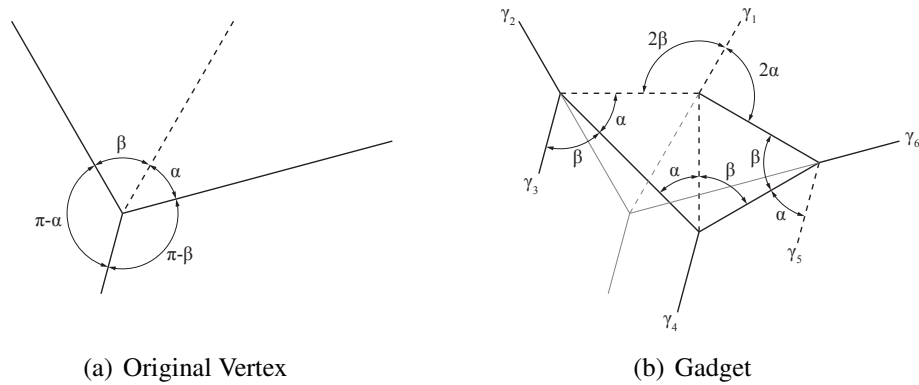


Figure 4.15: Triple parallel gadget. This gadget is rigidly foldable for $0 < \alpha, \beta < \pi/2$ and $\alpha \neq \beta$. The original vertex is superimposed with light weight on the gadget in (b).

another. We call this a set of triple parallel gadgets, shown in Figure 4.16(b). To form a set, the two gadgets must have equal values for α and β . A set of triple parallel gadgets may replace a combination of two vertices which are mirror-symmetric, as shown in Figure 4.16. A set of these

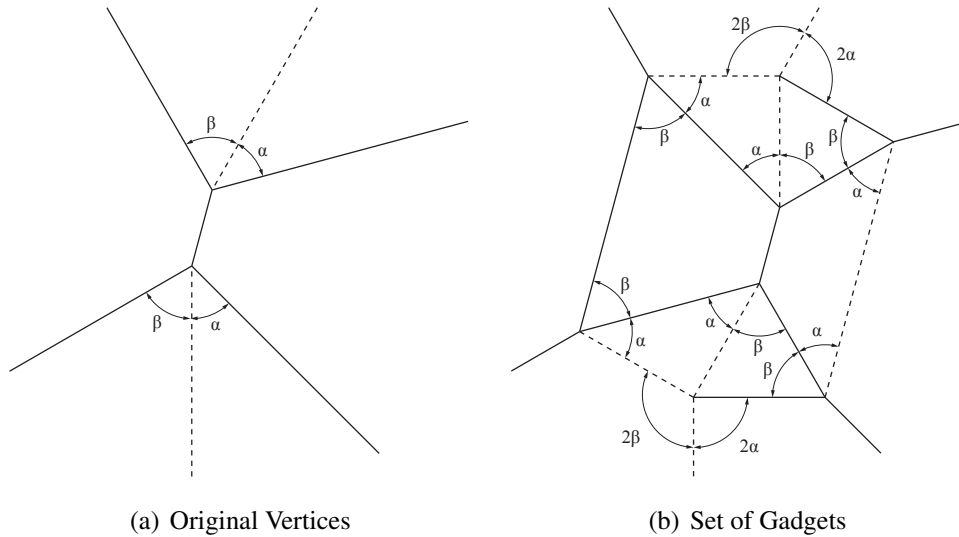


Figure 4.16: A set of triple parallel gadgets

gadgets adds a third dihedral angle to the set of vertices (Figure 4.16(a)) where this third angle is entirely contained in the set of gadgets.

4.4.3 Level Shifters

A level shifter is an origami gadget that has found use in formal origami design, and shows up often in origami in the form of a “spread sink” [43]. As its name suggests it is used to bring together two sections of an origami pattern which are at different levels. Level shifters allow for selective widening of origami patterns [43]. A level shifter in its most basic form is rigidly foldable. Figure 4.17 shows an asymmetric level shifter. Two independent input angles (α_1, α_2) fully define the gadget. The gadget is flat foldable, therefore, all other angles may be calculated by recalling that opposite sector angles in a vertex sum to π . A chain of level shifters has three unique fold angles. Two angles intertwine along the direction of the chain and a third angle passes through the horizontal creases.

Symmetric Level Shifter

A special case of the level shifter gadget occurs when $\alpha_1 = \alpha_2$. This creates a symmetric level shifter and we use α to designate the input angle. The dihedral angles for each of the hor-

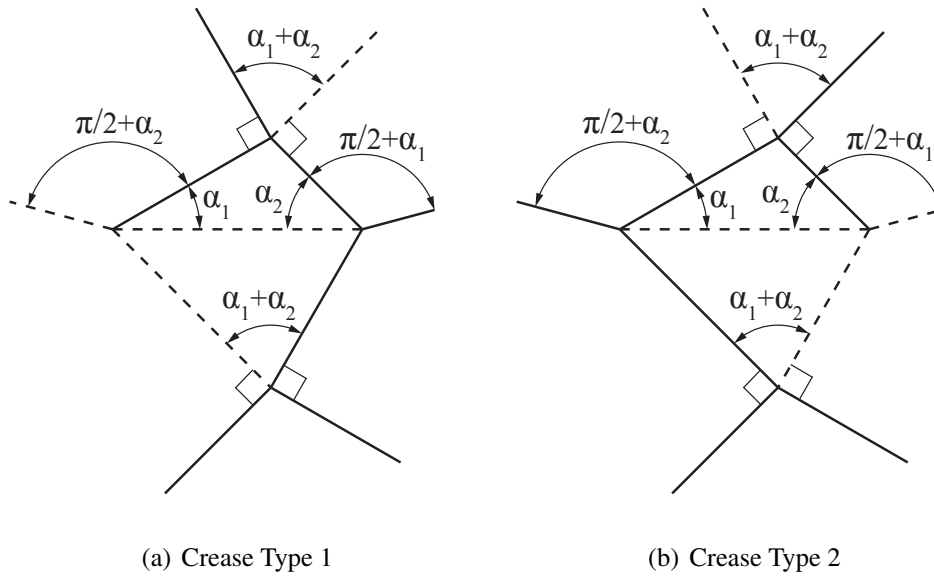


Figure 4.17: Asymmetric level shifter. This gadget is rigidly foldable for $0 < \alpha_1, \alpha_2 < \frac{\pi}{2}$ and $\alpha_1 + \alpha_2 \neq \frac{\pi}{2}$. (a) and (b) show the two possible crease assignments. The gadget may also be mirrored across itself and remain rigidly foldable. All vertices in this gadget are flat foldable (opposite sector angles sum to π).

horizontal crease lines in Figure 4.18(b) are equal. Therefore, this gadget may be useful in creating large tessellations which do not self-intersect.

4.5 Directly Modified Rigidly Foldable Patterns

In this section we explore modifications that can be made to existing rigidly foldable tessellations. These modifications use the gadgets presented previously to directly replace existing portions of the tessellations.

4.5.1 Miura-ori with Corner Gadget

By replacing the vertices of a Miura-ori tessellation with corner gadgets, the tessellation shown in Figure 4.19 is created. This tessellation has the same overall motion as the Miura-ori, however, the dimensions of the tessellation in its final, folded state are changed, as can be seen by comparing Figures 4.8(c) and 4.19(c). Also, when constructed using hinges with finite stiffness, this configuration is stiffer than the original Miura-ori.

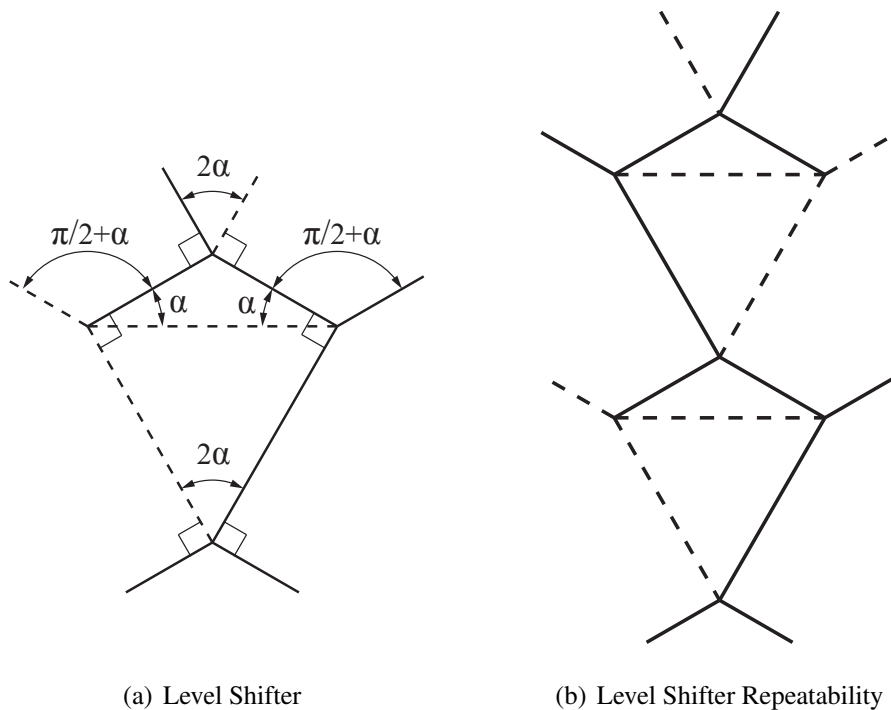


Figure 4.18: Symmetric level shifter. This gadget is rigidly foldable for $0 < \alpha < \frac{\pi}{2}$ and $\alpha \neq \frac{\pi}{4}$. This gadget may be repeated by mirroring itself and repeating as seen in (b).

4.5.2 Baretto’s “Mars” with Corner Gadget

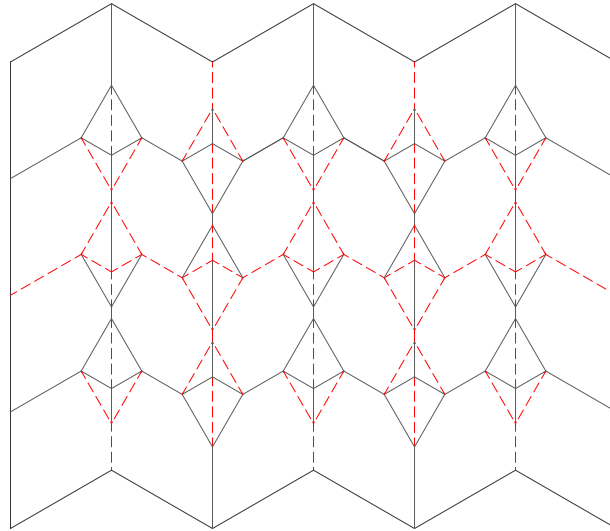
As with the Miura-ori, the “Mars” tessellation may be modified by replacing vertices with corner gadgets. Such a resulting tessellation is shown in Figure 4.20. This tessellation has the same motion as the “Mars”, however, like with the modified Miura-ori, the footprint of the final flat position is changed.

4.6 New Rigidly Foldable Patterns

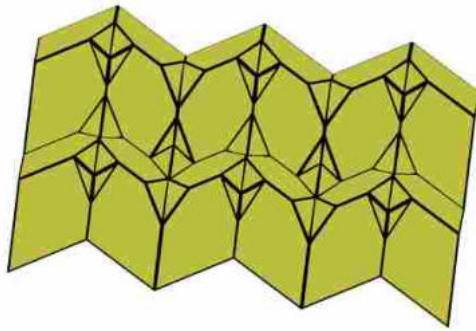
We present several new rigidly foldable patterns in this section. Many of these patterns were constructed using the previously mentioned gadgets.

4.6.1 Dual Square Twist Tessellation

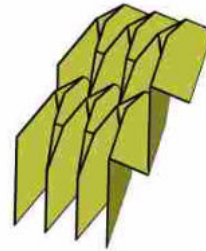
A special case of a generalised quadrilateral mesh origami occurs when only two different vertices are used. These vertices, along with their inversions are used to create the tessellation



(a) Fold pattern



(b) Partially folded position



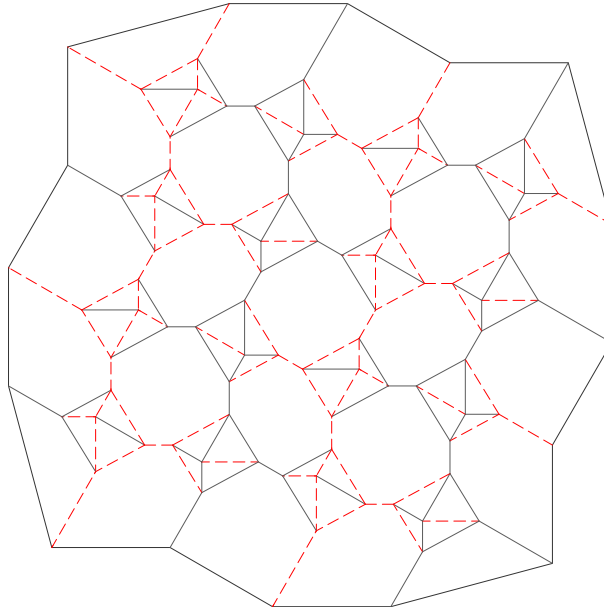
(c) Mostly folded position

Figure 4.19: Miura-ori pattern with corner gadgets

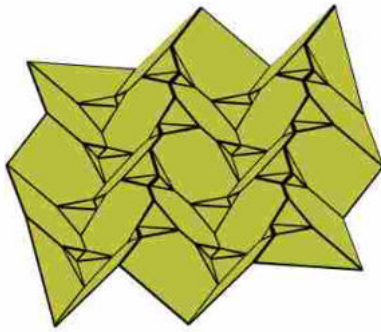
shown in see Figure 4.21. This tessellation contains many repetitions of square twists with two twist angles. It is rigidly foldable for $0 < \alpha \leq \beta < 90^\circ$. Note that the case where $\alpha = \beta$ results in the “Mars” tessellation. This tessellation contains four unique dihedral angles. Every other set of mostly vertical chains have equal fold angle magnitudes, as do every other set of mostly horizontal chains.

4.6.2 Alternating Level Shifter Tessellation

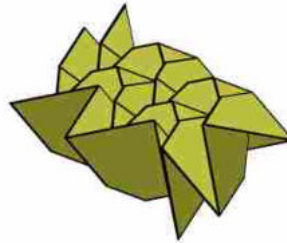
This tessellation is created by attaching chains of level shifters in opposite directions. The chains are arranged so that adjacent chains are in alternate directions and are connected using hexagons (see Figure 4.22). This tessellation is rigidly foldable for any rigidly foldable level



(a) Fold pattern



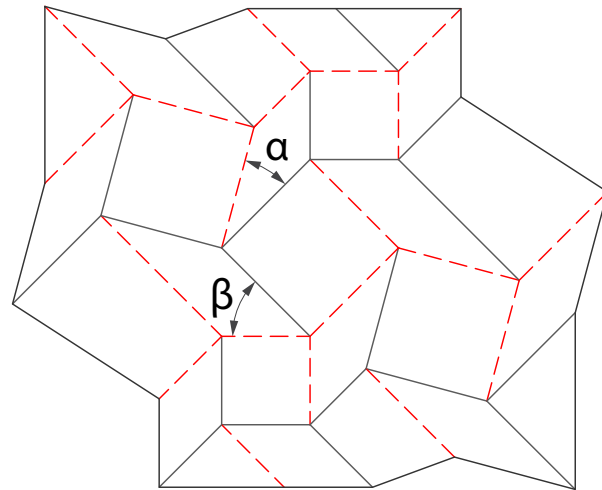
(b) Partially folded position



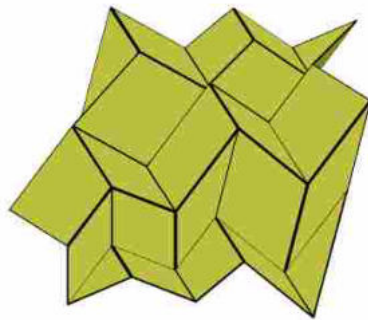
(c) Mostly folded position

Figure 4.20: Barreto's "Mars" with corner gadgets

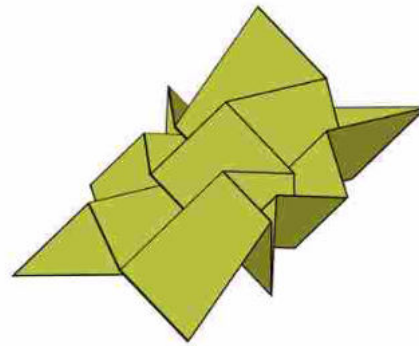
shifter. Figure 4.22 shows the simplest form of this tessellation, however, chains of different level shifters may also be joined together. As is shown in Figure 4.23, these chains will not be parallel. This tessellation contains two unique fold angles for each uniquely angled level shifter chain and another unique fold angle for all of the creases between chains.



(a) Fold pattern



(b) Partially folded position

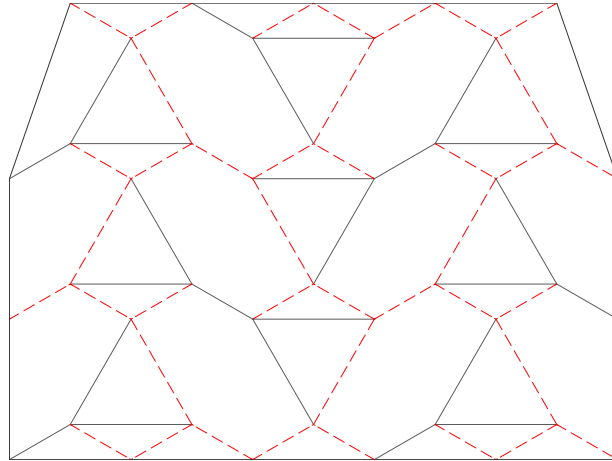


(c) Mostly folded position

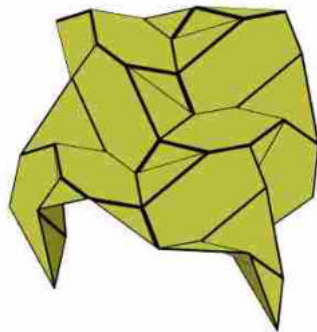
Figure 4.21: Dual square twist tessellation

4.6.3 Level Shifter Tessellation

This tessellation is created by attaching chains of level shifters in the same direction. These chains are attached using pentagons (see Figure 4.24). This tessellation is rigidly foldable for any rigidly foldable level shifter. As with the previously mentioned tessellation, this tessellation may also include chains of level shifters with different angles and still be rigidly foldable. However, in this case, each chain remains parallel while the crease lines separating the chains are no longer parallel (see Figure 4.25). This tessellation contains two unique fold angles for each uniquely angled level shifter chain, another and another unique fold angle for all of the creases between chains.



(a) Fold pattern



(b) Partially folded position



(c) Mostly folded position

Figure 4.22: Alternating level shifter tessellation

Also, each set of collinear folds may have its own unique dihedral angle or it may be equal to another set, depending on the orientation.

4.6.4 Miura-ori and Level Shifter Combination

Level shifter chains may be combined with Miura-ori patterns to construct new tessellations such as that shown in Figure 4.26. When this occurs, level shifter chains with mountain folds separating the triangles act as valley-like folds during the intermediate folding positions as shown in the centre in Figure 4.26(b). Likewise, level shifter chains with valley folds separating the triangles act as mountain-like folds during the intermediate positions as shown on the right and left in Figure 4.26(b). As the pattern approaches the final position, these level shifter chains become

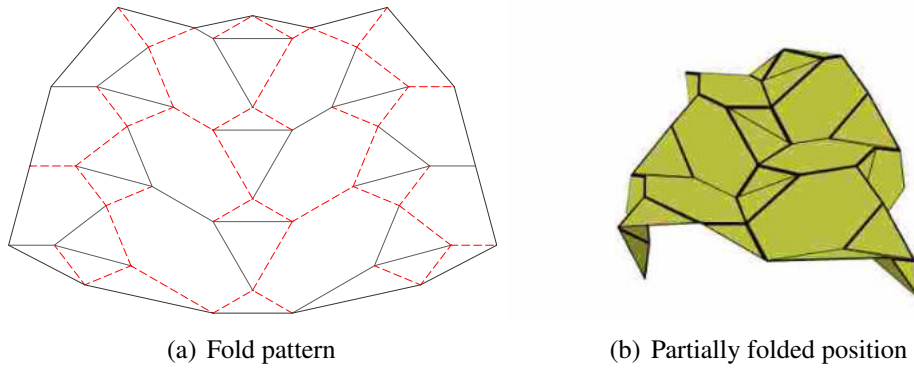


Figure 4.23: Non-parallel alternating level shifter tessellation

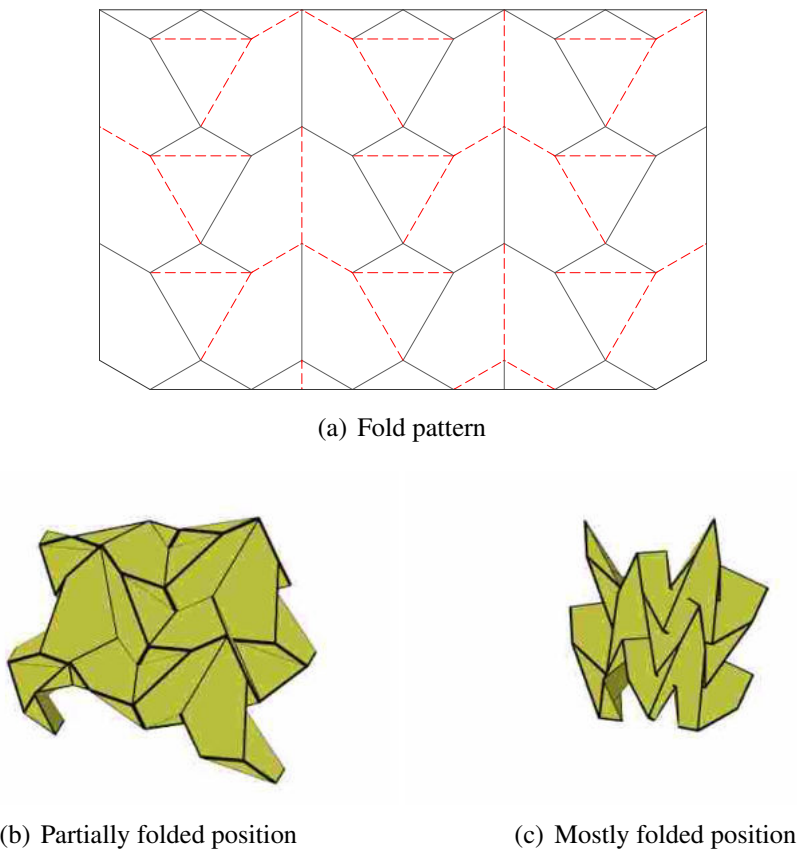


Figure 4.24: Level shifter tessellation

flat again as shown in Figure 4.26(c). The tessellation shows has four unique fold angles (two that intertwine on each level shifter chain, one for each collinear chain and a third for all connecting creases).

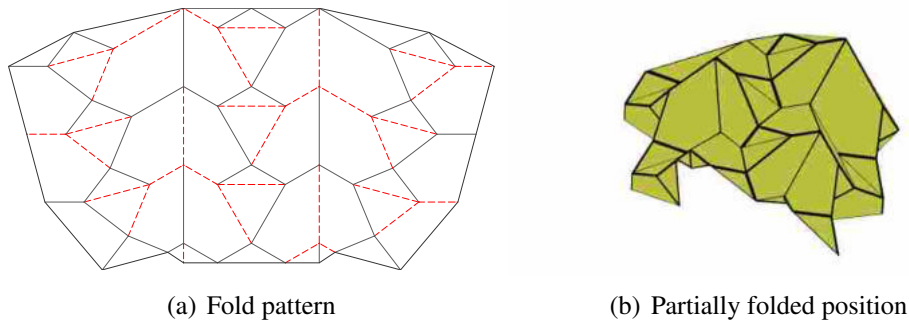


Figure 4.25: Non-parallel level shifter tessellation

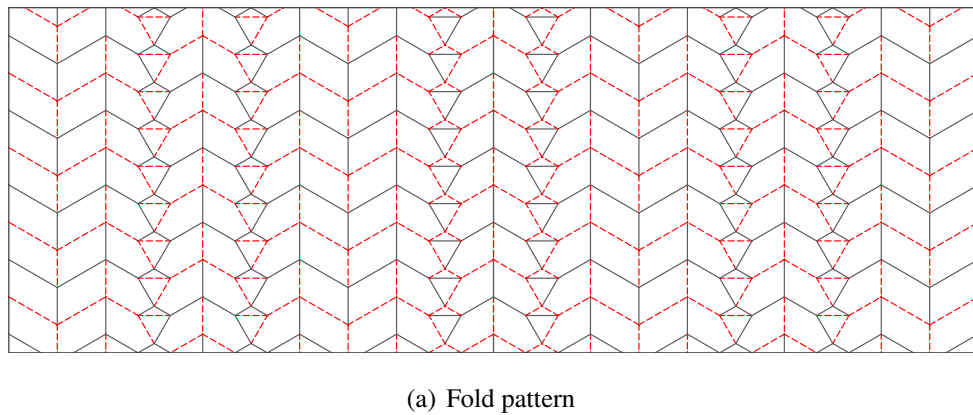
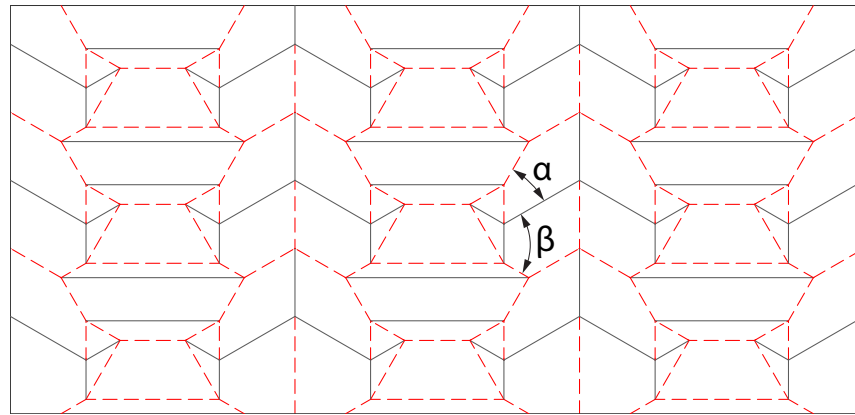


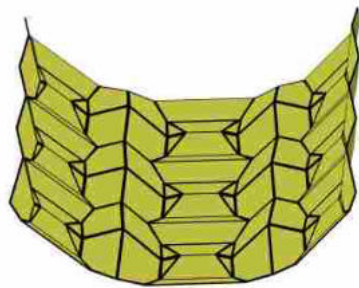
Figure 4.26: Combination of Miura-ori and level shifter patterns

4.6.5 Triple Parallel Tessellation

As with the level shifter gadget, the triple parallel gadget may also be used in many different combinations with the Miura-ori pattern. Figure 4.27(a) provides one example where alternating chains of the Miura-ori are replaced with chains of back-to-back level shifters. The gadgets are arranged so that the three parallel folds from each gadget meet the three parallel folds from another gadget. This tessellation is rigidly foldable under the same conditions that the gadgets are rigidly foldable. However, as is shown in Figure 4.27(c), global self-intersection occurs before the final



(a) Fold pattern



(b) Partially folded position



(c) Mostly folded position

Figure 4.27: Triple parallel tessellation

flat state. This tessellation includes three unique fold angles; the vertical crease chains are of equal angle, all folds stemming from these chains are of equal angle, and each set of triple parallel gadgets forms a third fold angle. (This third angle follows the rectangles formed by the set of triple parallel gadgets.)

4.7 Conclusion

This chapter has identified and categorized existing rigidly foldable origami tessellations. Using the method of fold-angle multipliers, several origami *gadgets* have been designed which may facilitate the modification of creation of rigidly foldable origami tessellations. New rigidly foldable origami tessellations involving these gadgets have been presented. These tessellations have final geometries that are more compact in one dimension than their counterparts. Because rigid foldability can be a critical feature for origami applications in materials other than paper,

the identification of rigidly foldable tessellations, introduction of rigidly foldable gadgets, and examples of how to create new tessellations by combining these concepts lays the foundation for future application.

CHAPTER 5. CONCLUSIONS AND RECOMMENDATIONS

5.1 Summary

This research focused on two types of origami with potential for applications in the design of deployable and foldable arrays of spatial mechanisms: the kaleidocycle and rigidly foldable origami. Chapter 2 analyzed the multistable behavior of compliant kaleidocycles. It was shown that kaleidocycles may be designed to have up to four positions of stable equilibrium and that these positions may be tuned to be sharply or neutrally stable.

Chapter 3 presented a new method, fold-angle multipliers, to evaluate rigid foldability. This method provides a way for determining if an origami pattern is rigid foldable without the requirement of solving systems of nonlinear equations. This method was used to evaluate origami twists and define seven theorems which govern the conditions for rigid foldability of these twists.

Chapter 4 used the fold-angle multiplier method to characterize and compare existing rigidly foldable tessellations and to create new origami “gadgets”. New tessellations were designed by modifying existing tessellations and using gadgets.

5.2 Conclusions

It has been shown that compliant kaleidocycles may be designed with one, two, three, or four positions of stable equilibrium, depending on the stiffness and orientation of the flexures. The degree of stability of stable positions may be designed to vary from sharp to neutrally stable. With the possibility of continuous revolution and multistable behavior, the kaleidocycle has the potential to increase the scope for compliant mechanisms in engineering applications.

Additionally, a method was described for evaluating the rigid foldability of origami tessellations. This method was applied to origami twists to discover what parameters allow an origami twist to be rigidly foldable. It was shown that there is no possible configuration for a rigidly fold-

able triangle twist. It was also shown that many possible rigidly foldable quadrilateral twists exist. A method for determining twist angles for a rigidly foldable regular polygon twist was presented and this method was used to calculate all possible twist angles for rigidly foldable regular polygons of degree eight or less.

Existing rigidly foldable origami tessellations were categorized and compared. Using the method of fold-angle multipliers, several origami *gadgets* were designed which may facilitate the modification of creation of rigidly foldable origami tessellations. Using the newly presented gadgets as tools, new rigidly foldable origami tessellations were designed. These tessellations have final geometries that are more compact in one dimension than their counterparts.

Because rigid foldability can be a critical feature for origami applications in materials other than paper, the evaluation of origami twists, identification of rigidly foldable tessellations, introduction of rigidly foldable gadgets, and examples of how to create new tessellations by combining these concepts lays the foundation for future application.

5.3 Recommendations

Although the relative motion of kaleidocycle links can be easily described by two angles, the 3D motion is much more complex. This complexity makes actuation and application difficult. For kaleidocycles to have new applications, a better understanding of the 3D motion of the links would be required.

This work presented an analysis of flat-foldable origami patterns composed of degree-4 vertices. However, non-flat-foldable patterns and vertices of higher degree were not considered. Because non-flat-foldable origami can achieve motion not possible with flat-foldable origami, analysis of these types of origami would increase the possibilities of origami-inspired designs.

Real material used in construction are not completely rigid. Although this work only considers rigidly foldable tessellations, it is possible that almost rigidly foldable tessellations may be used in the design of structures and mechanisms incorporating compliance in the members. A relationship between the product of fold-angle multipliers in a polygon and the strength-to-stiffness ratio required for the material could be explored.

REFERENCES

- [1] Miura, K., 1985. “Method of packaging and deployment of large membranes in space.” *Institute of Space and Astronautical Science*, **618**, pp. 1 – 9. 1, 19, 36, 44
- [2] Zirbel, S. A., Lang, R. J., Thomson, M. W., Sigel, D. A., Walkemeyer, P. E., Trease, B. P., Magleby, S. P., and Howell, L. L., 2013. “Accommodating thickness in origami-based deployable arrays.” *Journal of Mechanical Design*, **135**. 1, 19, 36
- [3] Francis, K. C., Blanch, J. E., Magleby, S. P., and Howell, L. L., 2013. “Origami-like creases in sheet materials for compliant mechanism design.” *Mechanical Sciences*, **4**, pp. 371 – 380. 1, 19, 36
- [4] Huffman, D. A., 1976. “Curvature and creases: A primer on paper.” *IEEE Transactions on Computers*, **C-25**, pp. 1010 – 1019. 1, 21, 36, 40
- [5] Wu, W., and You, Z., 2010. “Modeling rigid origami with quaternions and dual quaternions.” *Proceedings of the Royal Society*, **466**, pp. 2155 – 2174. 1, 3, 36
- [6] Tachi, T., 2009. “Generalization of rigid foldable quadrilateral mesh origami.” In *Proceedings of IASS Symposium*. 1, 3, 37, 39, 47
- [7] Tachi, T., 2010. “Freeform rigid-foldable structure using bidirectional flat-foldable planar quadrilateral mesh.” In *Advances in Architectural Geometry 2010*. Springer. 1, 21, 37
- [8] Howell, L. L., 2001. *Compliant Mechanisms*. John Wiley & Sons, Inc. 1, 2, 5
- [9] Zhao, X., Hu, Y., and Hagiwara, I., 2011. “Shape optimization to improve energy absorption ability of cylindrical thin-walled origami structure.” *Journal of Computational Science and Technology*, **5**(3), pp. 148–162. 1
- [10] Tolman, S. S., Delimont, I. L., Howell, L. L., and Fullwood, D. T., 2014. “Material selection for elastic energy absorption in origami-inspired compliant corrugations.” *Smart Materials and Structures*, **23**(9). 1
- [11] Kuribayashi, K., Tsuchiya, K., You, Z., Tomus, D., Umemoto, M., Ito, K., and Sasaki, M., 2006. “Self-deployable origami stent grafts as a biomedical application of ni-rich tni shape memory alloy foil.” *Materials Science and Engineering*, **A 419**, pp. 131 – 137. 1, 19, 36
- [12] Pickett, G. T., 2007. “Self-folding origami membranes.” *EPL*, **78**. 1, 19, 36
- [13] Lebee, A., and Sab, K., 2010. “Transverse shear stiffness of a chevron folded core used in sandwich construction.” *International Journal of Solids and Structures*, **47**, pp. 2620 – 2629. 1, 19, 36

- [14] Chen, Y., You, Z., and Tarnai, T., 2005. “Threefold-symmetric bricard linkages for deployable structures.” *International Journal of Solids and Structures*, **42**(8), pp. 2287 – 2301. 2, 8
- [15] Luo, Y., Yu, Y., and Liu, J., 2008. “A retractable structure based on bricard linkages and rotating rings of tetrahedra.” *International Journal of Solids and Structures*, **45**, pp. 620 – 630. 2, 5, 6
- [16] Demaine, E. D., 2000. “Folding and unfolding linkages, paper, and polyhedra.” In *Revised papers from the Japanese conference on discrete and computational geometry*. 5
- [17] Delimont, I. L., Magleby, S. P., and Howell, L. L., 2015. “Evaluating compliant hinge geometries for origami-inspired mechanisms.” *Journal of Mechanisms and Robotics*, **7**(1). 5
- [18] Norton, R. L., 2008. *Design of machinery: and introduction to the synthesis and analysis of mechanisms and machines.*, 4 ed. McGraw Hill. 5
- [19] Engel, M., 2003. M. C. Escher kaleidocycles http://www.kaleidocycle.de/pdf/kaleidocycle_theory.pdf. 7
- [20] Baker, J. E., 1980. “An analysis of the bricard linkages.” *Mechanism and Machine Theory*, **15**(4), pp. 267–286. 7
- [21] Song, C.-Y., Chen, Y., and Chen, I.-M., 2014. “Kinematic study of the original and revised general line-symmetric bricard 6r linkages.” *Journal of Mechanisms and Robotics*, **6**(3). 8
- [22] Gan, W. W., and Pellegrino, S., 2006. “Numerical approach to the kinematic analysis of deployable structures forming a closed loop.” *Proceedings of the Institution of Mechanical Engineers*, **220**(7). 8
- [23] Gao, W., Huo, K., Seehra, J. S., Ramani, K., and Cipra, R. J., 2014. “Hexamorph: A reconfigurable and foldable hexapod robot inspired by origami.” *Intelligent Robots and Systems (IROS 2014), 2014 IEEE/RSJ International Conference on*, pp. 4598–4604. 8
- [24] Pendleton, T. M., 2006. “Design and fabrication of rotationally tristable compliant mechanisms.” Master’s thesis, Brigham Young University. 8
- [25] Chen, G., Zhang, S., and Li, G., 2013. “Multistable behaviors of compliant sarrus mechanisms.” *Journal of Mechanisms and Robotics*, **5**(2). 8
- [26] Oh, Y. S., and Kota, S., 2009. “Synthesis of multistable equilibrium compliant mechanisms using combinations of bistable mechanisms.” *Journal of Mechanical Design*, **131**(2). 8
- [27] King, C. W., Campbell, M. I., Beaman, J. J., and Sreenivasan, S. V., 2005. “Synthesis of multistable equilibrium linkage systems using an optimization approach.” *Structural and Multidisciplinary Optimization*, **29**(6), pp. 477–487. 8
- [28] Tachi, T., 2011. “Rigid-foldable thick origami.” In *Origami 5*. 19
- [29] Hull, T., 2003. “Counting mountain-valley assignments for flat folds.” *Ars Combinatoria*, **67**. 20, 21, 36, 38

- [30] Silverberg, J. L., Evans, A. A., McLeod, L., Hayward, R. C., Hull, T., Santangelo, C. D., and Cohen, I., 2014. “Using origami design principles to fold reprogrammable mechanical metamaterials.” *Science*. 36
- [31] Dai, J., and Caldwell, D., 2010. “Origami-based robotic paper-and-board packaging for food industry.” *Trends in Food Science & Technology*, **21**(3), pp. 153 – 157. 36
- [32] Balkcom, D., 2004. “Robotic origami folding.” PhD thesis, Carnegie Mellon University. 36
- [33] Buri, H., 2010. “Folding - folded plate structures.” PhD thesis, EP Federale de Lausanne. 36
- [34] Hull, T., 1994. “On the mathematics of flat origamis.” *Congressus Numeratum*, **100**, pp. 215–224. 36, 39
- [35] Schenk, M., and Guest, S. D., 2012. “Geometry of muira-folded metamaterials.” *PNAS*, **110**(9), pp. 3276 – 3281. 36
- [36] Wei, Z. Y., Guo, Z. V., Dudte, L., Liang, H. Y., and Mahadevan, L., 2013. “Geometric mechanics of periodic pleated origami.” *Phys. Rev. Lett.*, **110**. 36
- [37] Demaine, E. D., Demaine, M. L., Hart, V., Price, G. N., and Tachi, T., 2011. “(non)existence of pleated folds: How paper folds between creases.” *Graph. Comb.*, **27**, pp. 377–397. 36
- [38] Evans, T. A., Lang, R. J., Magleby, S. P., and Howell, L. L., 2015. “Rigidly foldable origami twists.” In *review in Origami6*. 37, 39, 40, 44, 47
- [39] Miura, K., 1969. “Proposition of pseudo-cylindrical concave polyhedral shells.” *Institute of Space and Aeronautical Science*. 43
- [40] Barreto, P. T., 1997. “Lines meeting on a surface: The ‘mars’ paperfolding.” *Origami Science & Art: Proceedings of the Second International Meeting of Origami Science and Scientific Origami*. 44
- [41] Yoshimura, Y., 1955. “On the mechanism of buckling of a circular cylindrical shell under axial compression.” *NACA TM 1390*. 45
- [42] Stavric, M., and Wiltsche, A., 2014. “Quadrilateral patterns for rigid folding structure.” *International Journal of Architectural Computing*. 45
- [43] Lang, R. J., 2011. *Origami Design Secrets: Mathematical Method for an Ancient Art, Second Edition*. CRC Press. 49, 55
- [44] Murray, G., 2013. Rotation about an arbitrary axis in 3 dimensions http://inside.mines.edu/fs_home/gmurray/ArbitraryAxisRotation, June. 71
- [45] Lando, S. K., and Zvonkin, A. K., 2004. *Graphs on Surfaces and Their Applications*. Springer. 75

APPENDIX A. DERIVATION OF THE RELATIONSHIP BETWEEN DIHEDRAL ANGLES IN A DEGREE-4 FLAT-FOLDABLE ORIGAMI VERTEX

We will consider a flat-foldable degree-4 vertex where the first panel (associated with α_1) is grounded in the x-y plane as shown in Figure A.1. The unit vector pointing from the vertex along the first crease (\vec{a}_1) is along the x-axis:

$$\vec{a}_1 = \begin{pmatrix} 1 \\ 0 \\ 0 \end{pmatrix} \quad (\text{A.1})$$

The unit vector (\vec{n}_1) which is normal to the first panel is along the z-axis:

$$\vec{n}_1 = \begin{pmatrix} 0 \\ 0 \\ 1 \end{pmatrix} \quad (\text{A.2})$$

Analysis of this vertex will use the 3D rotation matrix. A rotation matrix R giving a rotation by θ radians about the axis \vec{u} and using the shorthand notation of $c\theta \equiv \cos \theta$ and $s\theta \equiv \sin \theta$ is given [44] as

$$R(\theta, \vec{u}) \equiv \begin{pmatrix} c\theta + u_x^2(1 - c\theta) & u_x u_y(1 - c\theta) - u_z s\theta & u_x u_z(1 - c\theta) + u_y s\theta \\ u_x u_y(1 - c\theta) + u_z s\theta & c\theta + u_y^2(1 - c\theta) & u_y u_z(1 - c\theta) - u_x s\theta \\ u_x u_z(1 - c\theta) - u_y s\theta & u_y u_z(1 - c\theta) + u_x s\theta & c\theta + u_z^2(1 - c\theta) \end{pmatrix} \quad (\text{A.3})$$

where u_x , u_y , and u_z are the x-, y-, and z-components of \vec{u} , respectively.

This derivation will involve solving a loop closure equation for the vertex by evaluating the unit vectors for each of the crease lines (\vec{a}_i) and the unit vectors normal to each sector (\vec{n}_i).

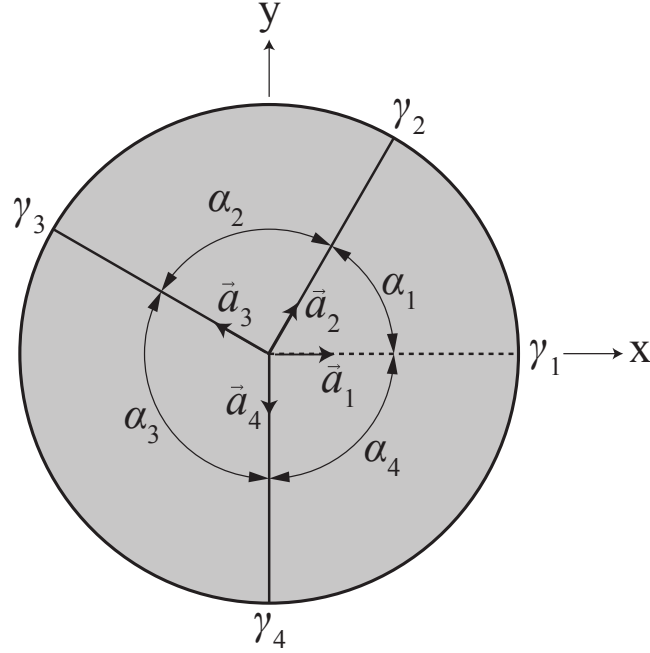


Figure A.1: Degree-4 flat-foldable origami vertex with sector angles (α_i), dihedral angles (γ_i) and unit vectors along each crease (a_i)

Using Equation (A.3), the unit vector along the second crease (\vec{a}_2) may be found by rotating \vec{a}_1 about \vec{n}_1 by the sector angle α_1 . Therefore,

$$\vec{a}_2 = R(\alpha_1, \vec{n}_1)\vec{a}_1 \quad (\text{A.4})$$

Similarly, the unit vector normal to the second panel (\vec{n}_2) may be found by rotating \vec{n}_1 about \vec{a}_2 by the dihedral angle γ_2 . Therefore,

$$\vec{n}_2 = R(\gamma_2, \vec{a}_2)\vec{n}_1 \quad (\text{A.5})$$

This same method can be used to find \vec{a}_3 ,

$$\vec{a}_3 = R(\alpha_2, \vec{n}_2)\vec{a}_2 \quad (\text{A.6})$$

Because of the complexity of these equations, it is simpler to work clockwise around the vertex from the original position than to continue closing the loop in the counterclockwise direc-

tion. The unit vector normal to the fourth panel may be found by rotation \vec{n}_1 about \vec{a}_1 by the negative of the dihedral angle γ_1 . Therefore,

$$\vec{n}_4 = R(-\gamma_1, \vec{a}_1)\vec{n}_1 \quad (\text{A.7})$$

Continuing evaluation around the vertex in the clockwise direction, while recalling from Equation (3.1) that $\alpha_3 = \pi - \alpha_1$ and $\alpha_4 = \pi - \alpha_2$ and from Equation (3.2) that $\gamma_3 = -\gamma_1$ and $\gamma_2 = \gamma_4$,

$$\vec{a}_4 = R(-\alpha_4, \vec{n}_4)\vec{a}_1 = R(\alpha_2 - \pi, \vec{n}_4)\vec{a}_1 \quad (\text{A.8})$$

$$\vec{n}_3 = R(-\gamma_4, \vec{a}_4)\vec{n}_4 = R(-\gamma_2, \vec{a}_4)\vec{n}_4 \quad (\text{A.9})$$

$$\vec{a}_3 = R(-\alpha_3, \vec{n}_3)\vec{a}_4 = R(\alpha_1 - \pi, \vec{n}_3)\vec{a}_4 \quad (\text{A.10})$$

The loop is then closed by equating Equations (A.6 and A.10). Evaluating Equations (A.4 - A.10) and equating these equations results in the following equality (once again using shorthand notation):

$$\begin{pmatrix} c\alpha_1 c\alpha_2 - c\gamma_2 s\alpha_1 s\alpha_2 \\ c\alpha_2 s\alpha_1 + c\alpha_1 c\gamma_2 s\alpha_2 \\ s\alpha_2 s\gamma_2 \end{pmatrix} = \begin{pmatrix} c\alpha_1 c\alpha_2 - c\gamma_2 s\alpha_1 s\alpha_2 \\ c\alpha_2 c\gamma_1 c\gamma_2 s\alpha_2 + c\alpha_1 c\gamma_1 s\alpha_2 + s\alpha_1 s\gamma_1 s\gamma_2 \\ -(c\alpha_2 c\gamma_2 s\alpha_1 + c\alpha_1 s\alpha_2)s\gamma_1 + c\alpha_2 s\alpha_1 s\gamma_2 \end{pmatrix} \quad (\text{A.11})$$

Using the symbolic mathematical software Mathematica, the solution to Equation (A.11) was found to be

$$\frac{\sin\left(\frac{1}{2}(\alpha_1 + \alpha_2)\right)}{\sin\left(\frac{1}{2}(\alpha_1 - \alpha_2)\right)} = \frac{\tan\left(\frac{1}{2}\gamma_2\right)}{\tan\left(\frac{1}{2}\gamma_1\right)} \quad (\text{A.12})$$

APPENDIX B. PROOF OF AVERAGE POLYGON SIZE

We will consider a mesh of k polygons with n_i as the number of vertices of the i^{th} polygon. (Such a mesh is shown in black in Figure B.1.) Now we divide each polygon into n_i triangles which have a common vertex at the center of the polygon (shown in green). Let V , E , and F be the number of vertices, edges, and polygons of the original graph (black). Let d be the degree of all interior vertices.

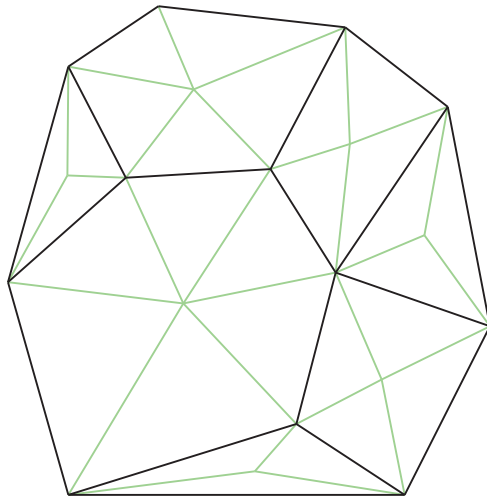


Figure B.1: Arbitrary polygon mesh with subdividing triangles

If we sum over all polygons, we can calculate the number of triangles N as follows:

$$N = \sum_{i=1}^k n_i \quad (\text{B.1})$$

Second, we sum over the edges. Each interior edge contributes two triangles while each boundary edge contributes only one. If there are E_b edges on the boundary, then

$$N = 2E - E_b \quad (\text{B.2})$$

Solving for E yields

$$E = \frac{1}{2}(N + E_b) \quad (\text{B.3})$$

Third, we sum over vertices. Assume that all interior vertices have degree d and boundary vertices have degree d_j (where j is the index of a boundary vertex). If m is the number of boundary vertices, then

$$N = dV - \sum_{j=1}^m (d - d_j) \quad (\text{B.4})$$

Solving for V results in

$$V = \frac{1}{d} \left(N + \sum_{j=1}^m (d - d_j) \right) \quad (\text{B.5})$$

According to the Euler characteristic [45],

$$V - E + F = 2 \quad (\text{B.6})$$

Solving for F yields

$$F = 2 + E - V \quad (\text{B.7})$$

Substituting in Equations (B.3) and (B.5) results in

$$F = 2 + \frac{1}{2}(N + E_b) - \frac{1}{d} \left(N + \sum_{j=1}^m (d - d_j) \right) \quad (\text{B.8})$$

Rearranging,

$$F = N \left(\frac{1}{2} - \frac{1}{d} \right) + \frac{1}{2}E_b - \frac{1}{d} \sum_{j=1}^m (d - d_j) + 2 \quad (\text{B.9})$$

Now the average polygon degree (n_{avg}) may be found:

$$n_{avg} = \frac{\sum_{i=1}^F n_i}{\sum_{i=1}^F 1} = \frac{N}{F} \quad (\text{B.10})$$

Substituting in Equation (B.8) yields

$$n_{avg} = \frac{N}{N\left(\frac{1}{2} - \frac{1}{d}\right) + \frac{1}{2}E_b - \frac{1}{d} \sum_{j=1}^m (d - d_j) + 2} \quad (\text{B.11})$$

Dividing both numerator and denominator by N results in

$$n_{avg} = \frac{1}{\left(\frac{d-2}{2d}\right) + \frac{1}{N} \left(\frac{1}{2}E_b - \frac{1}{d} \sum_{j=1}^m (d - d_j) + 2\right)} \quad (\text{B.12})$$

As the number of triangles (N) approaches infinity we reach the following:

$$\lim_{N \rightarrow \infty} n_{avg} = \frac{2d}{d-2} \quad (\text{B.13})$$

Thus for $d = 4$, $n_{avg} \rightarrow 4$. Note also that for $d = 3$, $n_{avg} \rightarrow 6$ and for $d = 6$, $n_{avg} \rightarrow 3$ as is found in the Diamond Tessellation. This equation is similar to the equation for the value of the interior angles of a regular polygon. As a result, n_{avg} is equal to the degree of the regular polygon that has interior angles equal to $2\pi/d$. For example, an array of regular hexagons of equal size contains only degree-3 vertices. Note that these conditions only hold as the number of polygons approach infinity. Therefore, degree-4 tessellations can be created which do not have an average polygon size of four if these tessellations do not repeat continuously.

APPENDIX C. CREASE PATTERNS FOR RIGIDLY FOLDABLE ORIGAMI TESSELLATIONS

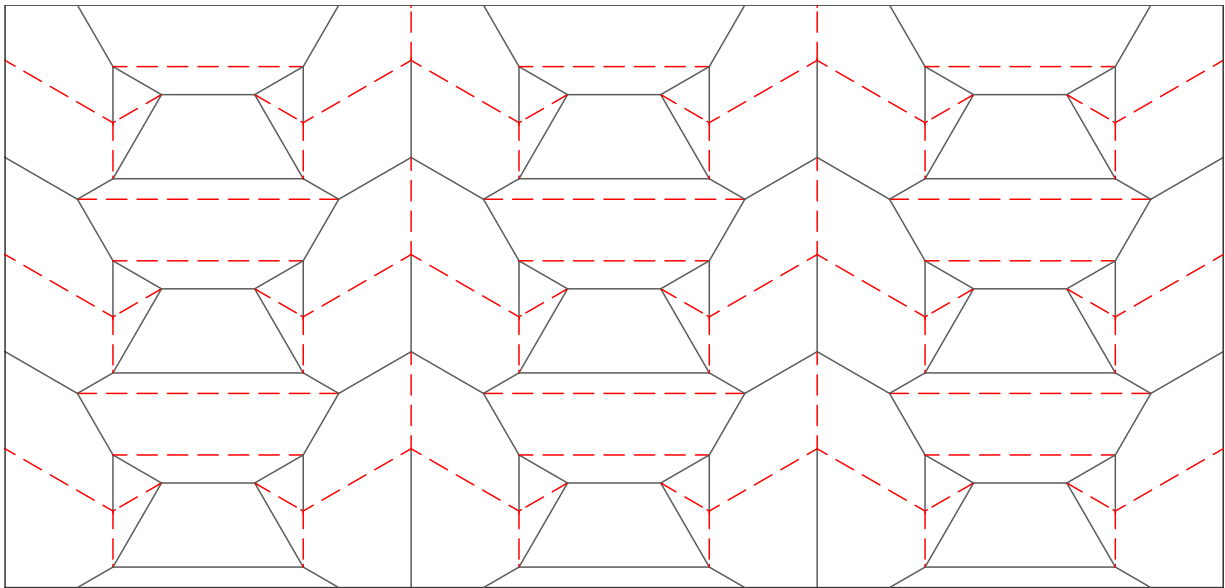


Figure C.1: Triple parallel tessellation. This tessellation is constructed using sets of triple parallel gadgets. Self-intersection generally occurs before the secondary flat position is reached.

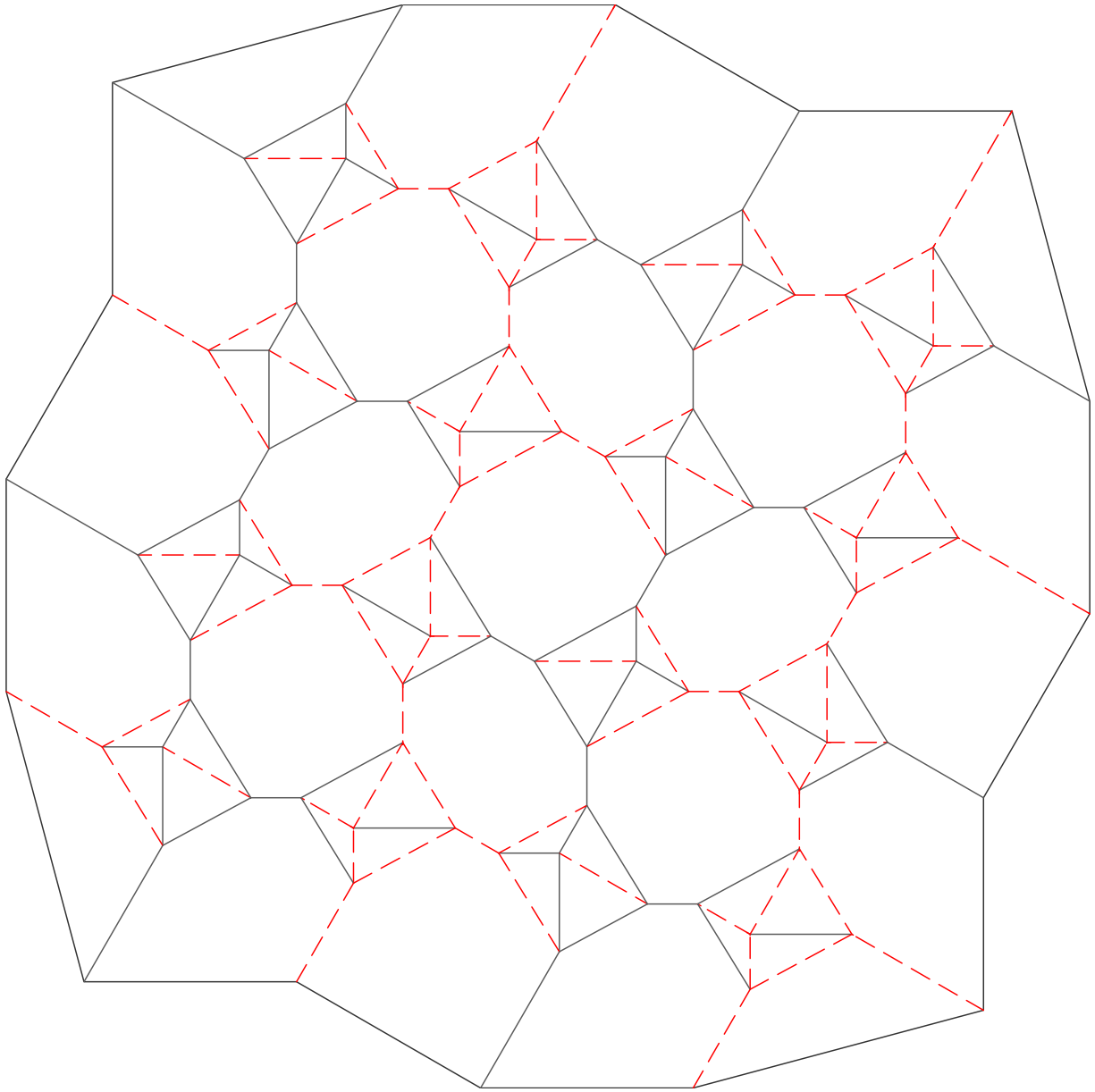


Figure C.2: Barreto's "Mars" with corner gadgets. This tessellation modifies Barreto's "Mars" by replacing vertices with corner gadgets. This replacement does not change the overall motion of the tessellation and the secondary flat position is obtainable without self-intersection.

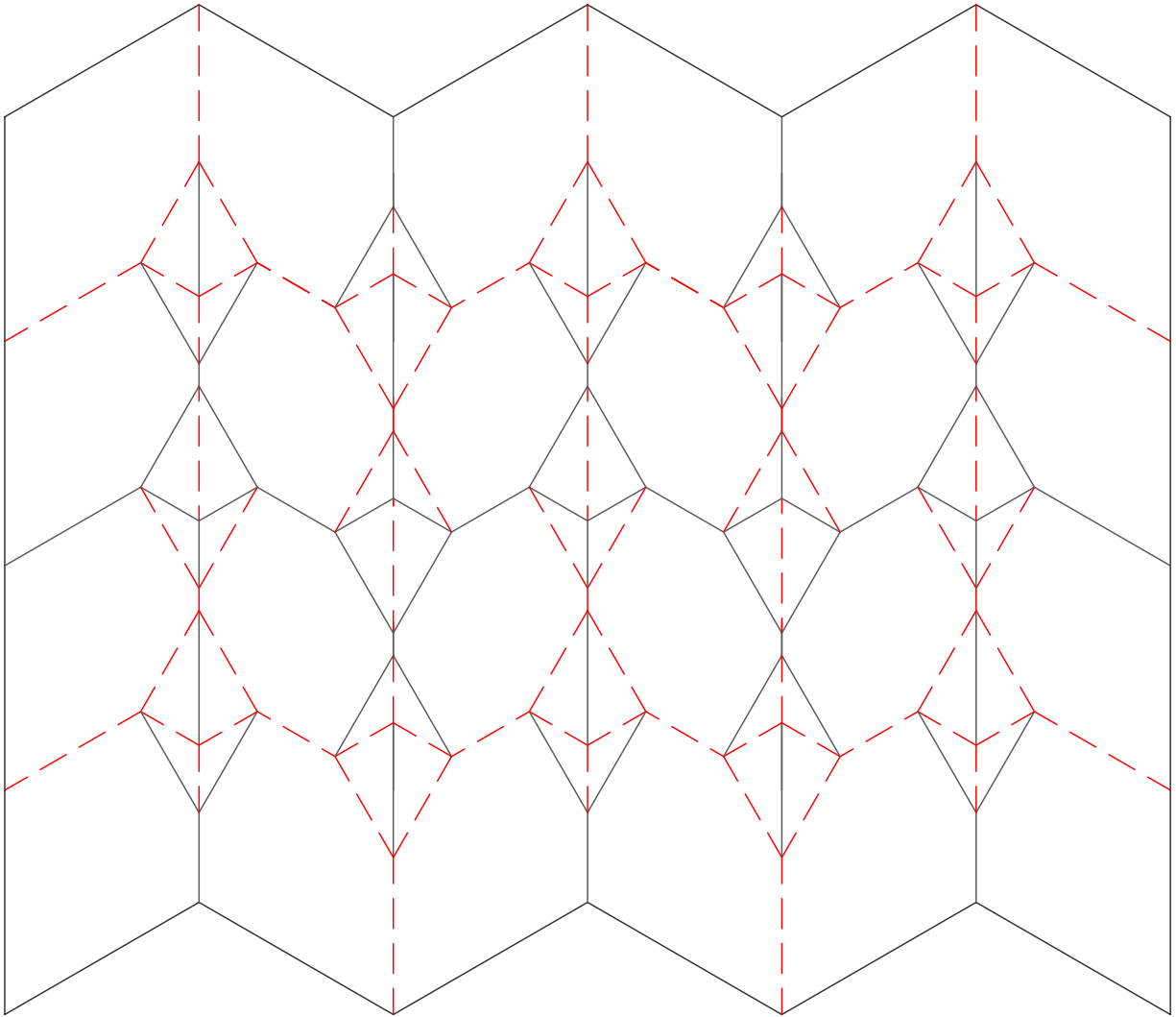


Figure C.3: Miura-ori pattern with corner gadgets. This tessellation modifies the Miura-ori by replacing vertices with corner gadgets. This replacement does not change the overall motion of the tessellation and the secondary flat position is obtainable without self-intersection.

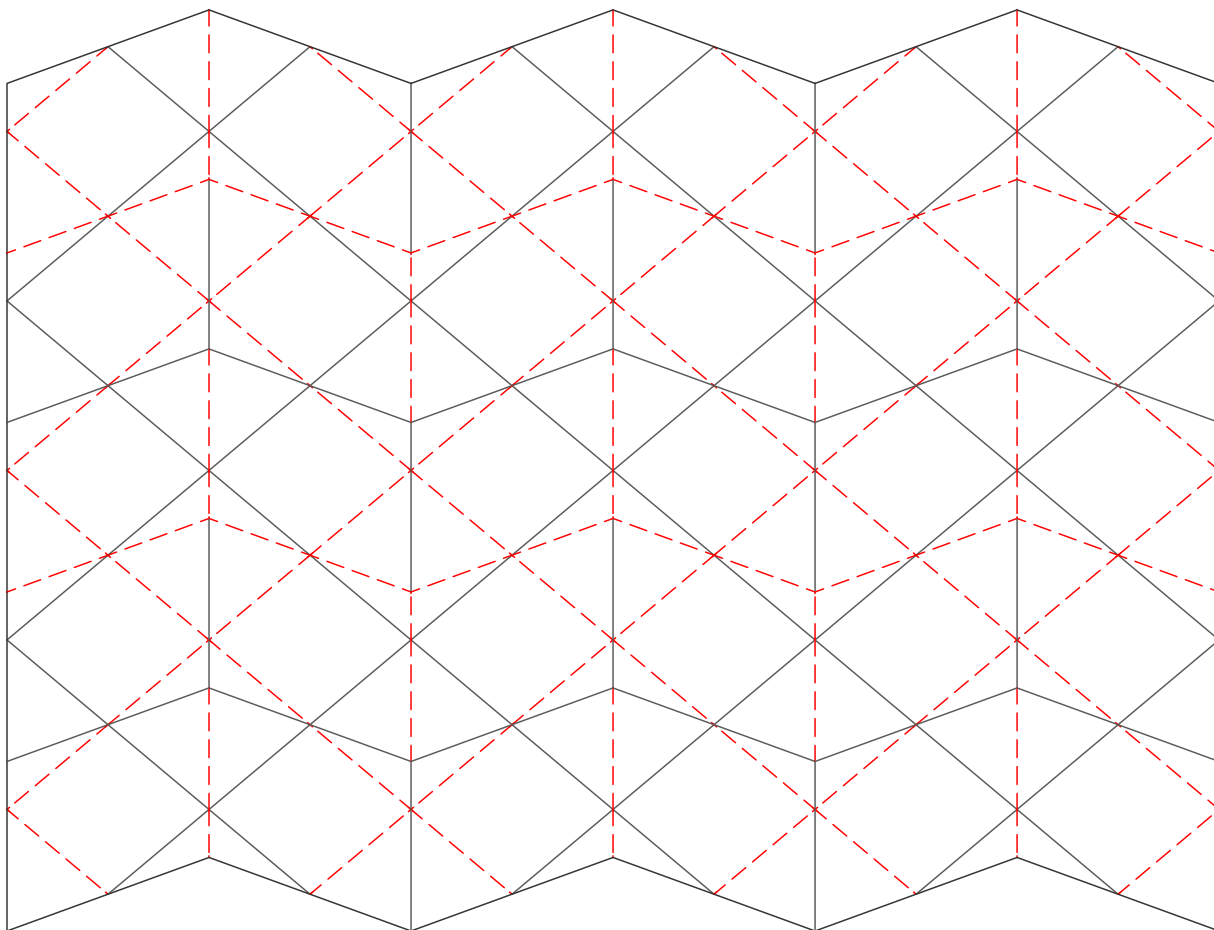


Figure C.4: Collapsed Miura-ori pattern with corner gadgets. This tessellation is created by eliminating creases between corner gadgets in the previous tessellation. As such, pairs of degree-4 vertices are combined to form degree-6 vertices. Even with the presence of degree-6 vertices, this tessellation has only one degree of freedom and the secondary flat position is obtainable without self-intersection.

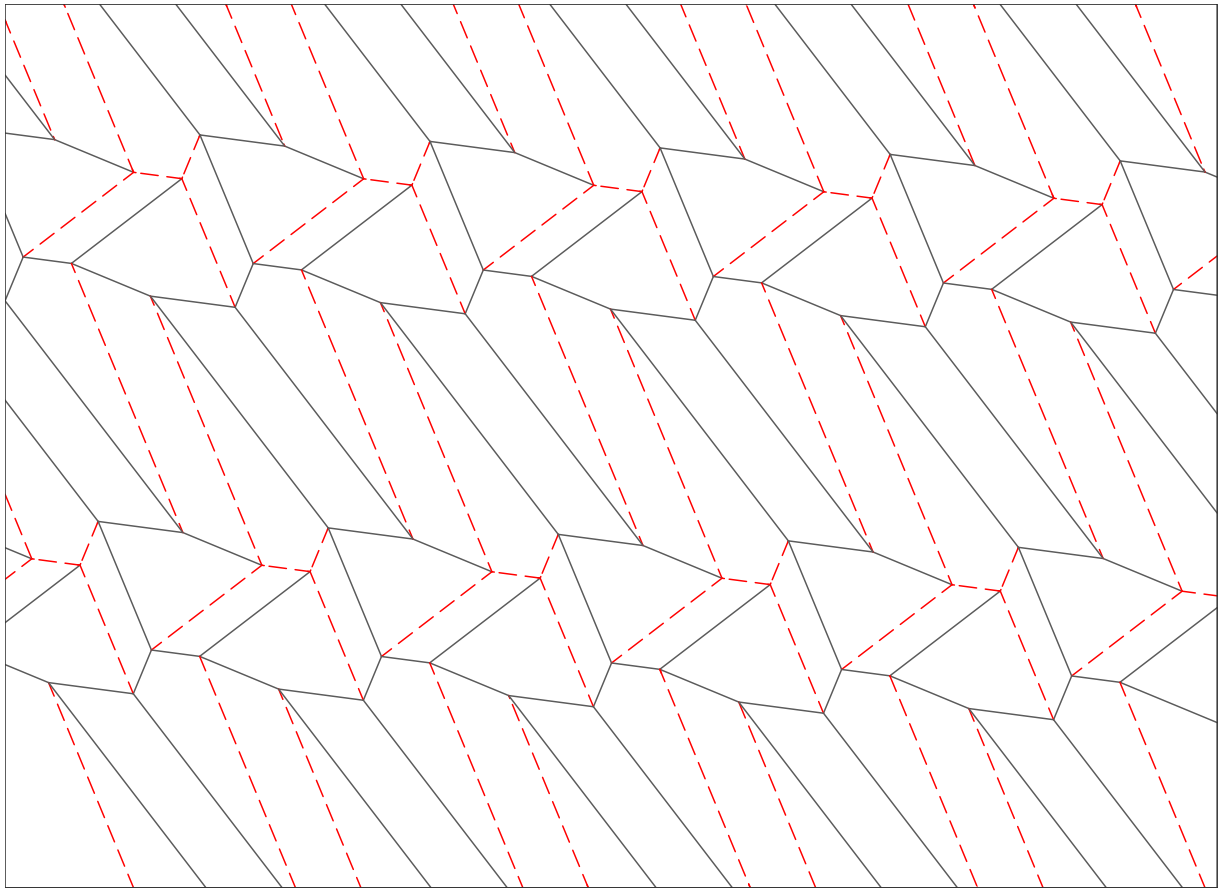


Figure C.5: Kite twist tessellation. This tessellation is constructed using two types of kite twists. Self-intersection generally occurs before the secondary flat position is reached.

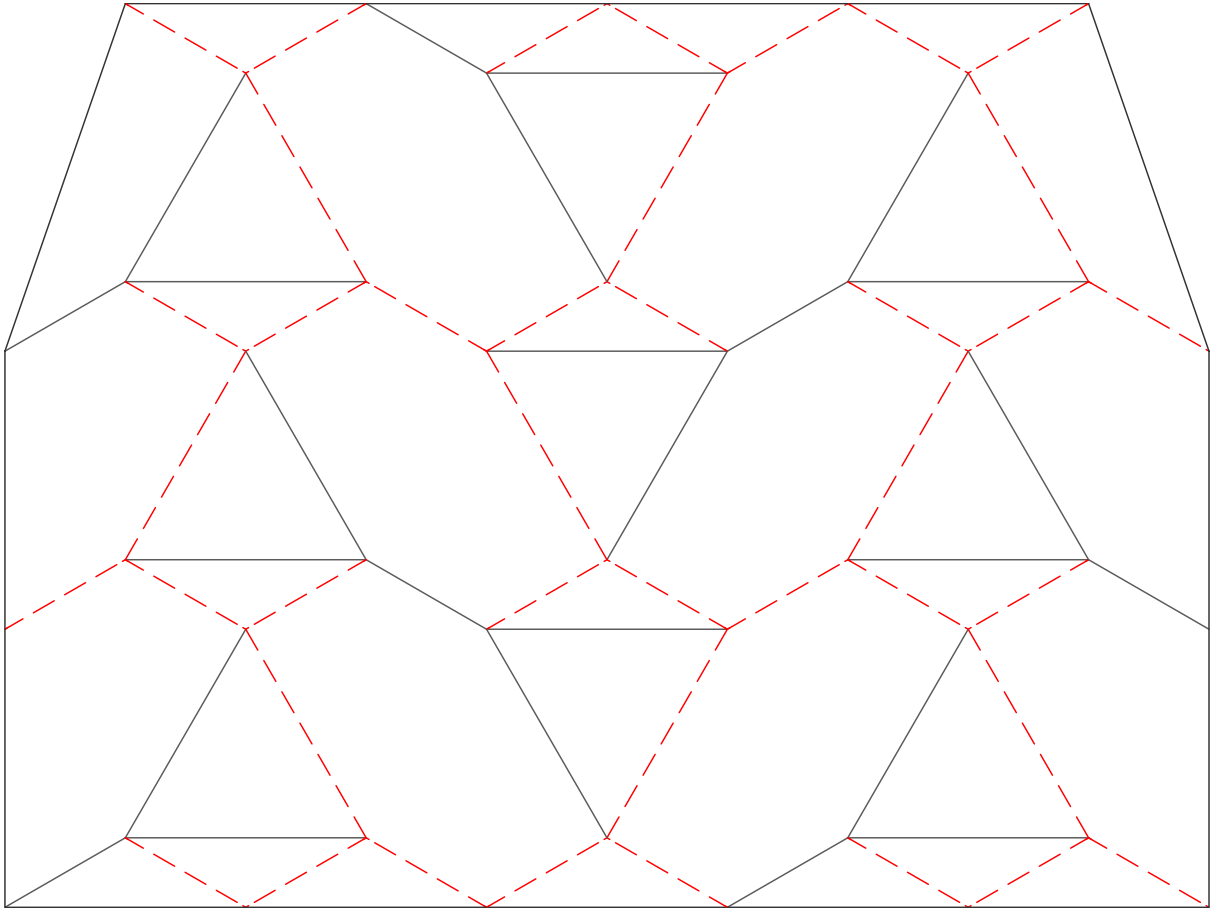


Figure C.6: Alternating level shifter tessellation. This tessellation contains parallel chains of level shifters which alternate in direction. The secondary flat position is obtainable without self-intersection.

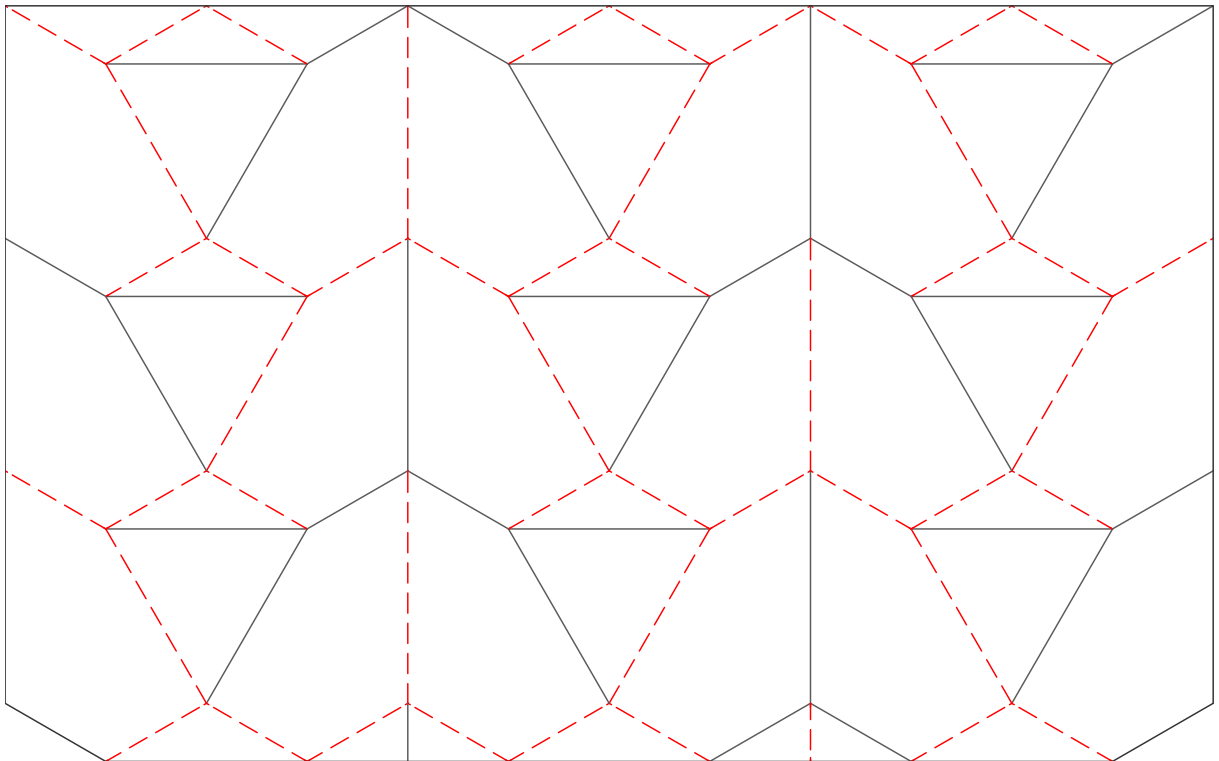


Figure C.7: Level shifter tessellation. This tessellation contains parallel chains of level shifters separated by vertical creases. Crease assignments of adjacent chains mirror each other. The secondary flat position is obtainable without self-intersection.

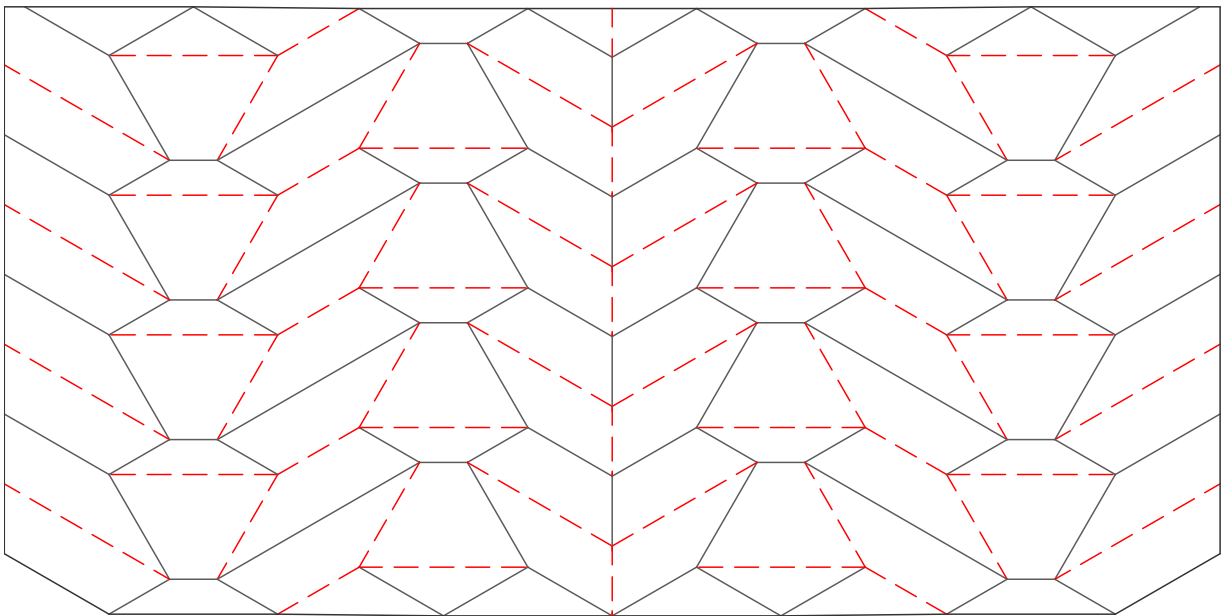


Figure C.8: Trapezoidal tessellation. This tessellation is constructed entirely of trapezoids and the secondary flat position is obtainable without self-intersection.

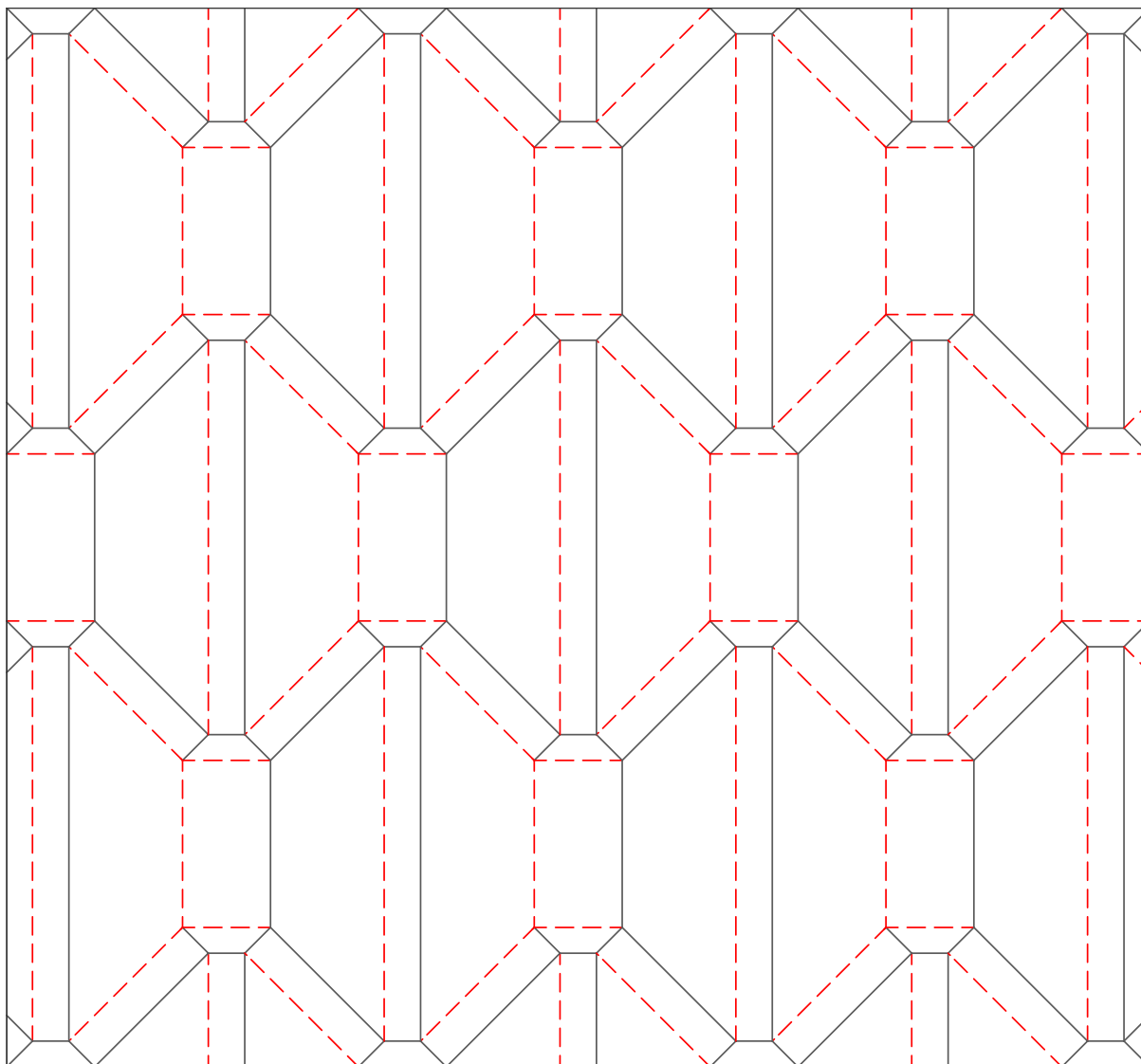


Figure C.9: Modified Yoshimura pattern. This tessellation is constructed by replacing creases on the Yoshimura pattern with pairs of creases with opposite parity and by replacing vertices with a rectangle and two isosceles trapezoids. The motion is similar to the Yoshimura pattern and self-intersection generally occurs before the secondary flat position is reached.

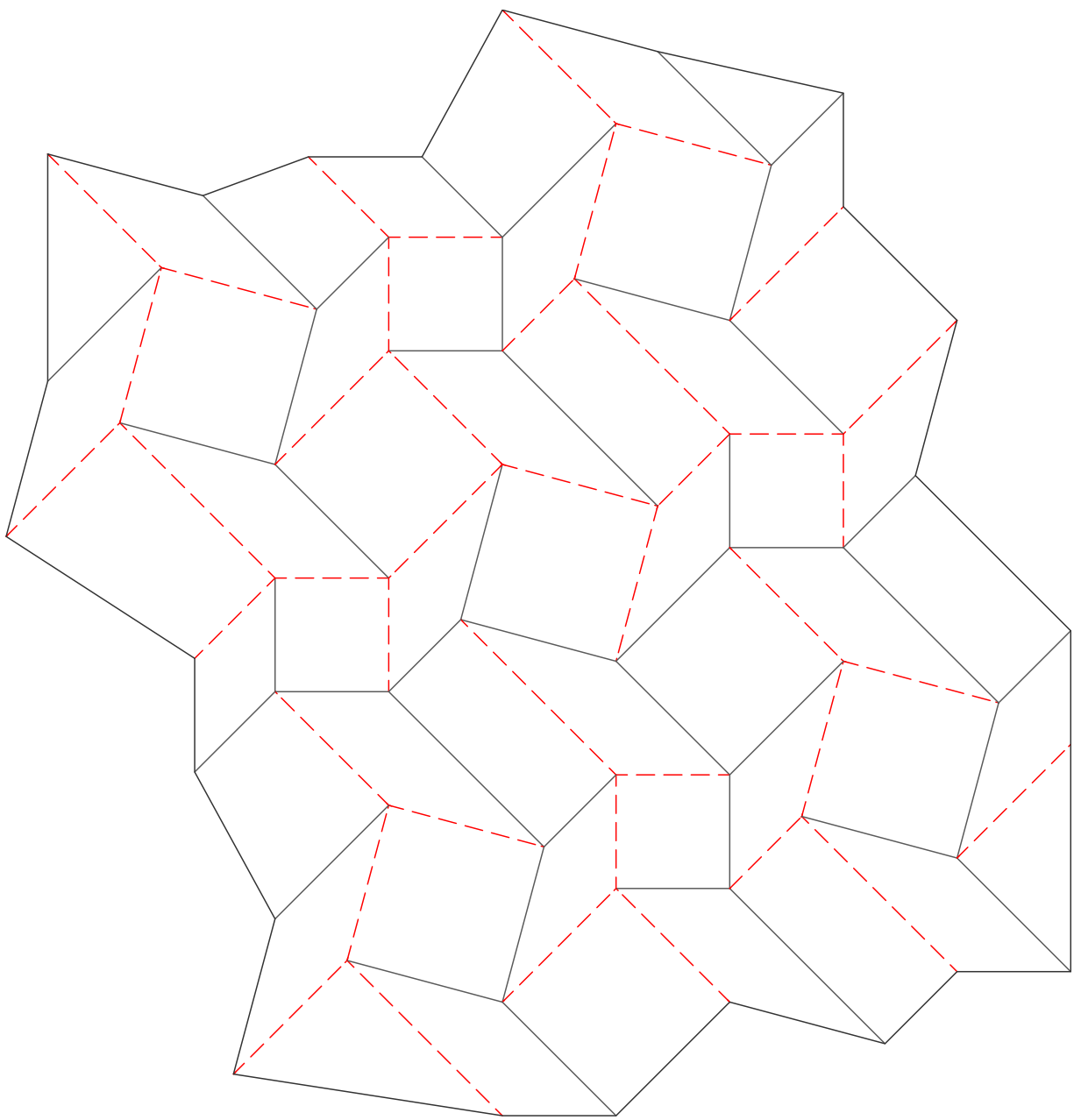


Figure C.10: Dual square twist tessellation. This tessellation contains square twists of two twist angles. The secondary flat position is obtainable without self-intersection.